Smart Materials in Medicine 7 (2026) 13–43

Contents lists available at ScienceDirect

Smart Materials in Medicine

journal homepage: www.keaipublishing.com/en/journals/smart-materials-in-medicine/

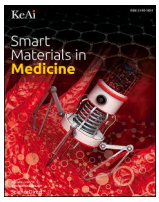

# Advanced nanomaterials for myocardial ischemia-reperfusion injury: Bridging precision imaging to targeted therapy

Jie Li[a,b,1], Muhammad Shafiq[c,1], Minghua Yao[d], Zehua Liu[e,*], Ruizhi Tian[b,f], Fangqiao Zheng[a,b], Chan Lu[a,b], Ming Ma[a,b,f,**]

[a] School of Chemistry and Materials Science, Hangzhou Institute for Advanced Study, University of Chinese Academy of Sciences, Hangzhou, 310024, PR China
[b] State Key Laboratory of High Performance Ceramics, Shanghai Institute of Ceramics, Chinese Academy of Sciences, Shanghai, 200050, PR China
[c] Research Center for Integrative Physiology & Pharmacology, Institute of Biomedicine, Faculty of Medicine, University of Turku, Turku, Finland
[d] Department of Medical Ultrasound, Shanghai General Hospital, School of Medicine, Shanghai Jiaotong University, Shanghai, 200080, PR China
[e] Drug Research Program, Division of Pharmaceutical Chemistry and Technology, Faculty of Pharmacy, University of Helsinki, FI-00014, Helsinki, Finland
[f] Center of Materials Science and Optoelectronics Engineering, University of Chinese Academy of Sciences, Beijing, 100049, PR China

ARTICLE INFO

*Keywords:*
Myocardial ischemia-reperfusion injury
Nanomaterials
Anti-inflammatory therapy
Diagnosis
Cardiac tissue repair

ABSTRACT

Myocardial ischemia-reperfusion injury (MIRI) is a major cause of heart failure, driven by oxidative stress, inflammation, and rapid loss of cardiomyocytes. Traditional therapies for MIRI remain limited, largely due to poor cardiac targeting and an absence of real-time diagnostic capabilities. Recently, various nanomaterials (NMs) have been extensively developed and applied to achieve more precise and effective treatment of MIRI, owing to their favorable biosafety and functional tunability. This review comprehensively summarizes the latest research progress on functional NMs in diagnostic imaging and therapeutic interventions for MIRI. In the context of diagnostic imaging, *in vitro* nano-biosensors enable the early detection of MIRI biomarkers, while NM-enhanced imaging modalities provide high diagnostic precision at the *in vivo* level and support real-time therapeutic guidance. Therapeutically, NMs can be leveraged as direct antioxidative agents, vehicles for targeted gene therapy, and platforms for combination regimens including gas therapy, stem cell therapy, and circadian rhythm modulation, to enhance myocardial repair. By synthesizing these advancements, this review provides conceptual and technological insights that could guide the future of nanomedicine-enabled precision cardiovascular care.

## 1. Introduction

Myocardial injury, encompassing conditions such as acute myocardial infarction (AMI) and procedure-related ischemic damage (e.g., percutaneous coronary intervention (PCI)-induced injury), continues to be a major contributor to global morbidity and mortality [1]. Among these, myocardial ischemia-reperfusion injury (MIRI) presents a particularly critical and paradoxical challenge: while timely reperfusion is essential to restore blood flow and salvage ischemic myocardium, it also initiates a cascade of deleterious processes that exacerbate tissue damage. Besides, intracellular calcium overload can disrupt ionic homeostasis and promote hypercontracture, protease activation, and mitochondrial injury [2]. Excess calcium further induces an opening of the mitochondrial permeability transition pore, a pivotal event that dissipates mitochondrial membrane potential, impairs adenosine triphosphate (ATP) synthesis, and activates necrotic and apoptotic pathways [3]. In parallel, the abrupt oxygen supply during reperfusion triggers a burst of reactive oxygen species (ROS), aggravating oxidative damage to lipids, proteins, and DNA, thereby amplifying mitochondrial dysfunction [4]. Beyond classical necrosis and apoptosis, regulated cell death modalities such as pyroptosis, a caspase-1-driven inflammation-promoting pathway, and ferroptosis, characterized by iron overload and lipid peroxidation, have also been implicated in the loss of cardiomyocytes (CMs) during MIRI [5–7]. These processes are closely

* Corresponding author.
** Corresponding author. School of Chemistry and Materials Science, Hangzhou Institute for Advanced Study, University of Chinese Academy of Sciences, Hangzhou, 310024, PR China.
*E-mail addresses:* zehua.liu@helsinki.fi (Z. Liu), mma@mail.sic.ac.cn (M. Ma).
Peer review under the responsibility of KeAi Communications Co., Ltd
[1] J.L. and M.S. are co-first authors and contributed equally to this manuscript.

https://doi.org/10.1016/j.smaim.2025.12.003
Received 11 October 2025; Received in revised form 18 December 2025; Accepted 26 December 2025
Available online 29 December 2025

intertwined with an intense inflammatory response involving immune cell infiltration, cytokine release, and endothelial cell (EC) dysfunction, all of which further impair myocardial recovery and contribute to adverse cardiac remodeling [8]. Despite progress in revascularization techniques and pharmacotherapy, MIRI remains a major clinical obstacle and a key driver of the long-term burden of ischemic heart disease [9].

Accurate diagnosis and real-time monitoring of MIRI progression are critical for effective therapeutic decision-making. Nonetheless, traditional imaging modalities often suffer from limited sensitivity, less specificity, and poor spatiotemporal resolution [10,11]. The discovery of intrinsically functional nanomaterials (NMs), such as cerium oxide ($CeO_2$) nanoparticles (NPs), manganese oxide ($MnO_2$), gold nanoclusters, and superparamagnetic iron oxide NPs (SPIONs), has significantly enhanced the diagnostic precision of MIRI through integration with advanced imaging techniques (e.g., computed tomography (CT), fluorescence imaging (FI), photoacoustic imaging (PAI), magnetic resonance imaging (MRI), etc.) [12–16]. These NMs offer multimodal imaging potential, while concurrently participating in oxidative stress regulation as well as inflammation regulation. In particular, nano-biosensing technologies have recently been developed to detect dynamic biochemical signals, such as ROS, inflammatory cytokines, and cardiac biomarkers with high sensitivity and selectivity as well as spatial resolution [17–19]. These biosensors may enable an earlier yet precise readout of myocardial pathology, suggesting their considerable promise for real-time monitoring of ischemic heart diseases. Though diverse biosensor platforms have been primarily evaluated in myocardial infarction (MI) models, they share overlapping pathophysiological features with MIRI, particularly in terms of oxidative stress and inflammatory responses. This commonality provides valuable mechanistic insights and technical references for the development of diagnostic strategies targeting reperfusion injury. These diagnostic advances also establish the basis for imaging-guided therapeutic strategies, in which pathological information feeds directly into spatiotemporally matched treatment decisions.

From a therapeutic perspective, current approaches for MIRI include mechanical reperfusion techniques, ischemic conditioning strategies, and advanced interventional procedures [20–22]. On the other hand, pharmacological agents (e.g., antioxidants, anti-inflammatory drugs) still face challenges such as insufficient cardiac targeting, narrow therapeutic windows, poor bioavailability, systemic toxicity, and a lack of real-time diagnostic feedback. Extensive clinical trials investigating candidates like cyclosporine, TRO40303, and elamipretide have failed to demonstrate consistent cardio-protection or acceptable safety in large-scale populations [23–25], partly due to pharmacokinetic constraints such as low myocardial accumulation and rapid systemic clearance [26,27]. Emerging therapeutic modalities, such as gene therapy, microRNA (miRNA) modulation, stem cell transplantation, and exosome-based treatments, offer great promise [28–30], yet their clinical translation is hindered by inefficient delivery and a hostile ischemic microenvironment, compromising therapeutic viability [31,32]. Functional NMs offer a compelling solution by not only enhancing cargo delivery efficiency but also directly participating in therapeutic pathways, including ROS scavenging, mitochondrial protection, anti-apoptotic effects, and immune modulation. Recent studies have also identified circadian rhythm as a crucial regulator of MIRI susceptibility and nanomedicine efficacy [33–35]. Chrono-pharmacological analyses suggest that the therapeutic outcome of NMs is significantly influenced by biological timing, thus demanding chrono-synchronized material design [36]. By integrating intrinsic bioactivity with time-controlled release, these NMs can achieve spatiotemporal precision aligned with endogenous cardiac rhythms.

Importantly, the boundary between diagnosis and treatment is becoming increasingly blurred. Functional nanoplatforms enable diagnostic imaging to guide, monitor, and personalize therapeutic interventions, thereby enhancing overall therapeutic efficacy and minimizing off-target effects. The convergence of intrinsically functional NMs with imaging, biosensing, catalytic medicine, gas therapy, and circadian modulation heralds a transformative shift toward precision cardiovascular nanomedicine [37–40].

The primary objective of this review is to highlight recent advancements in the application of intrinsically functional NMs for MIRI theranostics (Fig. 1). Unlike traditional nanocarriers that primarily act as passive drug delivery tools, this review highlights NMs with intrinsic functionalities. These include advanced imaging capabilities, such as magnetic resonance and optical fluorescence, along with a range of therapeutic effects, including anti-oxidative and anti-inflammatory activities, efficient cytoplasmic delivery, and anti-apoptotic properties. We systematically summarize the application of *in vitro* nano-biosensors for an earlier detection of MIRI, along with the integration of NMs and diverse imaging modalities to further broaden diagnostic precision in MIRI models. Different types of imaging platforms, such as CT, FI, PAI, and MRI can significantly improve diagnostic accuracy and facilitate real-time, imaging-guided interventions. Moreover, we explored the therapeutic strategies enabled by these multifunctional NMs: (1) the application of nanozymes for direct therapy of MIRI, (2) strategies for enhancing targeted gene therapy, with a focus on biomimetic membrane modifications and (3) combined delivery of intrinsically multifunctional NMs with complementary technologies, such as gas therapy, stem cell therapy, and circadian rhythm to further complement myocardial tissue repair process. This review aims to provide a conceptual and technological framework for the future development of smart NMs with built-in functionalities for precision cardiovascular therapy.

## 2. Diagnostic imaging of MIRI based on NMs

NMs have revolutionized the detection and imaging of myocardial injury, encompassing conditions such as MIRI and MI, by offering unprecedented precision, sensitivity, and multi-scale resolution. Intriguingly, unique physical and chemical features of NMs, including tunable size, high surface-area-to-volume ratio, and versatile surface chemistries may help develop highly responsive contrast agents, molecular probes, and biosensing platforms [41,42]. Through the encapsulation or conjugation of functional moieties, such as metallic ions, magnetic NPs, and fluorescent dyes, NMs can appreciably enhance imaging performance across diverse modalities, including CT, FI, PAI and MRI [43–45]. In addition to the applications of NMs for *in vivo* imaging, they are also being increasingly applied as *in vitro* biosensing platforms, thereby enabling an earlier yet point-of-care detection of cardiac biomarkers with high sensitivity and selectivity [46]. These technologies complement imaging-based strategies by facilitating rapid biochemical assessment of myocardial injury in clinical or perioperative settings. A unique advantage of NMs is their ability to be functionalized with targeting ligands to detect MIRI-related biomarkers, such as cardiac troponins, ROS, and inflammation-related adhesion molecules. This allows active localization to the injured myocardium alongside enhanced spatial and pathological specificity [47]. This molecular targeting may not only facilitate high-contrast imaging of infarcted tissue but may also help detect initial molecular alterations prior to structural remodeling [48]. It is noteworthy that most of the diagnostic nanoplatforms utilized in MI models can also be applicable or adaptable to MIRI contexts, in part, due to the shared biomarker profiles and pathophysiological mechanisms underlying ischemic cardiac events. Further, the inherent modularity of nanoplatforms provides a seamless bridge toward theranostics—wherein diagnostic and therapeutic functions are integrated into a single system. These approaches hold considerable promise for personalized management of myocardial injury as discussed in the following sections.

### 2.1. *In vitro* nanoscale biosensor

Earlier yet accurate detection of myocardial injury is central to an effective clinical intervention and prognosis. Of emerging diagnostic

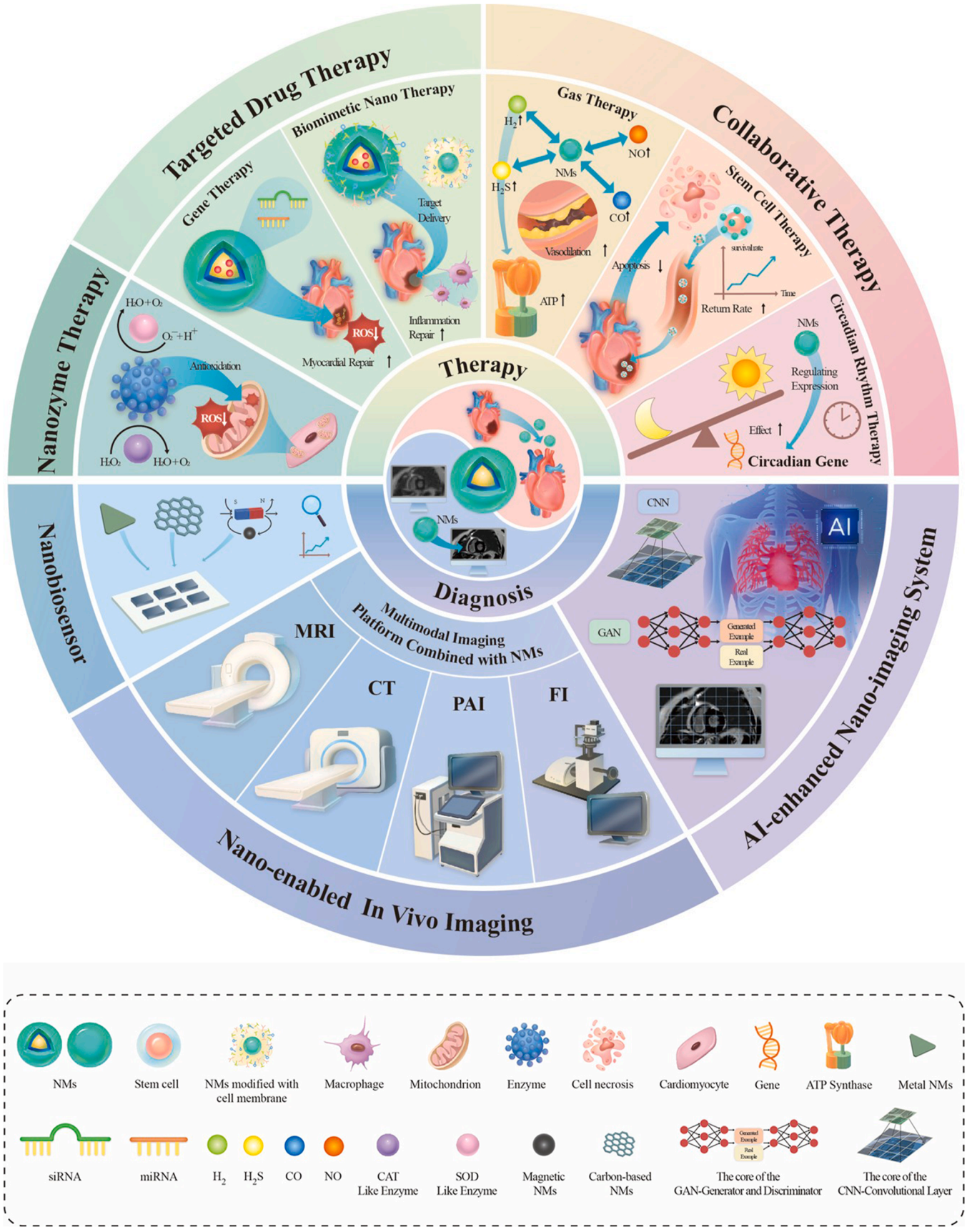


**Fig. 1.** An overview of multifunctional NMs for MIRI diagnosis and treatment.

strategies, *in vitro* nanoscale biosensors have garnered increasing attention due to their high sensitivity, rapid response, and adaptability to the point-of-care settings. These platforms, often integrating NMs (i.e., noble metal NPs, carbon-based nanostructures, two-dimensional (2D) materials, etc.) exhibit high surface area-to-volume, enhanced electron mobility, and tunable biocompatibility [46,49,50]. These characteristics enable ultrasensitive detection of trace-level cardiac biomarkers, including Cardiac Troponin I (cTnI), Cardiac Troponin T (cTnT), Creatine Kinase-Myocardial B (CK-MB), and myoglobin [51–53]. Unlike conventional immunoassays or clinical biochemistry techniques, nano-biosensors offer unique advantage of real-time, multiplexed, and miniaturized detection systems, and they can be additionally tailored for an early-stage diagnosis as well as continuous monitoring [54,55]. Further, by engineering nanointerfaces for selective molecular recognition, these sensors can achieve high specificity even in complex biological milieu (e.g., serum, whole blood, etc.) [56]. The integration of electrochemical, optical, or piezoelectric transduction mechanisms further broadens the diagnostic efficacy of nano-biosensors. In this section, we will highlight contemporary advances in the design and application of *in vitro* nano-biosensors for myocardial injury, with particular emphasis on the role of NMs in improving the analytical performance of biosensors. To illustrate the translational prospect of these platforms in cardiovascular diagnostics, we will describe the representative sensing strategies, detection principles, and signal amplification methods.

Among various nano-biosensor platforms, electrochemical strategies

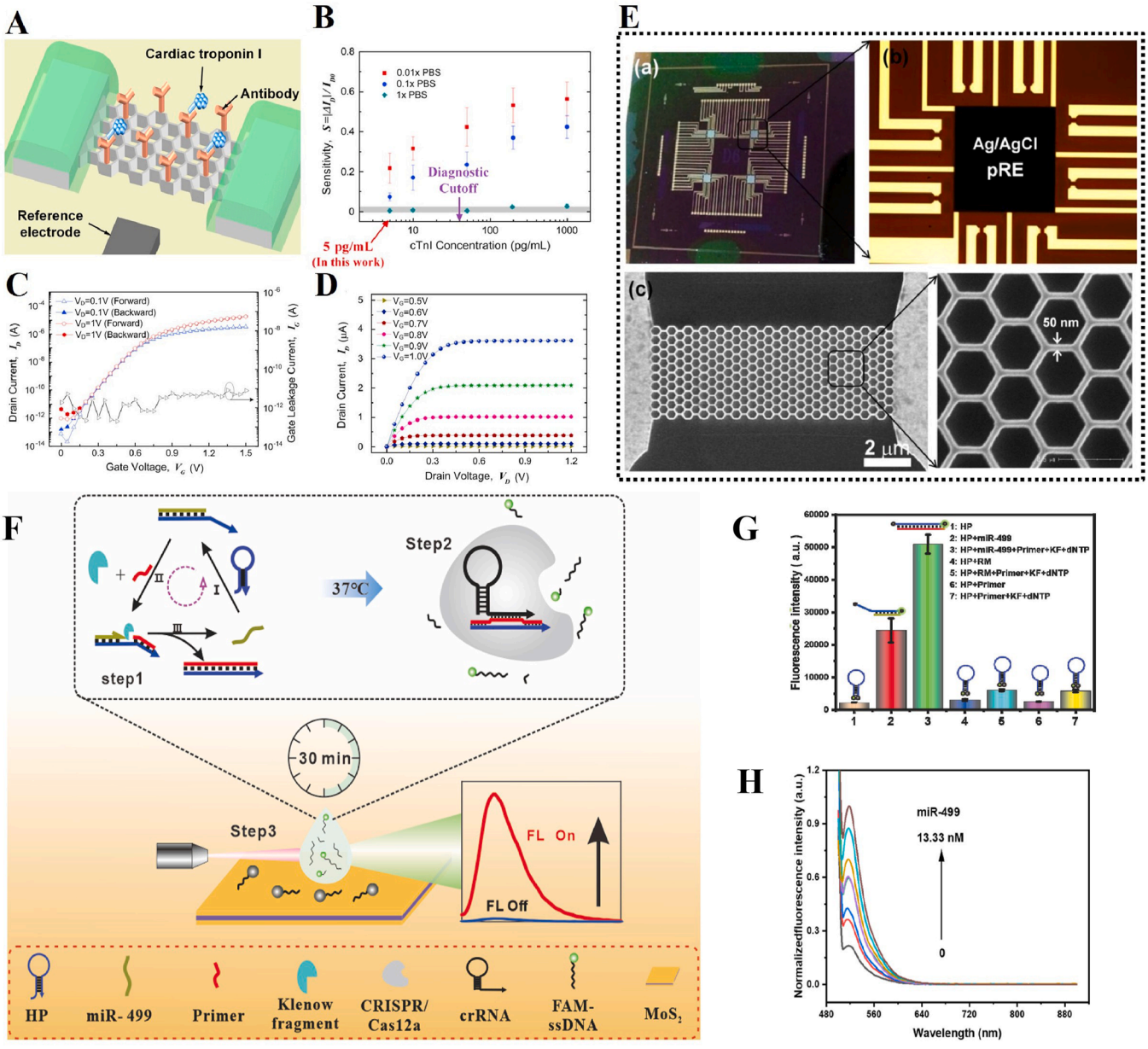


**Fig. 2.** Sensing architectures and performance for cardiac biomarker detection. (A) Schematic diagram of SiNW-FET biosensor functionalized with anti-cTnI antibodies for label-free detection. (B) Sensor's response to cTnI under varying phosphate buffered saline (PBS) conditions, highlighting improved sensitivity in low-ionic-strength buffers; LOD: 5 pg/mL. (C) Log-scale transfer curves (ID–VG and IG–VG) of the fabricated devices. (D) Output characteristics (ID–VD) of HCNW-FETs. (E) Device characterization: (a) Optical image of HCNW-FET chip with 32 sensors; (b) On-chip Ag/AgCl pseudo-reference electrode; (c) SEM image of 50 nm-wide honeycomb nanowire array. Reprinted with permission from Ref. [58]. (F) Schematic illustration of the dual-amplification strategy combining SDA, CRISPR/Cas12a, and $MoS_2$-based signal modulation. (G) Fluorescence signal comparison, demonstrating the enhanced amplification of the integrated SDA-Cas12a system. (H) Quantitative analysis: fluorescence spectra and corresponding calibration curve for miR-499 detection. Reprinted with permission from Ref. [62].

remain widely adopted, thanks to their high signal fidelity, simplicity, and compatibility with portable systems. For instance, the sensor developed by He et al. integrated porous metal-organic frameworks (MOFs) with conductive reduced graphene oxide (rGO), which provided a substantial electroactive surface area and facilitated efficient electron transfer [57]. The introduction of chitosan not only enhanced the stability of the sensing film but also significantly improved its capacity for the immobilization of specific antibodies against cTnI. This biosensor achieved a limit-of-detection (LOD) 0.008 ng/mL with a linear range of 0.01–50 ng/mL, demonstrating excellent specificity and reproducibility for cTnI detection in human serum samples, thereby underscoring its significant potential for application in complex biological matrices.

Similarly, an advanced yet highly sensitive strategy for cTnI detection utilized a honeycomb nanowire (HCNW) architecture-based silicon nanowire field-effect transistor (SiNW-FET) platform [58]. This periodic structure enhanced channel width and introduced multiple conduction pathways, enhancing both the sensing surface area and electrical performance. Anti-cTnI monoclonal antibodies were covalently immobilized on the NW surface, enabling selective capture of cTnI. Upon binding, negatively-charged cTnI molecules induce surface charge modulation and alter the carrier concentration in the channel. This change in conductance arises from a field-effect, where the local electric field generated by biomolecular interactions governs charge transport. This mechanism enables label-free, real-time, and highly specific detection of cTnI with enhanced sensitivity (Fig. 2A). The SiNW-FET achieves peak sensitivity in the sub-threshold regime (Fig. 2B), where even trace levels of cTnI result in pronounced current shifts. This enhanced sensing performance is primarily due to the reduced ionic strength of the surrounding environment, which weakens Debye screening effect; the latter refers to the tendency of ions in the solution to shield or “mask” electric charges on molecular surfaces. Under low-salt conditions, this shielding is minimized, allowing the electrical signals from surface-bound cTnI molecules to more directly influence the sensor's channel conductance. However, this reliance on low ionic strength may pose challenges for direct clinical application, as physiological fluids such as serum or whole blood typically exhibit high ionic strength (~150 mM), which can significantly attenuate sensor response due to enhanced Debye screening. Recent literature has emphasized this limitation, identifying it as a key bottleneck in the translational application of FET-based biosensors [59]. To circumvent this limitation, different types of strategies have been proposed, including the dilution or desalting of samples, as well as surface functionalization with polyethylene glycol (PEG)-based coatings or the application of short-chain affinity ligands (i.e., aptamers). These approaches can help minimize the effective Debye length and preserve sensing performance in complex matrices [60]. Moreover, buffer optimization studies suggest that intermediate ionic strengths (e.g., ~50 mM) may provide a practical compromise between biological compatibility and detection fidelity [61]. These approaches represent promising directions to enhance the clinical robustness of SiNW-FET biosensors. More importantly, the SiNW-FET enabled rapid (within 1 min), label-free detection using as little as 1 μL of sample, and achieved a remarkably low LOD (5 pg/mL)—well below the clinical threshold for diagnosing AMI (Fig. 2C). The conductance response curves further revealed a distinct dose-dependent behavior across a wide dynamic range (0.01–100 ng/mL), with optimal signal resolution under low ionic strength (0.01 × PBS) conditions due to reduced Debye screening (Fig. 2D). The physical implementation of the sensor was shown through a top-down view of the chip layout with multiple integrated FETs, an on-chip silver/silver chloride (Ag/AgCl) pseudo-reference electrode, and a scanning electron microscopy (SEM) image of the HCNW array composed of ~50 nm-wide individual NW (Fig. 2E). This design supports robust microfabrication, intense signal amplification, and seamless integration with microfluidic components. Collectively, the platform exhibited high sensitivity and selectivity, which was also validated using C-Reactive Protein (CRP) and Alpha-Fetoprotein (AFP) interference testing, illustrating its considerable promise for point-of-care cardiac (PoC) diagnostics.

In the context of MIRI, nucleic acid biosensors also represent a promising approach for early detection of miRNAs. Li et al. developed a sensitive biosensor by integrating CRISPR/Cas12a (clustered regularly interspaced short palindromic repeats (CRISPR)/CRISPR-associated protein 12a) with molybdenum disulfide ($MoS_2$) nanosheets for the detection of miR-499, a cardiac-specific microRNA relevant to cardiac injury [62]. This system employs a dual-amplification strategy: the miR-499 target first initiates strand displacement amplification (SDA) and generates numerous Protospacer adjacent motif (PAM)-containing double-stranded DNA amplicons, which subsequently activates the trans-cleavage activity of Cas12a to cleave fluorophore-labeled single--stranded DNA reporters. $MoS_2$ nanosheets act as efficient fluorescence quenchers, suppressing the background noise *via* pi-pi (π–π) stacking (Fig. 2F). Upon Cas12a activation, short DNA fragments are released from the $MoS_2$ surface, resulting in significant fluorescence recovery and enabling sensitive detection (Fig. 2G). The assay achieves a broad linear range (0.1–13.33 nM) and a low LOD of 381.78 pM within 30 min (Fig. 2H), demonstrating high specificity and reliable recovery in the human serum. This rapid, isothermal, and antibody-free method offers considerable potential for point-of-care diagnostics in MIRI.

Beyond extensively studied nano-biosensor modalities, a range of complementary strategies has emerged to enrich the diagnostic toolkit for myocardial injury. For instance, Shanmugam et al. developed a flexible electrochemical sensing array based on gold/zinc oxide (Au/ZnO) nanostructured electrodes that enabled the simultaneous detection of cTnI, cTnT, and myoglobin (Mb) with high specificity and minimal signal interference partly due to the uniform electrical performance across multiplexed sensor arrays and distinct antibody functionalization. The platform achieved LOD as low as 1 pg/mL for each biomarker, with negligible cross-reactivity and consistent baseline impedance between sensor elements [63]. Similarly, Liu et al. reported an indium oxide ($In_2O_3$) nanoribbon-based FET biosensor fabricated *via* shadow mask lithography, which enabled rapid and ultrasensitive detection of cTnI and B-type natriuretic peptide (BNP) (LOD: 0.24 pg/mL; response time <1 min) [64]. For optical sensing, Yola et al. constructed a fluorescence sensor incorporating boron nitride (BN) quantum dots embedded within a molecularly imprinted polymer matrix, achieving high selectivity, reusability, and an LOD of 3 pg/mL [65]. Collectively, these approaches demonstrate the versatility of NM-enabled platforms, which range from electrochemical and field-effect to optical systems, in improving sensitivity, multiplexing, and assay speed. Despite considerable promise of NM-based biosensors, challenges such as NMs reproducibility, signal drift in complex biological samples, and poor integration with clinical workflows continue to impede the translation. Therefore, alternative approaches, such as scalable NMs synthesis, surface stabilization, and system-level integration may help circumvent these limitations and help realize the clinical potential of nano-biosensors in PoC cardiovascular diagnostics.

### 2.2. NM-mediated diagnostic imaging of MIRI

Nano-enabled imaging constitutes a cornerstone in the precise diagnosis of MIRI. Leveraging their intrinsic physicochemical properties, such as tunable size and high surface area-to-volume ratio, NMs serve as versatile scaffolds for engineering high performance contrast agents and probes across different types of imaging modalities including CT, FI, PAI, and MRI [66,67]. A pivotal advancement lies in the active targeting capability of nano-enabled sensors conferred through the conjugation of NMs with ligands specific to MIRI biomarkers (e.g., cTnTs, ROS) [68]. These nano-enabled sensors may not only help achieve high-contrast imaging of injured myocardium but they may also enable the detection of molecular-level alterations preceding structural damage. Moreover, the inherent modularity of NMs may provide a direct pathway toward integrated theranostics, where diagnostic imaging and targeted therapy are unified within a single platform [69]. In this

section, the specific implementations of nano-enabled platforms for CT, FI, PAI, MRI, and multimodal imaging are systematically summarized. Additionally, a comparative overview of representative NM-based platforms and their key performance metrics, such as spatial resolution and targeting specificity, across all imaging modalities is provided in Table 1.

### 2.2.1. NMs for enhanced CT imaging

CT, such as coronary CT angiography (CTA), is routinely used in clinical cardiology to non-invasively visualize coronary anatomy and assess vascular patency. Owing to its excellent anatomical resolution and rapid acquisition speed, CT plays an important role in diagnosing ischemic heart disease and evaluating myocardial injury [83–85]. While traditional CT contrast agents, e.g., iodinated compounds offer good short-term enhancement, they face challenges including the lack specificity, rapid clearance from the circulation, and risk of nephrotoxicity, which restrict their utility for targeted or prolonged cardiac imaging [86,87]. In contrast, NM-based imaging agents, particularly gold NPs (AuNPs) may offer both improved imaging quality as well as enhanced contrast intensity. Most importantly, owing to a facile functionalization method, Au NPs enable targeted labeling of specific ligands, which can additionally facilitate the recognition of NPs by specific cell types or pathological tissues within the heart, thus improving imaging specificity and reducing systemic toxicity [88].

Accurate longitudinal tracking of macrophages (MΦs) in myocardial injury has long been hampered by a central mechanistic challenge: NPs leakage from labeled cells and undesired re-uptake by endogenous phagocytes, which obscures whether imaging signals truly reflect MΦs infiltration or merely redistributed particles. To address this issue, researchers have developed a glucose-modified, zwitterion-anchored gold NPs system (AuNPs-zwit-glucose) that integrates two design elements: (1) Glucose transporter (GLUT)-1–mediated endocytosis through surface glucose capping (Fig. 3A), and (2) lysosomal de-glycosylation that leaves a zwitterionic-only shell, effectively preventing secondary uptake after initial release (Fig. 3B) [89]. This structure enables rapid yet efficient MΦs labeling within 4 h without impairing cell viability or cytokine secretion. Functionally, labeled MΦs display strong and dose-dependent CT attenuation, with Hounsfield Units scaling linearly with both extracellular labeling concentration and intracellular gold content (Fig. 3C–F). In a mouse MI model, this nanoplatform enables non-invasive CT visualization of MΦs infiltration into infarcted myocardium, where signal intensity was progressively increased from day 4 to day 9 post-injection (Fig. 3G). Moreover, zwitterionic surface coatings can significantly reduce non-specific protein adsorption and NPs aggregation, thereby enhancing colloidal stability and extending systemic circulation time [90]. These properties contribute to the sustained intracellular retention of AuNPs within MΦs and reduce signal loss due to extracellular leakage or redistribution. However, the tracking stability of AuNPs-zwit-glucose beyond 9 days yet remains to be deciphered. Since NPs–biomembrane interactions, intracellular fate, and immune-mediated clearance can vary substantially across biological systems [91], it is imperative to study long-term (>14 days) biodistribution, degradation behavior, and batch-to-batch reproducibility of AuNPs-zwit-glucose to fully validate this platform for longitudinal MIRI imaging.

Owing to the high spatial and temporal resolution of CT, a major challenge in regenerative imaging remains effective *in vivo* tracking of therapeutic agents at the cellular and subcellular levels. To circumvent this limitation, extracellular vesicles (EVs) — particularly exosomes have emerged as promising natural nanocarriers due to their ability to modulate inflammatory responses, enhance angiogenesis, and facilitate tissue repair in injured myocardium [92]. Nonetheless, poor electron density and nanoscale size (30–100 nm) of EVs impede direct visualization with conventional CT imaging. Gong et al. employed glucose-labeled AuNPs for modification of mesenchymal stromal cells (MSC)-derived exosomes (MSC-Exo) (Fig. 3H) [71]. The modification of NPs with glucose increased their uptake through GLUT-1–mediated transport, ensuring minimal disruption to membrane integrity and avoiding vesicle aggregation. Upon intramyocardial injection into a mouse model of MI, micro-CT imaging at 4 h post-injection revealed a distinct radiopaque signal confined to the infarcted myocardium (Fig. 3I), indicating efficient retention of gold NPs (GNP)-labeled MSC-Exo in the infarcted myocardium. The signal was sustained and was additionally expanded at 24 h (Fig. 3J), with minimal off-target distribution in other organs, *i.e.,* liver, spleen, and kidney. This non-invasive imaging platform may enable real-time, high-resolution tracking of exosomal therapeutics *in vivo*, thereby offering valuable insight into the biodistribution and retention of NPs *in vivo*, which may also have implications for the development of exosome-based personalized therapies for cardiac tissue repair.

Therefore, the integration of AuNP-based CT molecular imaging enables precise and quantitative tracking across multiple biological scales—from inflammatory cells such as MΦs to EVs like exosomes. This strategy not only enhances imaging sensitivity and temporal resolution but also provides critical mechanistic insights into the dynamic processes of cell migration and therapeutic agent distribution during myocardial repair.

### 2.2.2. NMs for enhanced FI

FI, with its real-time and high-resolution advantages, has demonstrated significant value in clinical diagnosis as well as treatment of ischemic heart disease. While FI may not match the spatial resolution or tissue penetration of modalities, such as CT or MRI, the safety profile of FI makes it a suitable modality for long-term or live-cell tracking studies [93]. Furthermore, the development of fluorescent molecular probes, which can specifically bind to myocardial injury markers may provide additional information for the detection and spatial localization of damaged myocardium, facilitating the early diagnosis and assessment of myocardial injury [94].

Recent advancements in NM-based imaging have provided valuable insights into oxidative stress during MIRI. Luo et al. developed a near-infrared (NIR) light-activated dual-responsive nanoprobe for the simultaneous and controllable detection of hydrogen polysulfide ($H_2S_n$) and sulfur dioxide ($SO_2$) in MIRI models (Fig. 4A) [95]. The probe exhibited high sensitivity for $SO_2$, with a linear detection range of 0.1–50 μM and a detection limit of 0.24 μM (Fig. 4B). In HeLa cells, the probe quantitatively tracked endogenous $SO_2$ and $H_2S_2$ levels under metabolic modulation, showing distinct fluorescence responses (Fig. 4C). In an H9C2 CMs model of MIRI, the probe revealed a significant upregulation of both species, which was markedly attenuated by the ferroptosis inhibitor Fer-1 (Fig. 4D). Consistent with cellular findings, *in vivo* fluorescence quantification in mouse cardiac tissues confirmed elevated signals in I/R-injured myocardium; the intensity was increased approximately by 32 % compared to controls, and partial recovery upon Fer-1 treatment (Fig. 4E). This NIR-light-activatable nanoprobe enables quantitative, spatiotemporally resolved monitoring of redox dynamics during reperfusion, thereby offering a promising tool for the elucidation of oxidative stress in MIRI. Similarly, Zhang et al. developed a NIR ratiometric nanoprobe for real-time monitoring of $ONOO^-$ during myocardial reperfusion (Fig. 4F) [96]. The probe demonstrated high sensitivity with a detection limit of 0.085 μM (Fig. 4G). In a rat MIRI model, it quantitatively revealed that antioxidant drugs delivered *via* the nanoprobe effectively suppressed $ONOO^-$ burst during reperfusion (Fig. 4H). When administered as free drugs to account for pharmacokinetics, the probe further showed that drug half-life critically determined *in vivo* efficacy, with atorvastatin and resveratrol exhibiting sustained antioxidative effects, unlike carvedilol (Fig. 4I). This work highlights the utility of NIR nanoprobes for real-time evaluation of antioxidative therapies and the importance of pharmacokinetics in MIRI treatment.

A major limitation of FI is its restricted tissue penetration. Upconversion NMs (UCNMs) address this by converting NIR light into visible

**Table 1**
Summary of functional NMs for MIRI imaging.

| Category | Name | Spatial Resolution | Signal Intensity | Contrast Persistence | Target Specificity | Ref. |
|---|---|---|---|---|---|---|
| **NMs for enhanced CT imaging** | CNA35-AuNPs | Molecular imaging at ~0.3 mm resolution enables precise scar delineation in thick myocardial walls (1–2 mm) | Significantly increased, myocardial scar regions reached up to ~220 HU at 6 h post-injection | Prolonged intravascular enhancement (142–160 HU) sustained up to 6 h | High specificity to collagen in myocardial scar tissue; minimal off-target signal | [70] |
| | Gold NPs-labeled exosomes | Nominal resolution of 7.5 μm with micro-CT scanner | Gold NPs detected at 4 h and expanded by 24 h post-injection | Exosomes retained in the myocardium for up to 24 h, with limited distribution in other organs | High MI retention; minimal off-target accumulation in liver/spleen/kidney | [71] |
| | AuNPs-zwit-glucose | / | Strong CT signal at 6 h, sustained up to 24 h in infarct area | Longer blood circulation and selective accumulation in infarct MΦs | Signal mainly in infarct zone, minimal in liver/spleen/lung | [72] |
| **NMs for enhanced FI** | Yb/Tm/GZO@$SiO_2$ | Confocal imaging at 50 μm scale | NIR (830 nm) emission intensity ↑ ~12 × vs. uncoated UCNPs (upconversion NPs) | ≥7 days retention in myocardium post-injection of 6 mg/kg | Fl localized in myocardial tissue, minimal off-target signals | [73] |
| | DPNPs | / | Bright FL under confocal imaging; stable signal *in vitro* | Maintained signal during cellular uptake and imaging (up to 24 h) | Selective accumulation in HeLa cells, low background signal | [74] |
| **NMs for enhanced MRI** | Fluorescent iron oxide NPs | In-plane resolution: 100 × 100 μm; slice thickness: 0.5 mm | T2 hypointensity* in infarct zones due to labeled monocyte infiltration | Imaging performed 24 h post-injection, signal present in infarct region | Accumulation of labeled monocytes/MΦs in infarct area | [75] |
| | GCD-PEG-QK | / | Significant T2-weighted hypointensity in infarct area at 24 h post-injection | Signal detectable at 24 h, correlating with VEGFR targeting and accumulation | Selective binding to VEGFR overexpressed in infarct myocardium | [76] |
| **NMs for enhanced PAI** | CREKA-ICG-LIP NPs | System resolution: ~300 μm | PA signal in infarct region ↑ 3.2 × vs. control at 3 h post-injection | Enhanced signal maintained from 0.5 h to 6 h, peaking at ~3 h | Selective fibrin binding in infarcted myocardium, minimal off-target signal | [77] |
| | AS-I/S NCs | / | NIR-II PA signal intensity ↑ 2.1 × in infarct area vs. control at 12 h post-injection | Signal detectable from 1 h to 24 h, peak at 12 h | Accumulation in infarct myocardium, minimal in liver/spleen | [78] |
| | OPN@PFP-DiR NPs | / | PA signal ↑ 3.4 × in fibrotic myocardium vs. control at 8 h post-injection | Signal maintained from 1 h to 24 h, with peak at 8 h | Selective binding to osteopontin in fibrotic regions | [79] |
| | HI@PSeP-IMTP | PACT: Organ/Tissue level; FI: Cellular level | NIR signal increase of ≈32 %; PA signal increase of ≈40 % in MIRI region | Peak signal intensity at 8 h post-injection, providing a multi-hour imaging window | Selective accumulation in ischemic myocardium *via* IMTP-cTnI interaction, with minimal off-target retention in major organs | [69] |
| **NMs for enhanced multimodal imaging** | IMTP-$Fe_3O_4$-PFH NPs | MRI: In-plane 156 μm; FI: Cellular level (ex vivo histology) | MRI T1 signal ↑ 23.6 % at 4 h, persists to 24 h; NIRF: Strong signal at infarct zone at 4 h; FI: Clear ex vivo signal in infarct myocardium | All modalities showed stable enhancement from 1 h to 24 h, peak at 4 h | Specific fibrin binding in infarcted myocardium with minimal off-target signal | [80] |
| | CNA35-GNR/PFP@NPs | MRI: In-plane 140 μm; slice thickness 0.7 mm; PAI: ~300 μm | MRI T1 signal ↑ 27.3 % in fibrotic myocardium at 6 h; PAI signal ↑ 3.1 × at 6 h; NIRF signal localized and bright at fibrosis site | All modalities show enhancement from 1 h to 24 h, peak around 6 h | Selective binding to type I collagen in fibrotic myocardium, minimal off-target accumulation | [81] |
| | SCIO-ICG-CRT-CPPs NPs | MPI: ~1 mm voxel size; MRI: In-plane 140 μm | MPI signal in infarct zone ↑ 3.5 × vs. baseline at 6 h; MRI T2* signal ↓ due to iron accumulation; FI: Strong NIR signal in I/R myocardium | MPI and FI signals persisted from 1 h to 24 h, peak at 6 h | Specific to ferroptosis-associated iron overload in ischemia-reperfusion myocardium | [82] |

**Note**: **NMs**, nanomaterials; **HU**, Hounsfield units; **NIR**, near-infrared light; **MI**, myocardial infarction; **FI**, fluorescence imaging; **CT**, computed tomography; **CNA35**, a peptide for targeting collagen fibers; **AuNPs-zwit-glucose**, AuNPs-zwitterionic-glucose; **Yb/Tm/GZO@$SiO_2$**, Yb/Tm/Ga-doped ZnO@$SiO_2$; **DPNPs**, Boc-Tyr-Trp dipeptide-based NPs.

**PA**, photoacoustic imaging; **VEGFR**, vascular endothelial growth factor receptor; **NIR-II**, second near-infrared window; "**↑ 2.1 ×** " indicates that the NIR-II PA signal intensity in the infarct area was 2.1 times higher than that in the control area at 12 h post-injection; **GCD-PEG-QK**, Gadolinium-doped carbon dots conjugated with polyethylene glycol and QK peptide; **CREKA-ICG-LIP NPs**, Cysteine-arginine-glutamic acid-lysine-alanine-conjugated indocyanine green-loaded lipid NPs; **AS-I/S NCs**, Au–Se core–shell nanocomposites modified with ischemic myocardium-targeting peptide and mitochondria-targeted antioxidant peptide; **OPN@PFP-DiR NPs**, Osteopontin-targeted, perfluoropentane/DiR co-loaded PLGA NPs.

**IMTP**, ischemic myocardium-targeting peptide; **cTnI**, cardiac troponin I; **NIRF**, near-infrared fluorescence; **MPI**, magnetic particle imaging; **MRI**, magnetic resonance imaging; **PACT**, photoacoustic computed tomography; **CNA35-GNR/PFP@NPs**, a peptide for targeting collagen fibers-modified Au NPs/perfluoropentane lipid NPs; **SCIO-ICG-CRT-CPPs NPs**, the NPs which are consisting of superparamagnetic cubic iron oxide nanoparticles (SCIO NPs) conjugated with indocyanine green (ICG), TfR1-targeting peptides (CRT), and cell-penetrating peptides (CPPs); **IMTP-$Fe_3O_4$-PFH NPs**, ischemic myocardium-targeted peptide–$Fe_3O_4$–perfluorohexane NPs; **HI@PSeP-IMTP**, Hesperadin and ICG assembled in PLGA-Se-Se-PEG-IMTP.

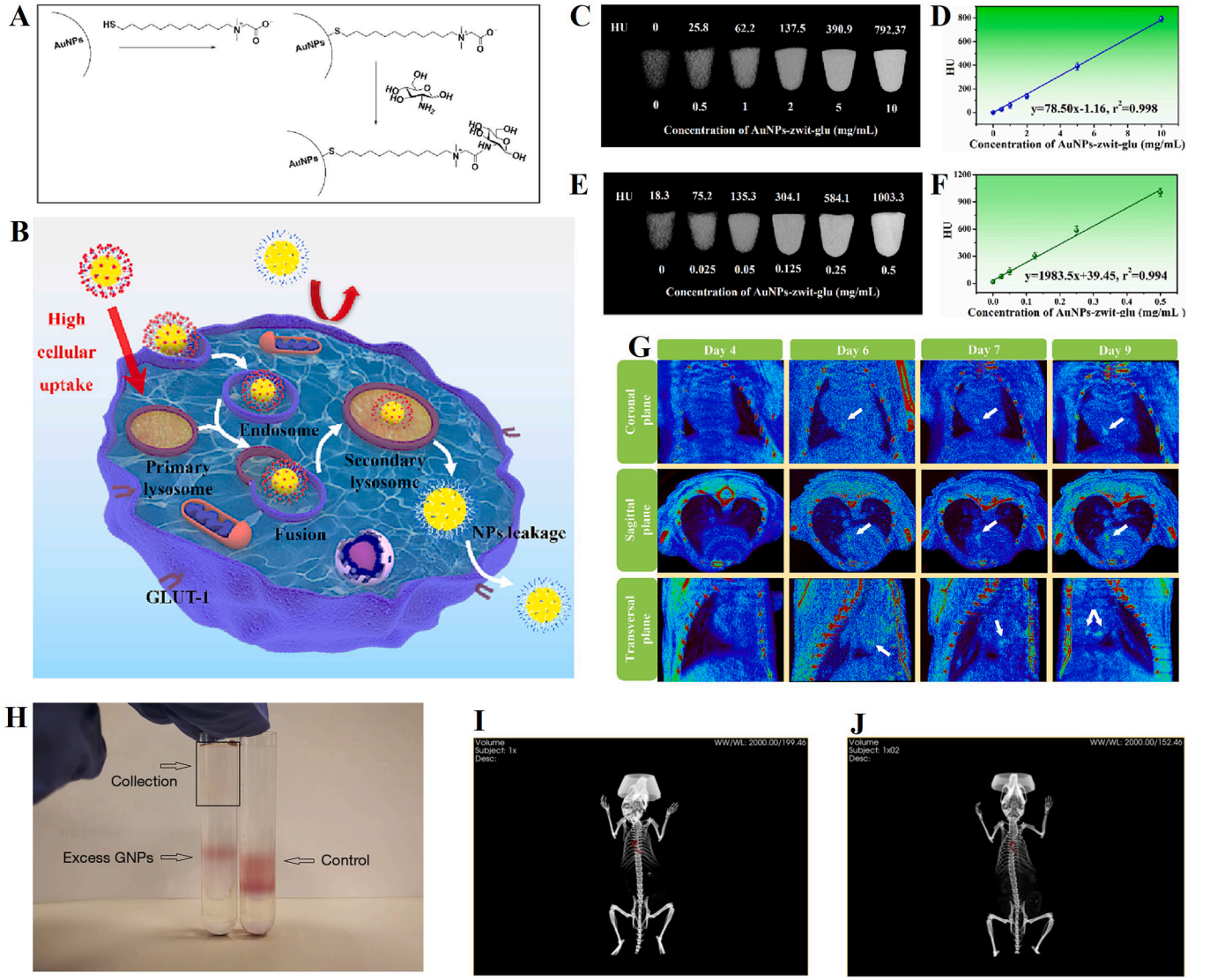


**Fig. 3. Gold NPs-assisted CT imaging of cell and exosome distribution in infarcted myocardium.** (A) Schematic diagram for the synthesis of AuNPs-zwit-glucose *via* surface hydrolysis. (B) Proposed uptake mechanism of NPs in MΦs, involving intracellular hydrolysis and exposure of the zwitterionic surface. (C, D) *In vitro* CT imaging of AuNPs-zwit-glucose: (C) CT images at varying concentrations; (D) linear correlation between Hounsfield units (HU) and concentration of NPs. (E, F) CT imaging of MΦs labeled with AuNPs-zwit-glucose: (E) CT images of cell pellets at increasing NPs concentrations; (F) corresponding linear increase in HU values. (G) *In vivo* CT imaging shows progressive signal enhancement in infarcted myocardium at day 4, 6, 7, and 9 after injection of AuNP-labeled MΦs (white arrows). Reprinted with permission from Ref. [89]. (H) GNP-labeled exosomes separated from free NPs via density gradient ultracentrifugation (exosome sample vs. GNP-only control). (I, J) Micro-CT at 4 h (I) and 24 h (J) post-injection shows sustained cardiac retention of GNP-labeled MSC-Exo in the infarcted heart with minimal off-target distribution. Reprinted with permission from Ref. [71].

emission. Li et al. developed core–shell nanostructures composed of a silica-coated, gallium-doped ZnO core and an ytterbium (Yb)-enriched shell, which significantly improved light absorption and energy-transfer efficiency [73]. Under NIR illumination, these NPs produced bright red fluorescence in the myocardium, with detectable signals persisting for up to 7 days post-injection, highlighting their potential for longitudinal *in-vivo* imaging.

Besides UCNMs, alternative FI strategies have emerged through innovative NMs design. Sivagnanam et al. reported zinc-coordinated tyrosine-tryptophan (Tyr-Trp) dipeptide NPs, which displayed strong fluorescence in the visible light range [74]. These peptide-based NMs combine excellent photostability with physiological compatibility, maintaining stable emission across a broad pH range and at temperatures for up to 75 °C. The resistance of these peptide-based NMs to photobleaching enables real-time tracking of cellular processes within the dynamic cardiac microenvironment. Fluorescent NMs have also been leveraged for molecular diagnostics of cardiac injury. For instance, Anju et al. engineered antibody-functionalized gold nanoclusters as a highly sensitive fluorescence immunosensor for cTnI detection [97]. This system exploits the unique fluorescence of gold nanoclusters alongside a quenching-recovery mechanism, allowing precise biomarker quantification. These NM-based immunosensors meet the pressing clinical need for rapid and accurate cardiac biomarker detection.

These collective advances in fluorescent NMs technology have appreciably widened the capability of myocardial imaging and diagnostics. By improving signal stability, extending imaging duration, and increasing detection sensitivity, fluorescent materials may help overcome limitations associated with cardiac FI. Moreover, these NMs can also be integrated with existing imaging modalities, which can provide a more comprehensive assessment of myocardial injury as well as repair processes, potentially transforming both research and clinical practice in cardiovascular medicine. Future developments in this field

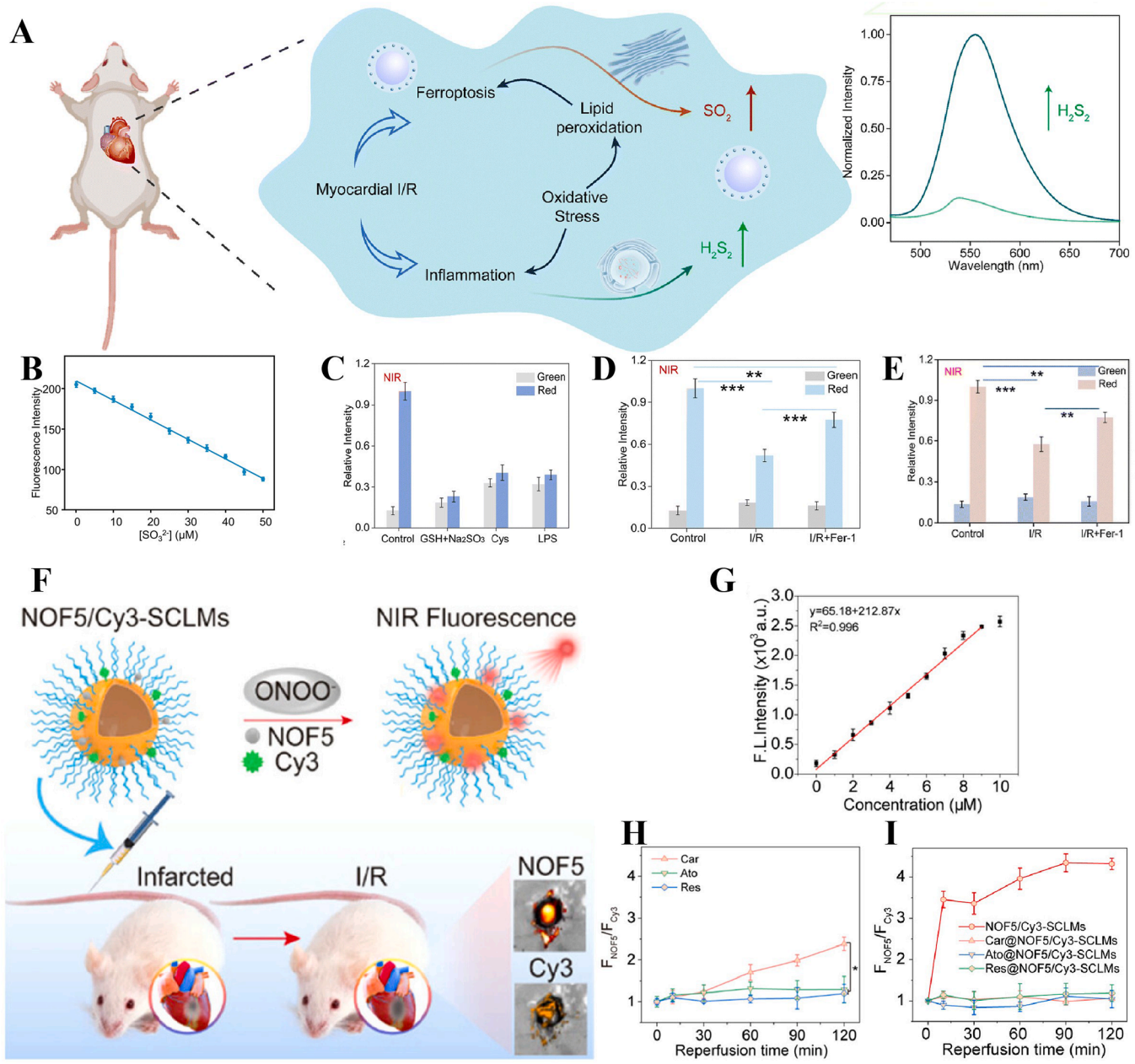


**Fig. 4. Real-time monitoring of biochemical processes in MIRI using NIR nanoprobes.** (A) Design of a NIR-light-activated nanoprobe for simultaneous detection of $H_2S_n$ and $SO_2$ in MIRI. (B) Linear fluorescence response of the probe to $SO_2$ ($Na_2SO_3$), showing high sensitivity. (C) Endogenous $SO_2/H_2S_2$ levels in HeLa cells under metabolic stimulation (Cys, GSH + $Na_2S_2O_3$, LPS). (D) Fluorescence intensity changes in H9C2 cells during I/R injury and after Fer-1 treatment. (E) *In vivo* fluorescence quantification in mouse hearts showing elevated $SO_2/H_2S_2$ in I/R and recovery with Fer-1. Reprinted with permission from Ref. [95]. (F) Schematic of a ratiometric nanoprobe for real-time $ONOO^-$ imaging and drug evaluation in I/R hearts. (G) Linear detection of $ONOO^-$ with a limit of 0.085 μM. (H) Time-course fluorescence ratio ($F_{NOF5}/F_{Cy3}$) in rat hearts after treatment with antioxidant-loaded nanoprobes. (I) Pharmacokinetic influence on drug efficacy revealed by fluorescence ratio after free drug administration. Reprinted with permission from Ref. [96].

may focus on further improving tissue penetration depth and developing multifunctional probes capable of simultaneous imaging and therapeutic delivery.

### 2.2.3. NMs for enhanced PAI

PAI is a novel multimodal imaging technique that combines optical contrast with ultrasound (US) penetration depth, demonstrating unique advantages for precise diagnosis and treatment of ischemic heart disease [98]. In recent years, the introduction of NMs has brought revolutionary breakthroughs to this technology. Nanoprobes, with their tunable optical properties, excellent biocompatibility, and active targeting capabilities, have significantly enhanced the imaging sensitivity and specificity of PAI [99,100]. Zhang et al. developed a fibronectin-targeted NPs system to enhance PAI for the non-invasive detection of ischemia injured area [77]. The NPs incorporate indocyanine green (ICG), which exhibits strong absorption in the NIR region. The NPs effectively encapsulate and protect ICG from degradation, thereby extending its circulation time *in vivo* and enhancing PAI performance. Using a MIRI model, the NPs demonstrated targeted accumulation in the ischemia injured area as well as diagnosis with a PA signal. In addition, these NPs were surface-functionalized with fibronectin-targeting pentapeptide sequence, e.g., cysteine-arginine-glutamic acid-lysine-alanine (CREKA), which enabled specific binding to fibronectin-rich tissues in the myocardial ischemia area. Fibronectin, an extracellular matrix (ECM)

protein is expressed following myocardial injury and plays a pivotal role in cardiac repair by enhancing vascular permeability as well as facilitating the migration of fibroblasts.

A recently developed theranostic nanoprobe, designated HI@PSeP-IMTP, integrates targeting, self-reporting, and combination therapy for MIRI (Fig. 5A and B) [69]. The nanoprobe was constructed from a ROS-responsive polymer core crosslinked *via* diselenide bonds and conjugated with an ischemic myocardium-targeting peptide (IMTP). The core is co-loaded with the CaMKIIδ inhibitor hesperadin (a therapeutic agent) and the NIR dye indocyanine green (ICG). Fig. 5B depicts its functional mechanism: upon accumulation in the ischemic heart, local ROS trigger the release of ICG and hesperadin, enabling real-time dual-modal imaging (NIR and PAI) of the injury site. Therapeutically, hesperadin inhibits inflammatory signaling while the diselenide bonds scavenge ROS, synergistically reducing oxidative stress and inflammation. This approach significantly reduced key inflammatory markers and improved cardiac function, demonstrating a targeted, self-monitoring nanoplatform for MIRI theranostics. This contemporary work aligns with and extends earlier foundational research focused on nanoplatforms with integrated antioxidative properties. Sun et al. designed a theranostic nanoplatform based on gold–selenium core–shell nanocomposites (AS-I/S NCs) for the treatment of MIRI [78]. The system consists of gold nanorods coated with a selenium nanoshell and further functionalized with an IMTP and a mitochondria-targeted antioxidant peptide (SS31), enabling precision targeting and synergistic antioxidant activity (Fig. 5C). *In vitro,* AS- I/S NCs demonstrated potent free radical scavenging capacity, as confirmed by standard radical scavenging assays (Fig. 5D). In a rat MIRI model, intravenous administration of AS-I/S NCs significantly restored cardiac function, evidenced by a marked recovery of the ejection fraction (EF) (Fig. 5E). These findings indicate that AS-I/S NCs represent an integrated nanotheranostic platform that combines targeted delivery, antioxidant protection, and functional cardiac recovery for MIRI therapy.

Notably, while AS-I/S NCs exhibit strong NIR-II absorption, the intrinsic attenuation of PA signals across myocardial depth remains an important factor influencing full-thickness MIRI assessment. Existing PAI studies have shown that PA signal intensity may progressively decrease from the epicardial surface toward the endocardial layer due to wavelength-dependent optical scattering and acoustic attenuation in dense cardiac tissue [101]. For instance, fibrin-targeted or ICG-liposome PA probes demonstrated sufficient contrast to delineate infarcted myocardium, yet their detectability and signal-to-noise ratio were noticeably reduced in deeper myocardial regions, reflecting a depth-related attenuation trend [102]. Therefore, while AS-I/S NCs may offer superior optical absorption and enhanced PAI performance, further investigations quantifying PA signal distribution at different myocardial depths would be crucial to confirm their suitability for full-thickness MIRI detection.

Herein, the discussed literature demonstrates the capability of NM-based strategies to significantly enhance PAI for myocardial injury assessment by overcoming its intrinsic limitations. By integrating molecular targeting units (e.g., fibronectin-binding or ischemic homing peptides), these nano-agents can improve the accumulation at diseased sites, thereby enhancing signal-to-noise ratio and enabling the detection of earlier and subtler pathological changes. Besides, the incorporation of contrast agents with high absorption in the NIR window, especially NIR-II, substantially augments the penetration depth and spatial resolution of PAI, addressing one of the major constraints of conventional optical imaging. Co-delivery of multiple therapeutic components, including anti-oxidative compounds may help the nanoprobe to not only visualize but also mitigate oxidative stress, thereby showcasing a theranostic approach from mere diagnosis. Collectively, these nanoscale designs effectively leverage the high sensitivity and functional imaging capacity of PAI while compensating for its limitations in depth penetration and biological specificity, offering a robust and multifunctional tool for the precise detection and management of MIRI.

#### 2.2.4. NMs for enhanced MRI

MRI is a non-invasive imaging modality that utilizes strong magnetic fields and radiofrequency pulses to generate high-resolution anatomical images. Compared to conventional techniques such as X-ray or CT, MRI offers superior soft tissue contrast and is particularly advantageous for imaging organs such as the brain, spinal cord, joints, and heart [103–105].

Superparamagnetic iron oxide NPs (SPIONs) have emerged as effective MRI contrast agents due to their strong influence on T2 (Transverse relaxation time) and T2* (effective Transverse relaxation time). Montet-Abou et al. demonstrated that intravenously injected fluorescently labeled SPIONs are rapidly cleared from circulation by the reticuloendothelial system (RES), particularly accumulating in monocytes (MCs) [75]. Following myocardial injury, these SPION-labeled MCs are passively recruited to the injury site, producing localized signal hypo-intensity in T2*-weighted MRI. Enhanced contrast is ascribed to the superparamagnetic nature of SPIONs, which induces local magnetic field inhomogeneity, accelerates dephasing of transverse magnetization, and shortens T2/T2* relaxation times. This manifests as darkened regions in MRI images corresponding to SPION-rich areas, thereby enabling the imaging of immune cell infiltration. Co-localization studies with $CD68^{+}$ MΦs further correlated MRI signal intensity with immune cell infiltration. This approach enables sensitive, non-invasive monitoring of immune responses *in vivo* without altering cell function, suggesting the potential translational applications of NPs for inflammation targeting and assessing therapeutic interventions in cardiovascular disease.

Gd is a widely used MRI contrast agent due to its strong paramagnetic properties, which facilitate proton relaxation and enhance signal intensity in T1-weighted imaging [106]. To improve targeting and biocompatibility of Gd, Li et al. designed a Gd-doped carbon dot nanoprobe conjugated with a vascular endothelial growth factor (VEGF) mimetic peptide, termed GCD-PEG-QK [76]. Briefly, $Gd^{3+}$ ions were encapsulated into the core of carbon dots, which can avoid the leakage of metal ions and reduce systemic toxicity. The QK peptide can interact with VEGF receptors, which are highly expressed in ischemic myocardial tissue, thereby helping to increase NP accumulation in the infarcted region. *In vivo* MRI confirmed that GCD-PEG-QK can significantly increase signal intensity in the infarcted myocardium compared to the free Gd-DTPA, especially within 30 min post-injection. The mapping of T1 relaxation time further showed enhanced signal intensity, in part, due to prolonged circulation and receptor-mediated retention in ischemic tissue. Unlike conventional Gd agents, this NP-based platform integrates imaging contrast, ischemic targeting, and therapeutic potential within a single system. The synergy of effective imaging and myocardial repair highlights the translational potential of nanoprobe for MRI-guided cardiovascular diagnostics and treatment.

Therefore, the incorporation of nanotechnology has markedly expanded the functional scope of MRI for MIRI treatment. Nano-scale contrast agents, including SPIONs and engineered gadolinium complexes can enhance imaging specificity through targeted accumulation while reduce toxicity risks associated with traditional agents. More importantly, these platforms may enable visualization of cellular-level processes in inflammation and integrate real-time imaging with therapeutic interventions, thereby elevating MRI from a diagnostic tool to a theranostic system. This evolution supports deeper mechanistic insight and personalized management of MIRI through multifunctional, longitudinal monitoring.

#### 2.2.5. NMs for enhanced multimodal imaging

The precise diagnosis of MIRI requires the integration of multidimensional pathological information, including anatomical structure (e.g., infarct size and cardiac morphology), functional parameters (e.g., ventricular motion and ejection fraction), and molecular or cellular dynamics (e.g., oxidative stress, inflammatory responses, and apoptosis) [107,108]. Since no single imaging modality can simultaneously

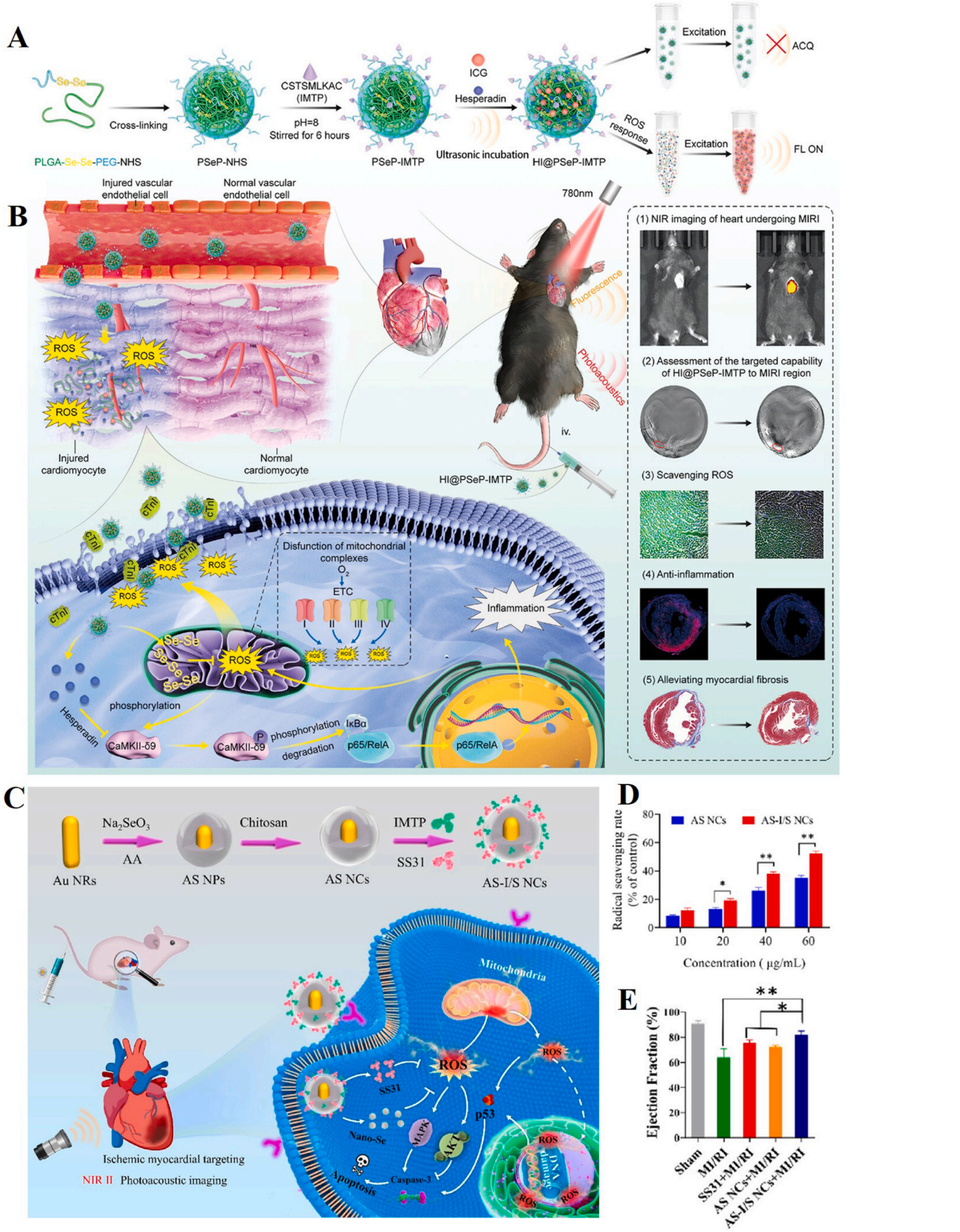


**Fig. 5. PAI-guided nanotheranostics for MIRI.** (A) Fabrication: conjugation of IMTP to a ROS-responsive PLGA-Se-Se-PEG polymer and co-loading of hesperadin (CaMKIIδ inhibitor) and ICG. (B) Function: targeted accumulation in MIRI region, ROS-triggered release, real-time dual-modal imaging (NIR/PA), and synergistic anti-inflammatory/antioxidant therapy. Reprinted with permission from Ref. [69]. (C) Schematic illustration of AS-I/S NCs structure and proposed mechanism for MIRI therapy. (D) *In vitro* antioxidant activity of AS-I/S NCs determined by ABTS radical scavenging assay. (E) Restoration of cardiac function (ejection fraction) in MI/RI rats after AS-I/S NCs treatment. Reprinted with permission from Ref. [78].

provide such a comprehensive diagnostic profile, the development of multimodal imaging strategies has become essential. Recent clinical data underscore the limitations of single-modality imaging and the growing need for integrated approaches. In myocardial infarction with nonobstructive coronary arteries, combining optical coherence tomography (OCT) with cardiac magnetic resonance (CMR) identified disease etiology in 84–100 % of cases, outperforming OCT alone (44 %) and CMR alone (74 %) [109,110]. Such findings illustrate that no single modality can fully capture the structural, functional, and tissue-level complexity of ischemic injury. Multimodal cardiovascular technologies, including hybrid PET/CT, PET/MRI, and echocardiography–MRI, further expand diagnostic capacity by integrating anatomical, metabolic, and hemodynamic data [111,112]. However, current multimodal systems remain limited by resolution mismatch, poor penetration, slow acquisition, and technical complexity [113]. Their low sensitivity to early molecular events also restricts timely diagnosis and monitoring [114].

NMs possess highly tunable surfaces and architectures that enable the co-loading or conjugation of diverse contrast agents onto a single platform [115,116]. This multifunctional capacity facilitates the convergence of complementary imaging signals and supports the spatially aligned acquisition of physiological and pathological information [117]. By leveraging the complementary advantages of various imaging techniques, such as high soft-tissue resolution of MRI, excellent temporal and spatial precision of CT, high sensitivity of FI, or optical–acoustic contrast of PAI, multimodal nanosystems offer a comprehensive and unified diagnostic profile. This unified approach enables clinicians to correlate structural changes with corresponding functional impairments and molecular-level disturbances, thereby significantly improving the accuracy and reliability of MIRI assessment. Furthermore, by incorporating targeting ligands that recognize specific biomolecular signatures of MIRI (e.g., ROS, adhesion molecules), NM-based multimodal platforms can further improve lesion-specific accumulation and contrast enhancement, thereby supporting earlier detection and more precise therapeutic monitoring [118].

Recent advances in NM-based contrast agents have further broadened the capability of multifunctional NMs for integrated diagnosis. Chen et al. developed ischemic myocardium-targeted peptide-conjugated SPIONs/perfluorohexane (PFH) NPs (IMTP-$Fe_3O_4$-PFH NPs) for targeted multimodal imaging of ischemic myocardium *via* integrating US imaging, PA, and MRI [80]. In this hybrid NP, SPIONs function as $T_2$-weighted MRI contrast agents and PA signal enhancers due to their superparamagnetic and optical absorption properties. PFH, encapsulated within the core, undergoes acoustic droplet vaporization under low-intensity focused US, generating microbubbles that enhance US contrast. Surface-conjugated IMTP peptides enable active targeting to hypoxic myocardial tissue, increasing local NP accumulation and improving imaging specificity. Together, these components synergistically enhance the sensitivity and accuracy of tri-modal imaging. In addition, Li et al. synthesized a collagen-targeting nanoprobe (CNA35-GP@NPs), consisting of Au NRs and PFH-loaded lipid NPs modified with CNA35 peptides (Fig. 6A) [81]. Au NRs enhanced NIR absorption and PA signal generation (Fig. 6B and C). Meanwhile, the high X-ray attenuation of Au led to stronger, concentration-dependent signal enhancement than iodine-based agents (Fig. 6D and E). In addition, PFH contributed to US contrast through LIFU-triggered phase transition. Building upon the aforementioned material design, it is anticipated that clinicians can readily utilize multiple imaging modalities to assess structural and functional alterations in lesions following the administration of these multifunctional NPs. Under the multimodal imaging framework established by Li et al., PAI is prioritized for quantitative evaluation of fibrosis given its collagen-specific targeting and strong histological correlation (Pearson r = 0.82). CT provides anatomical context and spatial localization, while US imaging enables real-time procedural guidance. Within this hierarchical integration, PAI acts as the definitive molecular readout, whereas CT and US imaging support anatomical correlation and reduce false positives, collectively enhancing diagnostic accuracy and reliability in detecting myocardial fibrosis. In another research, Yang et al. designed transferrin receptor-targeted cubic iron oxide NPs combining magnetic particle imaging (MPI) and MRI capabilities (Fig. 6F) [82]. The designed NPs exhibited a linear correlation between MPI signal intensity and infarct size as validated by triphenyltetrazolium chloride (TTC) staining. These NPs with multiple imaging capabilities can detect cardiac injury approximately 48 h earlier than that of the conventional imaging modalities, thereby offering significant diagnostic advantages for an earlier intervention. Overall, the aforementioned multimodal imaging nanoplatforms transcend the limitations of single-mode techniques by integrating complementary anatomical, functional, and molecular information, thereby offering an unprecedented panoramic view of MIRI.

## 3. Functional NMs for MIRI therapy

Building upon the advanced imaging and diagnostic nanoplatforms discussed in Section 2, which enable precise spatial and molecular characterization of MIRI, we now turn to therapeutic interventions that leverage these diagnostic insights for targeted treatment of underlying pathological processes, including oxidative stress, calcium overload, and inflammatory activation. Although reperfusion restores oxygen supply, it also initiates a harmful cascade comprising oxidative stress, inflammatory activation, apoptotic signaling, and metabolic dysregulation [119–121]. Conventional small-molecule therapeutics struggle to effectively modulate these pathological processes due to inherent limitations such as systemic toxicity, poor target specificity, and rapid clearance. In contrast, the advent of functional NMs represents a paradigm shift in MIRI treatment. These platforms are specifically engineered to overcome the drawbacks of conventional drugs by offering enhanced biocompatibility, targeted accumulation, and the ability to integrate therapeutic and diagnostic functions within a single platform—a theranostic approach that holds significant promise for personalizing and optimizing treatment efficacy [122,123]. This section focuses on a range of therapeutic mechanisms enabled by nanotechnology, particularly through the application of functional NMs. Key approaches include nanocatalyst-based direct intervention in MIRI, targeted strategies such as NPs-mediated gene delivery and bioinspired nanotherapeutics, as well as synergistic modalities that integrate nanotechnology with gas therapy, stem cell therapy, and the regulation of circadian rhythms.

### 3.1. Direct treatment: nanozyme therapy

Oxidative stress and inflammation induced by the restoration of blood flow in MIRI can induce significant damage to CMs [124]. Nonetheless, numerous clinical trials employing conventional small-molecule antioxidants, such as N-acetylcysteine, have yielded inconclusive results due in part to the short half-life of these antioxidants, thereby warranting robust yet sustainable anti-oxidative strategies [125]. Other direct treatment modalities, such as photothermal therapy and radiotherapy/chemotherapy, present distinct advantages and limitations. Photothermal therapy provides high specificity and minimal invasiveness albeit that its effectiveness is restricted by less tissue penetration and potential cytotoxicity concerns of photosensitive agents [126]. While radiotherapy is effective for deeper tissues, it poses risks of collateral damage and long-term cardiovascular complications [127,128].

Conversely, nanozymes have emerged as promising artificial catalysts, which effectively scavenge free radicals *via* different types of mechanisms. Nanozymes exhibit catalytic activities similar to natural enzymes (i.e., superoxide dismutase (SOD), catalase (CAT)), and they can enhance cellular antioxidant capacity by mimicking enzymatic reactions as well as convert free radicals into harmless molecules [129]. In

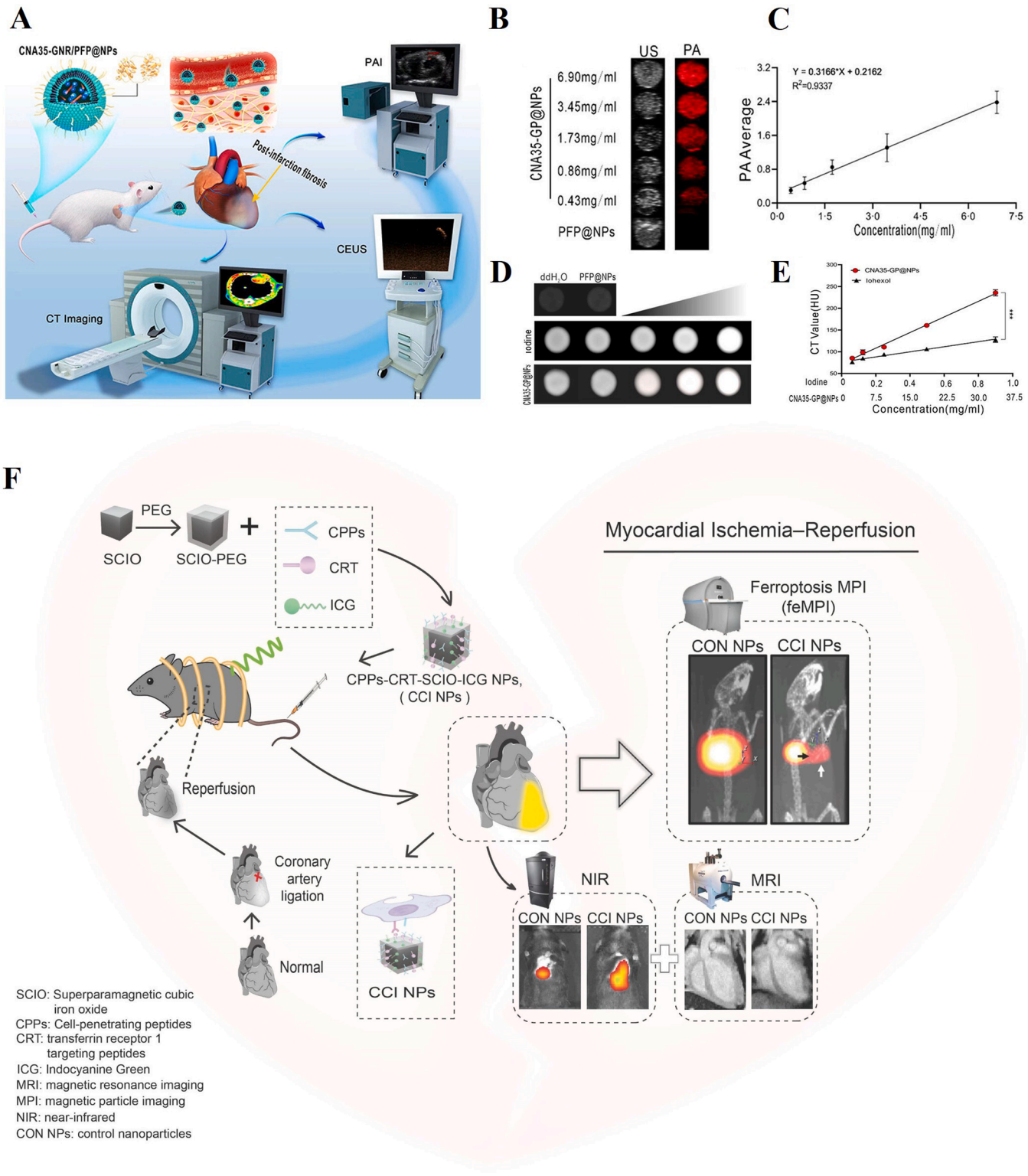


**Fig. 6.** Application of functional NMs in multimodal imaging of MIRI. (A) Multimodal imaging of CNA35-GP@NPs targeting local myocardial fibrosis in rats. (B, C) PA signals were increased with an increase in the concentration of CNA35-GP@NPs. NPs without GNRs (PFP@NPs) did not show an increase in signal intensity after irradiation. (D, E) CT contrast images of CNA35-GP@NPs showed a positive correlation between signal intensity and NP concentration *in vitro*. Reprinted with permission from Ref. [81]. (F) Multimodal NIR/MRI imaging of MIRI utilizing the targeted contrast agent CCI NPs. Reprinted with permission from Ref. [82].

addition, high specific surface area of nanozymes promotes efficient contact with free radicals, thereby enhancing scavenging efficiency [130]. These properties give nanozymes a distinct advantage over other direct treatment strategies, offering a more targeted and sustainable antioxidant approach with fewer side effects. Consequently, nanozymes hold broad potential for biomedical applications, especially in contexts requiring antioxidant and anti-inflammatory responses, such as MIRI (Table 2 illustrates the typical nanozymes for MIRI therapy).

**Table 2**
Summary of typical nanozymes for MIRI therapy.

| Name | Cargo | ROS Scavenging Mechanism | ROS Concentration | Optimal Material Concentration | Ref. |
|---|---|---|---|---|---|
| CNP | / | CNP eliminate ROS *via* $Ce^{3+}/Ce^{4+}$ redox cycling, mimicking antioxidant enzymes | 0.5 mM $H_2O_2$ | *In vitro*: 40 μg/mL CNP; *In vivo*: 0.6 mg CNP | [131] |
| CuCe NPs | Copper ions (Cu) | CuCe NPs attenuate ROS *via* GSH-triggered SOD1 activation and redox homeostasis enhancement | 250 μM $H_2O_2$ | *In vitro*: 2.5 μg/mL CuCe NPs | [132] |
| TA-Ce NCs | Tannic acid | TA–Ce NCs scavenge ROS *via* $Ce^{3+}/Ce^{4+}$ cycling with CAT- and SOD-like activities | 20 mM $H_2O_2$ | *In vitro*: 40 μg/mL TA–Ce NCs; *In vivo*: 2.69 ID%/g (bioavailability) | [133] |
| CeONZs | / | CeONZs scavenge ROS *via* CAT- and SOD-mimetic activities | 100 μM $H_2O_2$; 200 μM tert-butylhydroperoxide | *In vitro*: 0.375 μM | [134] |
| $Mn_3O_4$@PDA nanozyme | / | $Mn_3O_4$@PDA nanozyme mimics SOD activity to catalytically scavenge ROS | 200 μM $H_2O_2$ | *In vitro*: 10 μg/mL $Mn_3O_4$@PDA nanozymes | [135] |
| PB-MSCs | PB NPs | PB nanozymes enzymatically neutralize ROS, enhancing MSC resistance to oxidative stress | **25 μM–200 μM** $H_2O_2$ | *In vitro*: 200 μg/mL PB nanozyme; *In vivo*: 50 μg/mice | [136] |
| NP-SOD | SOD | NP-SOD scavenges superoxide *via* diffusion-driven catalytic dismutation through a porous membrane | 50 μM hypoxanthine; 0.2 U/mL xanthine oxidase | *In vivo*: 500 U/mL NP-SOD | [137] |
| CVNRs | / | CVNRs mimic SOD by catalyzing superoxide dismutation, effectively scavenging ROS | 150 μM homocysteine,5 μM $CuCl_2$ | *In vitro*: 20 μg/mL CVNRs | [138] |
| PtsaN-C | / | PtsaN-C scavenges ROS *via* Pt-$N_4$ single-atom catalytic sites with multienzyme-like activity | 10 mM $H_2O_2$; 100 ng/mL phorbol myristate acetate | *In vitro*: 1 μg/mL PtsaN-C | [139] |
| PBNz@PSC | PB nanozyme | PBNz@PSC scavenges ROS *via* enhanced SOD-like activity and AMPK pathway activation | 10 mM $H_2O_2$ | *In vitro*: 1 μg/mL PBNz@PSC | [140] |
| MnMSN-6 | $Mn^{2+}$, $Mn^{4+}$ | MnMSN catalytically scavenges ROS *via* $Mn^{2+}/Mn^{4+}$, suppressing NF-κB to induce anti-inflammatory MΦs polarization | $O_2^-$ (**60 mmol/L for** xanthine and **1 U/mL for** xanthine oxidase); •OH (**20 mmol/L $H_2O_2$** and **20 mmol/L $FeSO_4$**) | *In vitro*: 10 μg/mL MnMSN-6 | [141] |

**Notes: CNP**, cerium NPs; **CuCe NPs**, copper-deposited ceria NPs; **TA-Ce NCs**, tannic acid–cerium nanocatalysts; **CeONZ**, cerium oxide nanozymes; **PDA**, polydopamine; **PB**, Prussian blue.
**NMs**, nanomaterials; **TA-Ce**, tannic acid–cerium; **NP-SOD**, porous NPs-encapsulated superoxide dismutase; **CVNRs**, cerium vanadate nanorods; **PtsaN-C**, platinum single-atom nitrogen–carbon catalyst; **MnMSN-6**, Mn-loaded mesoporous silica nanozymes; **AMPK**, adenosine monophosphate-activated protein kinase; **NF-κB**, nuclear factor kappa-light-chain-enhancer of activated B cells; **MΦs**, macrophage.

### 3.1.1. *Cerium-based nanozymes*

Cerium, a rare-earth element, exhibits remarkable antioxidative capacity by catalytically scavenging ROS through a reversible redox cycle between its $Ce^{3+}$ and $Ce^{4+}$ states [142]. Nanoengineering cerium into cerium-based NPs (Ce NPs) further amplifies this effect by providing a high specific surface area, which increases the availability of reactive sites for neutralizing free radicals and other oxidative species [143].

Capitalizing on this foundation, diverse Ce-based NMs with tailored therapeutic properties have been developed. For instance, Wang et al. constructed myocardium-targeting TA-Ce nanocatalysts (TA-Ce NCs) *via* the self-assembly of tannic acid (TA) and $Ce^{4+}$ ions (Fig. 7A) [133]. These TA-Ce NCs effectively alleviated oxidative stress in CMs by scavenging key ROS, such as superoxide anions ($\cdot O_2^-$), hydrogen peroxide ($H_2O_2$), and hydroxyl radicals (·OH). This effect was primarily mediated by the $Ce^{3+}/Ce^{4+}$ redox couple (Fig. 7B). Consequently, treatment with TA-Ce NCs reduced infarct size and restored cardiac function, showing their robust cardioprotective potential. Despite promising preclinical efficacy of TA-Ce NCs in mitigating MIRI, several translational challenges must be addressed. A primary obstacle is the development of a scalable, reproducible synthesis under Good Manufacturing Practice (GMP) standards, which requires precise control over critical quality attributes including particle size, $Ce^{3+}/Ce^{4+}$ ratio, surface ligand density, and long-term colloidal stability—each being a key determinant of therapeutic performance and safety [144]. Furthermore, while acute toxicity appears limited in rodent models, comprehensive long-term biosafety assessments are lacking. The metabolic fate, potential chronic accumulation, organ-specific retention, and immunogenicity of TA-Ce NCs also yet remain to be characterized. Preclinical studies are also limited by the use of healthy animal models that do not recapitulate common clinical comorbidities such as diabetes, atherosclerosis, and hypertension, all of which can alter the NPs pharmacokinetics and pharmacodynamics of NPs. Moreover, poor understanding between TA-Ce NCs and endogenous antioxidant systems is also a critical gap. Although TA-Ce NCs exhibit ROS-scavenging activity through their $Ce^{3+}/Ce^{4+}$ redox cycle, their potential synergistic, additive, or antagonistic interactions with native antioxidant enzymes (e.g., SOD, CAT) remain largely unexplored. Elucidating this crosstalk is essential for rationally integrating TA-Ce NCs into the physiological antioxidant network without disrupting redox homeostasis [145].

Beyond simple catalysts, more sophisticated nanozymes have been designed to mimic endogenous antioxidant systems. Hang et al. engineered biomimetic cerium oxide nanozymes (CeONZs) to protect human pluripotent stem cell-derived CMs (hPSC-CMs) from oxidative damage [134]. These CeONZs exhibit high biocompatibility, enhanced cellular uptake due to their ~5 nm size, and sustained ROS-scavenging activity through redox cycling between $Ce^{3+}$ and $Ce^{4+}$. In MIRI, ROS such as superoxide anions ($O_2^-$) and hydrogen peroxide ($H_2O_2$) contribute to cellular apoptosis, inflammation, and mitochondrial dysfunction. The CeONZs target these ROS, prevents oxidative damage and cell death, thereby protecting CMs during MIRI.

In addition, Im et al. synthesized copper-deposited ceria NPs (CuCe NPs) by anchoring $Cu^+$ ions onto the surface of Ce NPs using a mild reduction process [132]. These NPs release bioavailable copper ions intracellularly, which function as cofactors to activate the antioxidant enzyme SOD1. The activated SOD1 effectively catalyzes the dismutation of superoxide anions ($O_2^-$) and hydrogen peroxide ($H_2O_2$), thereby

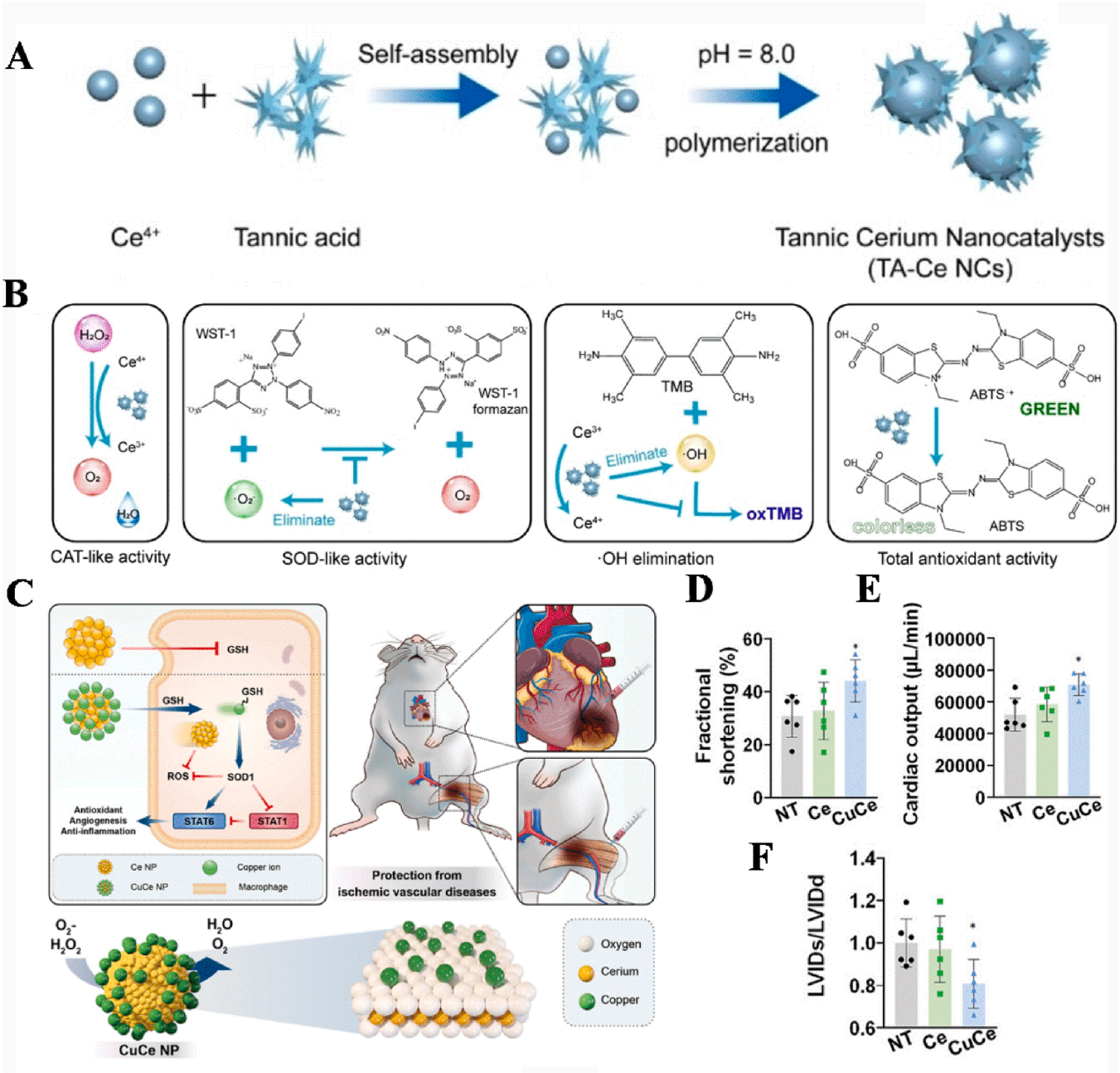


**Fig. 7. Antioxidant effect of Ce-containing NMs.** (A) Schematic illustration of the synthesis of TA-Ce NCs. (B) Schematic illustration of the anti-oxidative mechanism of TA-Ce NCs. Reprinted with permission from Ref. [133]. (C) Schematic illustration of the release of copper ions ($Cu^{2+}$) in a hind-limb ischemia model and myocardial ischemia model in mice. (D, E) The cardiac functions including the factional shortening and the cardiac output were significantly improved in the CuCe group. (F) The ratio of left ventricular end-diastolic dimension (LVIDd) to left ventricular end-systolic dimension (LVIDs) after 30 days of drug injection. Reprinted with permission from Ref. [132].

mitigating oxidative damage. The CuCe NPs also modulated inflammatory pathways, such as STAT1 and STAT6 (signal transducer and activator of transcription 1 and 6), to alleviate inflammation triggered by ROS accumulation (Fig. 7C). This dual action of ROS clearance and inflammation regulation can provide significant cardioprotection in MIRI (Fig. 7D–F). The combined effect of cerium and copper ions directly addresses oxidative stress and inflammation, key drivers of myocardial injury in MIRI.

### 3.1.2. *MOF-based nanozymes*

MOFs exhibit remarkable enzyme-mimetic activities owing to their well-defined porous structures, tunable metal clusters, and functional organic ligands [146–149]. These nanozymes primarily mimic CAT, SOD, and glutathione peroxidase (GPx) through tailored metal-active sites (e.g., Fe, Mn, Cu, Se, V) and optimized ligand environments [150–153]. For instance, CAT-like activity involves efficient $H_2O_2$ decomposition *via* both heterolytic and homolytic pathways with low energy barriers, while SOD-like performance relies on metal redox couples such as $Mn^{3+}/Mn^{4+}$ and $Cu^{+}/Cu^{2+}$ [154–156]. The GPx-like behavior is enhanced by elements such as selenium (Se) or vanadium (V) incorporated into the MOF architecture [151–153]. Key factors governing catalytic efficiency include metal ion identity and valence state, ligand electronic properties (e.g., nitro ($-NO_2$) or amino ($-NH_2$) groups fine-tuning electron transfer), pore confinement effects, and

synergistic interactions in bimetallic systems [157–159]. Such precise control over active sites and microenvironments enable MOF-based nanozymes to exhibit high catalytic activity and selectivity, making them highly promising for biomedical applications including mitigation of MIRI.

Rational integration of multiple metal sites and precise structural engineering within MOFs has significantly advanced the design of high-performance nanozymes for ROS scavenging and therapeutic applications. For instance, Xiang et al. developed a bimetallic nanozyme, where copper (Cu) and manganese (Mn) centers acted synergistically to confer dual SOD- and CAT-like activities, effectively mimicking enzymatic cascade reactions for enhanced ROS elimination (Fig. 8A and B) [160]. The synergy between the metal centers was maximized at a specifically optimized Cu:Mn molar ratio of 1:2, which was empirically determined to possess the highest catalytic activity and theoretically validated by density functional theory (DFT) calculations to have the most favorable reaction kinetics. The developed nanozyme exhibited superior catalytic rate and stability under physiological conditions compared to monometallic analogues, and notably reduced inflammation and mitigated myocardial injury in a MIRI model. Similarly, Liu et al. constructed a cascade nanozyme, by embedding platinum (Pt) NPs within a Mn-functionalized zirconium-porphyrin MOF [161]. The confined porous structure facilitated efficient substrate diffusion and electron transfer between active sites, leading to robust dual-enzyme activity and significantly stronger anti-inflammatory effects as compared to physically mixed controls.

In addition to classical MOFs, Prussian blue (PB) has emerged as a promising multifunctional nanozyme. It is a coordination polymer in which iron ions in different oxidation states are bridged by cyanide ligands, creating a redox-active framework. This unique structure enables the application of PB nanozymes in antioxidant and anti-inflammatory therapies [59]. Long et al. developed a polysaccharide-coated PB nanozyme (PBNz@PSC) with enhanced SOD-like activity, effectively scavenged ROS, promoted MΦs polarization from M1 to M2 phenotype, and improved cardiac function in MIRI models, outperforming conventional therapeutic agents (Fig. 8C–E) [140]. Compared to typical MOFs, PB nanozymes offer distinct advantages such as facile synthesis, high aqueous stability, inherent catalytic activity, and excellent biocompatibility, making them promising candidates for clinical translation [162].

In conclusion, nanozyme-based therapies, particularly those utilizing Ce-based and MOF-derived systems, show great promise for mitigating oxidative stress and inflammation in MIRI. Ce-based nanozymes, such as TA-Ce NCs and CuCe NPs, leverage the $Ce^{3+}/Ce^{4+}$ redox cycle to efficiently scavenge ROS, offering substantial protection against ischemic damage. In contrast, MOF-derived nanozymes, with their tunable metal nodes (e.g., Mn, Cu, Fe) and functional organic ligands, provide a versatile platform for mimicking a series of enzymatic activities, including SOD, CAT, and GPx-like functions, which are often enhanced through synergistic multi-metal sites. However, despite these advances, several key challenges remain, including optimizing targeting specificity to the ischemic myocardium, ensuring long-term safety and efficient metabolic clearance, and scaling up synthesis for clinical applications. Future research should prioritize the development of intelligent nanozymes that are responsive to the local microenvironment, as well as the integration of multimodal imaging capabilities for theranostic applications. Moreover, combining multiple catalytic activities within single platforms could enhance therapeutic outcomes. By overcoming these challenges, nanozyme-based therapies hold significant potential to become next-generation treatments for MIRI and other oxidative stress-driven cardiovascular diseases.

### 3.2. Targeted gene delivery based on NMs

Targeted drug delivery aims to improve therapeutic efficacy while minimizing side effects by delivering therapeutics precisely to specific cell types or tissues [163]. Unlike other NM-based approaches for MIRI, which broadly focus on mitigating oxidative stress or inflammation without targeting specific molecular pathways, gene therapy represents a shift towards precision medicine. Gene therapy allows for the selective regulation of specific molecular targets within infarcted myocardium, offering unprecedented precision in treatment [164,165]. Notwithstanding, the success of gene therapy depends on the development of advanced NMs capable of efficiently delivering genetic payloads. These NMs should facilitate crucial processes, including endosomal escape as well as cytoplasmic release to ensure maximal therapeutic efficacy. By overcoming these challenges, NM-based gene delivery systems can significantly enhance the versatility of gene therapy, expanding its potential for cardiovascular applications [166].

Given these considerations, different types of nanocarriers have been exploited for the sustained and controlled release of genetic materials, such as lipid NPs (LNPs), dendrimers, and MOFs. [38,167,168]. Nonetheless, cardiac-targeted gene delivery systems face unique biological barriers and design challenges. The dynamic perfusion, dense endothelium, and continuous mechanical activity of heart impede efficient vehicle accumulation and retention in the infarcted myocardium [169–171]. Moreover, most of the cardiac cells are terminally differentiated with limited proliferative capacity as well as reduced endocytic or phagocytic activity, which pose additional barriers for the intracellular delivery of therapeutic agents [172]. Consequently, cardiac gene delivery systems are often meticulously designed to improve cardiac targeting and enhance cell transfection efficiency.

Local delivery of NMs is one of the viable approaches to enhance cardiac accumulation of NMs and overcome limitations associated with systemic delivery of NPs. Chen et al. developed a conductive microneedle patch for the targeted myocardial delivery of microRNA-30d-loaded zeolitic imidazolate framework-8 NPs (miR-30d@ZIF-8 NPs) [173]. This strategy leverages the pH-responsive properties of ZIF-8 to enhance lysosomal escape and protect miRNA from degradation, significantly improving delivery efficiency. The therapeutic efficacy stems from dual function of miR-30d to reduce CMs apoptosis as well as suppress fibrotic remodeling, which may help address key pathological processes in MI. This localized delivery platform represents a significant advancement in cardiac gene therapy. Meanwhile, Zeng et al. designed fusogenic coiled-coil peptide modified LNPs, which efficiently transfected induced pluripotent stem cell-derived CMs (iPSC-CMs) than that of the LNPs [174]. The fusogenic peptide is composed of a pair of complementary coiled-coil peptides (CPE4/CPK4), conjugated to a cholesterol moiety *via* a PEG spacer; cholesterol moieties can promote cellular uptake of the carrier through an easier incorporation into lipid membranes as well as LNPs. Consequently, LNP-CPE4/CPK4 can trigger an efficient fusion between liposomes and cells, bypassing endosomal entrapment, and improve drug delivery.

As we know, the conventional approaches for localized drug delivery to the heart typically necessitate highly invasive surgical procedures, which impose considerable physical trauma and clinical risks on patients [175]. In contrast, systemic injection into the bloodstream remains the most convenient and non-invasive method for targeted delivery of genetic material.

Bionic nanomembranes, by mimicking the structure and function of cell membranes, not only enhance drug targeting capabilities but also integrate seamlessly with gene therapy to improve the stability and targeting of gene vectors [176,177]. This is particularly beneficial in the treatment of MIRI, where bionic nanomembranes demonstrate excellent synergistic effects. MΦs rapidly converge on the site of cardiac injury following myocardial damage, acting as master regulators that coordinate inflammation, tissue repair, and structural remodeling [178]. Inspired by the natural homing ability and phagocytic activity of MΦs, Lu et al. fabricated a MΦs membrane modified with hemagglutinin and receptor for advanced glycation end products (RAGE), and used it to coat NPs for small interfering RNA (siRNA) delivery [179]. In addition, Wang et al. developed MΦs -targeting nanocomplexes to co-deliver

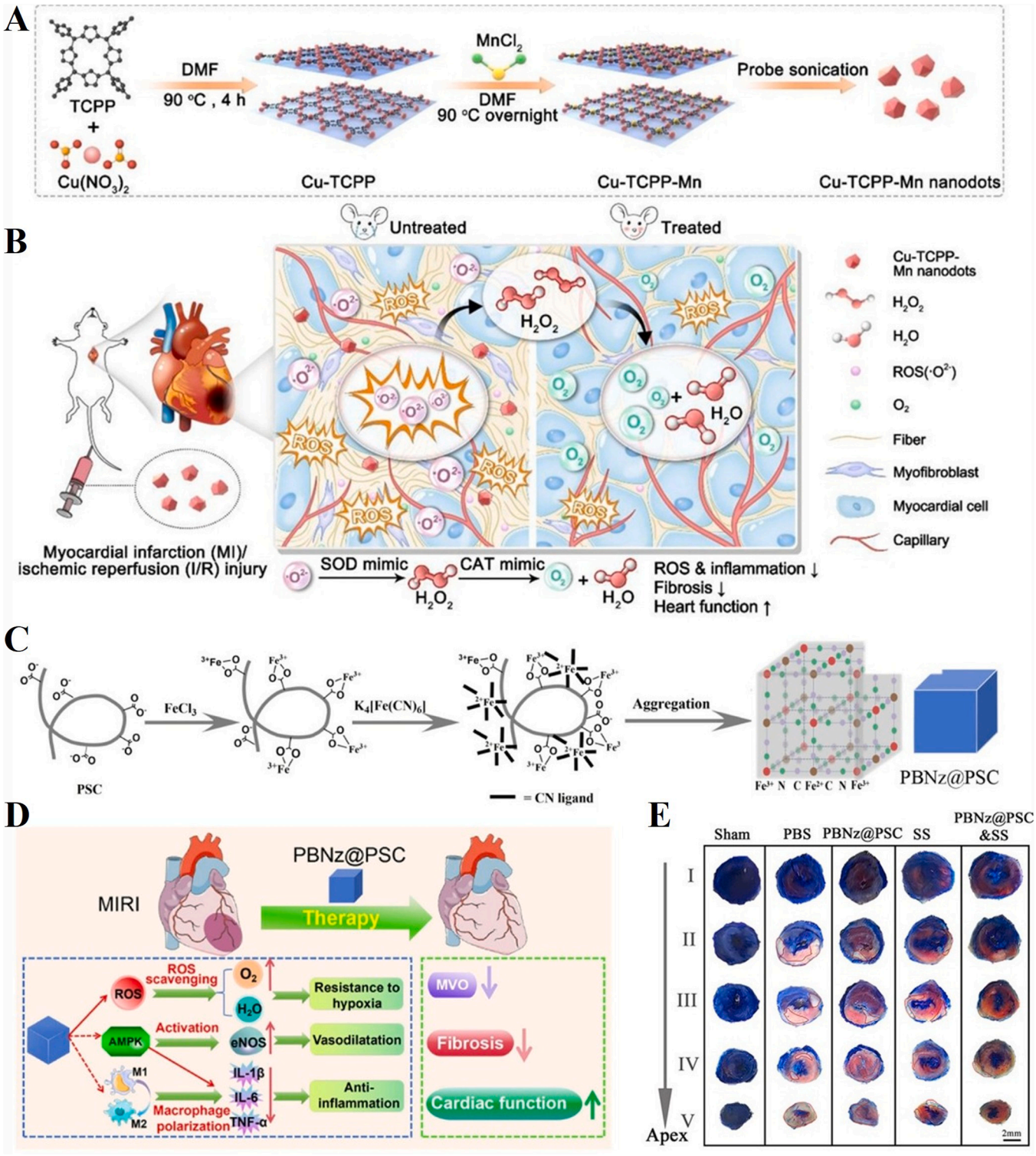


**Fig. 8. MOF-based nanozymes for MIRI treatment.** (A) Bimetallic nanozymes were prepared by solvothermal method, Mn and Cu were embedded in porphyrin, and MOF nanodots were prepared by sonication. (B) Bimetallic nanozymes demonstrated potent ROS scavenging, while promoting angiogenesis and cardiac repair in MIRI model. Reprinted with permission from Ref. [160]. (C) Schematic illustration of the synthesis of PBNz@PSC nanozymes. (D) PBNz@PSC treats MIRI by scavenging excess ROS, activating the AMPK (Adenosine Monophosphate-Activated Protein Kinase) signaling pathway, and promoting M1 MΦs polarization. (E) Evans blue/TTC staining distinguished myocardial viability: blue (viable), unstained (ischemic), red (reperfusion-salvaged), and necrotic (white, outlined in red). Reprinted with permission from Ref. [140].

siRNA targeting MOF and miRNA-21 for MIRI therapy. The combined delivery of siRNA and miRNA-21 efficiently silenced target genes, suppressed oxidative stress, and polarized MΦs toward an anti-inflammatory phenotype [180]. In another study, Zhou et al. developed platelet–macrophage hybrid membrane–coated nanocomplexes (BSPC@HM NCs) for targeted delivery of Sav1 siRNA, an upstream inhibitor of the Hippo pathway [181]. The hybrid membrane enables inflammation homing and microthrombus targeting, guiding the

nanocomplexes to ischemic myocardium (Fig. 9A). Upon reaching the acidic microenvironment, the membrane is shed, exposing the siRNA-loaded core and enhancing transfection efficiency (Fig. 9B–D). *In vivo* data showed siRNA release and gene silencing occurred selectively in the injured myocardium, with minimal activity in other tissues (Fig. 9G–I). Notably, the non-responsive control (BSPS@HM) failed to induce transfection despite similar tissue distribution, underscoring that both the local acidic environment and targeted accumulation are essential for successful gene delivery and transfection (Fig. 9E–J). Consequently, BSPC@HM NCs effectively silenced Sav1, reduced cardiomyocyte apoptosis, and promoted myocardial regeneration in MIRI models.

Machine learning (ML) has emerged as a transformative tool in material screening. By integrating computational simulations (e.g., molecular dynamic simulation (MDS), DFT, etc.) with ML algorithms (e.g., random forests, graph neural networks, etc.), researchers can rapidly predict key properties of NMs, including biocompatibility, drug-loading efficiency, and targeted delivery capability [182–184]. This data-driven approach can appreciably reduce experimental trial-and-error and accelerate the development of NP-based gene delivery technologies. Santos and our team et al. developed a diversity-oriented combinatorial screening strategy that integrates an automated microfluidics platform with computational-assisted analysis to systematically optimize polysaccharide-based nanocarriers for cardiac RNA interference (RNAi) therapy [185]. Ultimately, a NP formulation composed of the anionic polysaccharide endosomolytic phosphorylated β-glucan (EEPG) and the cationic cell-penetrating peptide (CPP) KALA was identified as the optimal carrier for targeted gene delivery in myocardial injury (Fig. 10A–C). This system, designated GluCARDIA, exhibits efficient siRNA delivery and robust RNAi silencing in MIRI model, thereby significantly attenuating cardiac fibrosis and improving cardiac function (Fig. 10D–I). Thus, this study enhances delivery efficiency by employing a diversity-oriented combinatorial formulation screening strategy using an automated microfluidics platform. Through stepwise evaluation, which includes NPs formation, siRNA encapsulation, biocompatibility, and gene silencing efficacy, and paired with computational interpretation, the authors identify optimal cationic–anionic pairings for efficient, targeted RNA delivery.

In conclusion, targeted gene therapy, offers a promising avenue for treating MIRI by enabling precise molecular targeting within the myocardium. The integration of gene therapy with advanced nanoplatforms, such as bionic nanomembranes, further enhances delivery efficiency, stability, and targeting accuracy. These innovations pave the way for more effective and personalized treatments for MIRI and other cardiovascular conditions. However, challenges remain in optimizing gene delivery systems, ensuring their stability and biocompatibility, and achieving targeted accumulation in specific cardiac tissues. Additionally, while nanoplatforms have shown potential in enhancing therapeutic outcomes, their clinical translation requires overcoming issues related to scalability, regulatory approval, and long-term safety. Future efforts should focus on refining NMs design to achieve higher improve therapeutic index, and minimize immune system interactions. Moreover, the integration of real-time monitoring through advanced imaging techniques will be crucial in assessing the efficacy of these therapies and

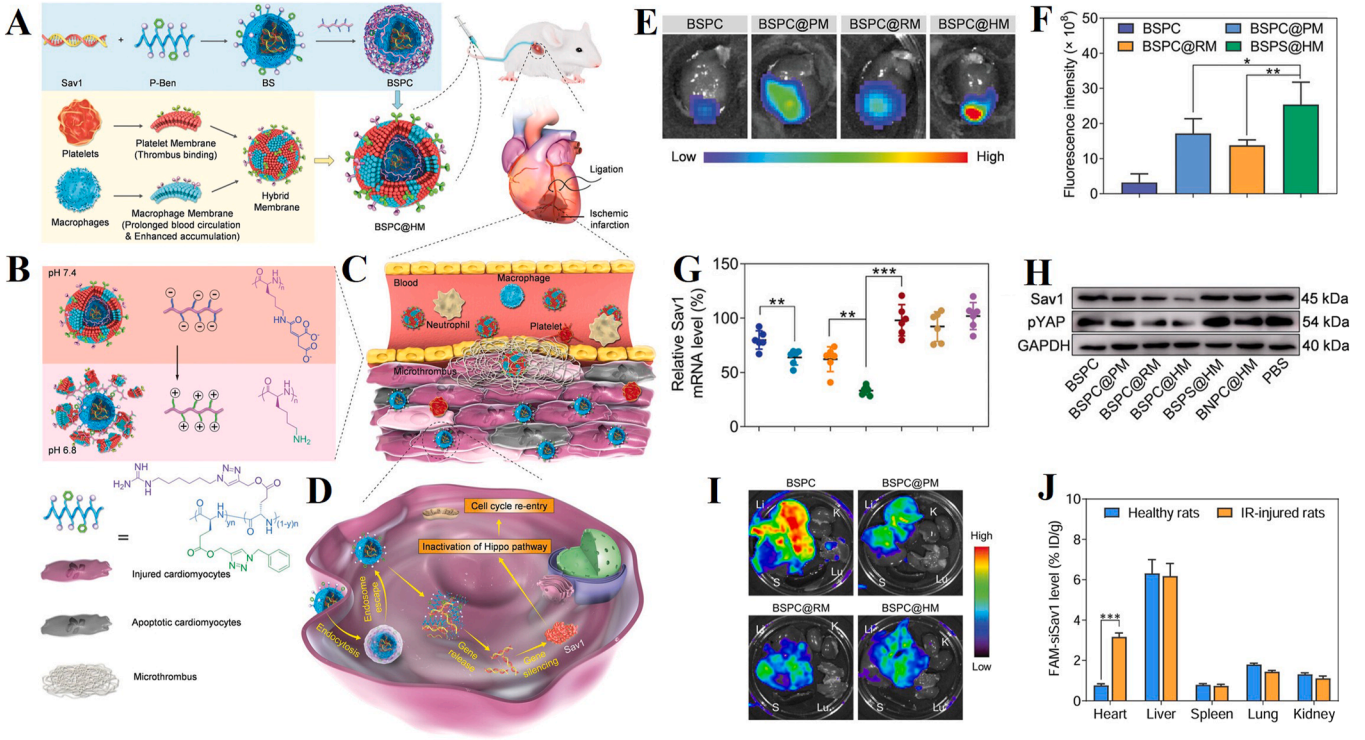


**Fig. 9. Biomimetic BSPC@HM NCs with HM reversible camouflage for gene therapy of MIRI.** (A) BSPC@HM nanocomplex is formed by coating a platelet- MΦs hybrid membrane (HM) onto a poly (L-lysine)-cis-aconitic acid (PC)-based core loaded with P-Ben/siSav1 (membrane-penetrating peptide and targeted siRNA). (B) In acidic (pH 6.8) conditions, the PC layer charge reverses, shedding the HM camouflage and exposing P-Ben/siSav1 to enhance cellular uptake and endosomal escape. (C) Intravenously injected BSPC@HM NCs selectively accumulate at MIRI sites. (D) Intracellular siSav1 silences the Sav1 gene, inhibiting the Hippo pathway to promote cardiomyocyte regeneration and suppress apoptosis. (E) *Ex vivo* imaging of rat hearts performed 6 h post-injection revealed myocardial accumulation of both BSPC@HM and BSPS@HM. (F) Quantification of fluorescence intensity confirms comparable heart distribution between BSPC@HM and BSPS@HM. (G) qRT-PCR analysis of Sav1 mRNA in ischemic myocardium; only BSPC@HM shows significant silencing. (H) Western blot of Sav1 and pYAP proteins in heart tissues, confirming gene silencing by BSPC@HM. (I) Biodistribution of BSPC@HM in major organs, showing low off-target accumulation. (J) BSPC@HM accumulation in IR vs. healthy hearts, showing ~4.1-fold enrichment in injured myocardium. Reprinted with permission from Ref. [181].

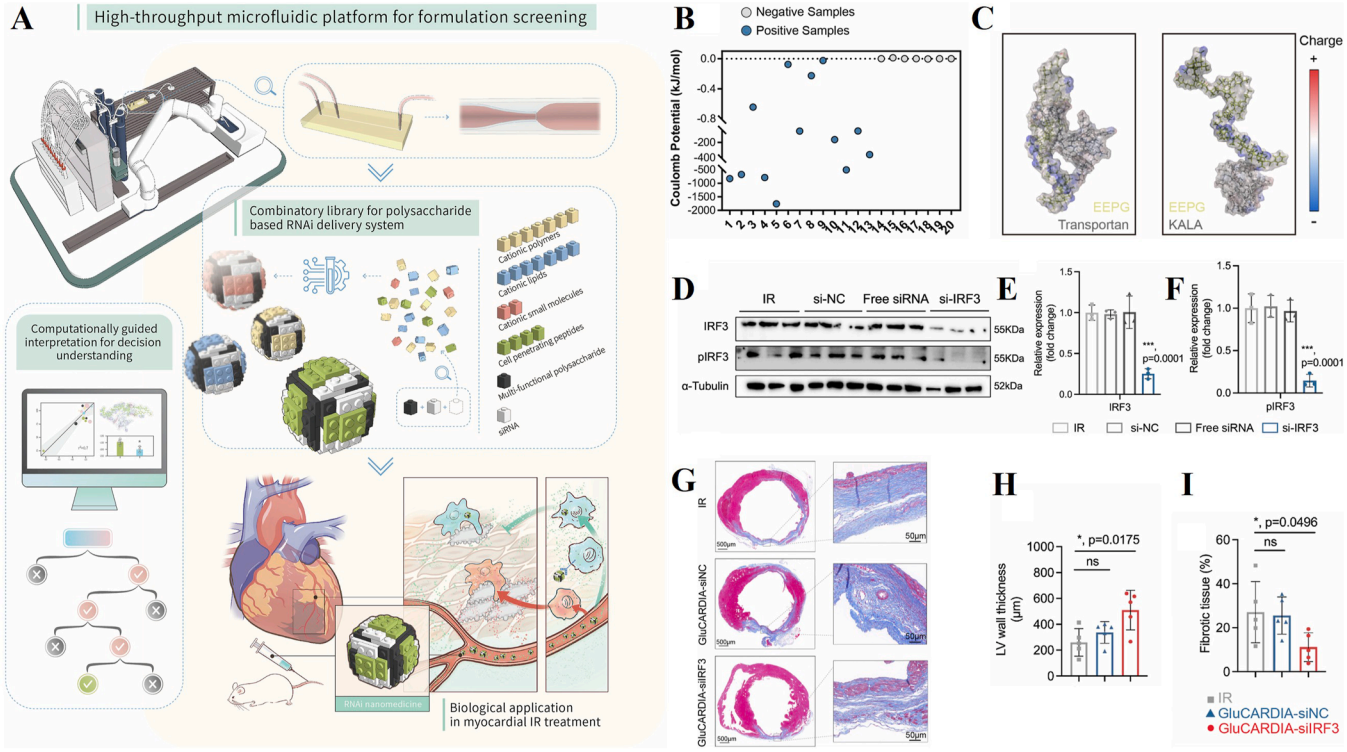


**Fig. 10. Rational design, targeted delivery mechanism, and therapeutic efficacy of polysaccharide-based RNAi nanocarriers (GluCARDIA NPs) in MIRI.** (A) High-throughput screening and optimization of polysaccharide-based RNAi nanocarriers. (B) MDS analysis of electrostatic interactions between cationic compounds and anionic polysaccharides. (C) Comparative binding conformations of EEPG-CPP complexes. (D, E) Western blot analysis of interferon regulatory factor 3 (IRF3) and phosphorylated IRF3 (p-IRF3) expression in myocardial tissue. GluCARDIA-siIRF3 NPs reduced both proteins by 70 % vs. controls (***$p < 0.001$). (F) Densitometric quantification of IRF3/p-IRF3 expression. (G) Masson's trichrome staining of myocardial fibrosis. (H) Left ventricular (LV) wall thickness in GluCARDIA-siIRF3 (1.02 ± 0.08 mm) vs. IR group (0.68 ± 0.05 mm, **$p < 0.01$). (I) Fibrosis area reduced by 57 % (12.3 ± 2.1 % vs. 28.7 ± 3.5 %, ***$p < 0.001$). Reprinted with permission from Ref. [185].

guiding clinical decision-making.

### 3.3. Combination therapy

MIRI encompasses intricate pathophysiological pathways. While advanced monotherapies, such as stem cell therapy, gasotransmitter-based approaches, and circadian rhythm interventions, demonstrate considerable mechanistic potential, their translation into clinical practice remains fraught with substantial challenges. Stem cell therapy is limited by poor engraftment and transient paracrine effects [186]. Gas transmitter-based approaches, utilizing molecules such as nitric oxide (NO), hydrogen sulfide ($H_2S$), carbon monoxide (CO) and hydrogen ($H_2$) suffer from extremely short half-lives and a lack of targeted delivery [187–189]. Besides, circadian rhythm interventions require precise temporal coordination, which is difficult to achieve in practice [190]. These inherent limitations underscore the inadequacy of singular strategies in addressing the multifaceted pathology of MIRI.

Nanotechnology provides a sophisticated convergence platform to systematically overcome these barriers through precise therapeutic manipulation. By engineering nanocarriers, such as liposomes, polymeric NPs, and biomimetic vesicles, key functional advances are realized: (*i*) Protected and targeted delivery: nanocarriers encapsulate and shield unstable agents (e.g., stem cell-derived exosomes, gas donors), enabling site-specific accumulation *via* surface-modified ligands (e.g., peptides targeting ischemic myocardium or activated endothelium), thereby enhancing local bioavailability while minimizing systemic exposure [191,192]. (*ii*) Intelligent responsive release: stimuli-responsive nanocarriers can sense pathological microenvironments (e.g., oxidative stress, acidic pH, enzyme overexpression) and trigger on-demand release of therapeutics, thus converting transient bioactivity into sustained, localized effects and improving therapeutic precision [193,194]. (*iii*) Multifunctional integration and synergy: The most distinctive advantage lies in co-delivering multiple therapeutic agents (e.g., antioxidants, anti-inflammatory drugs, pro-repair factors) within a single nanoplatform [195]. Recent advances highlight chrono-nanomedicine, where the efficacy of smart NPs is governed by circadian rhythms, with optimal myocardial repair achieved through time-dependent administration contingent upon an intact biological clock [196]. In this section, we will focus on introducing current research progress in integrating nanotechnology with the aforementioned monotherapies for combined treatment of MIRI.

#### 3.3.1. Engineering of NMs-Laden stem cells for MIRI treatment

While gene therapy enables precise modulation of disease-associated pathways at the molecular level, its capacity to orchestrate comprehensive tissue regeneration remains limited. In this regard, stem cell therapy offers a promising approach for myocardial repair through cellular replacement and paracrine effects. Stem cells, such as MSCs, can promote tissue regeneration, reduce inflammation, and improve cardiac function after myocardial injury. However, the clinical impact of stem cell-based strategies is often limited by factors such as poor cell survival, retention, and engraftment within the hostile microenvironment of MIRI [130,197–200].

To address these challenges, recent studies have explored the combination of stem cells with multifunctional NMs to enhance their therapeutic efficacy for MIRI treatment. One of the major limitations for the application of stem cells in MIRI is the rapid cell loss caused by the oxidative stress. Le et al. engineered MSCs by incorporating dopamine-modified manganese oxide nanozymes ($Mn_3O_4$@PDA) with SOD-like activity [135]. The $Mn_3O_4$@PDA effectively scavenged ROS, reduced

inflammation and enhanced cell survival in an oxidative stress environment (Fig. 11A). Furthermore, it also significantly improved the migration and homing of cells (Fig. 11B). While a direct assessment of paracrine factor secretion (e.g., VEGF, hepatocyte growth factor (HGF)) remains to be fully elucidated, the enhanced angiogenic and anti-fibrotic effects observed *in vivo*, coupled with transcriptomic data indicating a broadly augmented repair phenotype, strongly suggest a synergistic potentiation of the native paracrine functions of MSCs (Fig. 11C).

In addition to the advancements in antioxidant nanozyme-engineered MSCs, other studies have explored different nano-therapeutic approaches to enhance the efficacy of stem cell therapy in MIRI. Pan et al. developed Tempol-loaded β-cyclodextrin-based NPs (TPCD NPs) and further incorporated an $H_2O_2$-responsive compound, PBAP, into these NPs (Fig. 11D) [201]. These innovative NPs were used to engineer MSCs, enhancing their paracrine signaling. For example, it promotes the secretion of VEGF and HIF-1α (hypoxia-inducible factor 1-alpha), which is crucial for tissue repair and angiogenesis under oxidative stress conditions (Fig. 11E and F). The engineered MSCs demonstrated significant resistance to oxidative stress by scavenging ROS, improving mitochondrial protection, and enhancing their paracrine activity. Notably, under $H_2O_2$-induced oxidative stress, MSCs treated with TPCD NPs exhibited a marked increase in viability, with cell survival rising from 18.5 % in untreated MSCs to 79.4 % in TPCD NP-engineered MSCs, compared to 31.0 % with poly (boronate-ester--acrylamide) acrylate polymer (PBAP) alone. The combination of TPCD NPs with MSCs provided a strong protective effect against ROS-induced cell death, supported by the enhanced antioxidative properties of the NPs. Furthermore, this engineered MSCs exhibited significantly improved migration and adhesion capabilities, further boosting their potential for targeted therapy in ischemic tissues.

Overall, the combination of stem cells with multifunctional NMs offers a powerful strategy to overcome the limitations of stem cell therapy for treating MIRI. By enhancing cell survival, reducing oxidative stress, and improving migration and paracrine signaling, this approach not only promotes tissue repair and regeneration but also provides a more effective and targeted treatment compared to gene therapy alone. The incorporation of NMs into stem cell therapy significantly improves the stability, retention, and therapeutic efficacy of stem cells in the injured myocardium, offering a promising avenue for more effective MIRI treatment and potentially revolutionizing cardiovascular therapies.

### 3.3.2. NM-based gas therapy

Gas therapy has emerged as a key focus in modern cardiovascular treatment, utilizing gaseous species such as NO, $H_2S$, CO, and $H_2$. Despite the different molecules involved, their therapeutic effects primarily stem from several mechanisms that counteract MIRI. These include reducing oxidative stress and apoptosis, modulating inflammation, regulating mitochondrial function and autophagy, and promoting angiogenesis [202–205]. Gas therapy significantly reduces oxidative stress and inflammation induced during MIRI, thus alleviating reperfusion injury [206,207]. When combined with NMs, gas therapy shows considerable promise in treating MIRI. NMs, modified with cell-targeting moieties, enhance the bioavailability of gases, improve retention in ischemic tissues, and prolong release for better therapeutic outcomes. Additionally, controlled and sustained gas release at the injury site enables precise regulation of kinetics, minimizing systemic side effects. Moreover, therapeutics can be co-released with gaseous species to achieve synergistic effects [208,209]. These advantages make the combination of gas therapy and NMs a promising approach for MIRI treatment (Table 3 illustrates the typical strategies combining gas therapy with functional NMs).

NO is a multifunctional signaling molecule, which plays a pivotal role in cardiovascular homeostasis by inhibiting platelet adhesion, modulating cell growth and death, and inducing vasodilation, thereby protecting cardiovascular system from injury [219,220]. *In vivo*, NO synthesis from L-arginine (L-Arg) is catalyzed by NO synthase (NOS) in the presence of oxygen ($O_2$) and nicotinamide adenine dinucleotide phosphate (NADPH) [221]. The dysregulation of NOS activity can impair endogenous NO production, contributing to various pathological conditions [222]. Thus, modulating endogenous NOS activity or administering exogenous NO has emerged as a key therapeutic strategy. The concentration and release kinetics of NO are critical for its biological effects. While low concentrations of NO (1–30 nM) can promote vasodilation and angiogenesis through cyclic guanosine monophosphate (cGMP)-dependent pathways, higher concentrations of NO (~100 nM) can activate protein kinase phosphorylation, thereby exerting anti-apoptotic and tissue-protective effects. However, excessive NO levels (4400 nM) can trigger apoptosis [223]. Therefore, precise control over NO release is essential for therapeutic applications.

Presently, NO gas inhalation as well as administration of NO precursors is used in clinical scenarios albeit numerous challenges to achieve sustained and controlled release of NO *in vivo*, especially once NO donors are depleted [224]. To circumvent these limitations, different types of approaches have been used. Li et al. developed an NOS-like nanoplatform (NanoNOS) that recapitulated NOS function as well as catalyzed the constant concentration of NO under physiological conditions plausibly through a three-step mechanism: (*i*) NADPH oxidation to generate superoxide anions ($O_2^-$); (*ii*) conversion of superoxide anion ($O_2^-$) to hydrogen peroxide ($H_2O_2$) by SOD-like activity; and (*iii*) non-enzymatic oxidation of L-Arg by $H_2O_2$ to produce NO [210]. The administration of NanoNOS significantly suppressed the adhesion of monocytes to ECs, which was governed by exogenous stimuli, including oxidative stress and heavy metal ions. Consequently, NanoNOS alleviated myocardial injury. Moreover, the intrinsic photothermal effect of Au nanorods as well as reaction rate and NO generation efficiency of NanoNOS were increased with NIR excitation.

NMs based on noble metals may not only act as core platforms for catalytic reactions but they can also act as protective barriers for the substrates involved in these reactions. Following MIRI, an excessive ROS generated in myocardial tissue can oxidize NO to produce peroxynitrite ($ONOO^-$), thereby further exacerbating myocardial dysfunction [171]. Therefore, it is important to construct a platform capable of generating NO as well as protecting it from the oxidation. Wang et al. developed AASP (PCM-modified, L-Arg-loaded, selenium-coated gold nanocages). Moreover, L-Arg was loaded into PCM for NO release [211]. AASP can exert dual anti-oxidative and NO-modulating effects by: (*i*) scavenging ROS to prevent oxidative damage, (*ii*) sustaining NO bioavailability through total nitric oxide synthase (TNOS) activation, and (*iii*) inhibiting the conversion of NO to cytotoxic $ONOO^-$. The AASP preserved mitochondrial function by regulating the closure of mitochondrial permeability transition pore, maintaining ATP synthesis, and protecting mitochondrial integrity in CMs (Fig. 12A–C). The AASP conferred synergistic cardioprotection by concurrently addressing oxidative stress and NO dysregulation in MIRI. Xu et al. leveraged platelet membrane-coated NPs (B-P@PLT) for targeted NO delivery (Fig. 12D) [212]. B-P@PLT NP can target injured ECs and release NO under US stimulation (Fig. 12E). Consequently, B-P@PLT NPs promoted ECs function, increased revascularization and enhanced the survival of CMs due in part to the NO bioavailability at the injury site (Fig. 12F–H).

CO is an endogenous gas signaling molecule with well-recognized roles in myocardial protection and regeneration. CO exhibits multifunctional advantageous features, such as immuno-modulation, redox homeostasis, vasculogenic induction, which render it as an attractive candidate for MIRI therapy [225]. However, to fully leverage the therapeutic potential of CO as well as minimize its off-target effects and toxicity, an ideal CO-based therapy should enable site-specific, on-demand release within diseased myocardium. To achieve this, researcher have developed $ONOO^-$-responsive CO donors, which can react with elevated levels of $ONOO^-$ to activate the release of CO; $ONOO^-$ level is higher in ischemic MIRI model. For example, Zhang et al. synthesized a biomimetic CO nanogenerator (M/PCOD@PLGA), which was composed

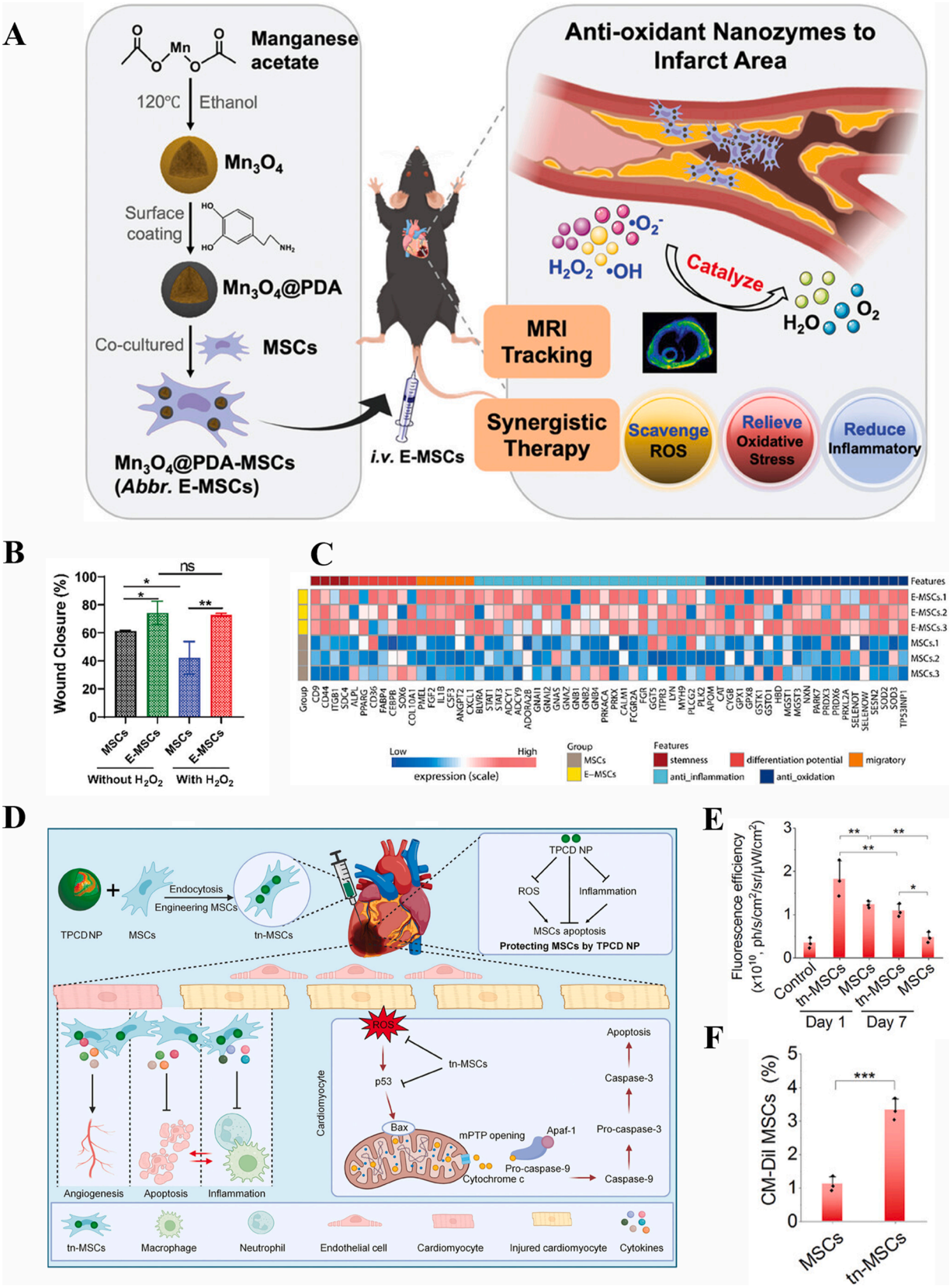


**Fig. 11.** NMs combined with stem cells for the treatment of MIRI. (A) Schematic illustration of the synthesis of $Mn_3O_4$@PDA-MSCs and their application for *in vivo* MRI tracking. (B) Wound closure using MSCs and E-MSCs ($Mn_3O_4$@PDA-MSCs) with different treatments (n = 3). (C) Differential gene expression pattern in E-MSCs by transcriptome sequencing analysis. Reprinted with permission from Ref. [135]. (D) Engineering MSCs *via* a TPCD NP for the treatment of MIRI. (E) MSCs-DiI and tn-MSCs-DiI were accumulated in isolated hearts of MIRI mice on day 1 and day 7 after myocardial injection. Quantitative analysis (F) of MSCs-DiI and tn-MSCs-DiI in isolated hearts on day 1 after myocardial injection. Reprinted with permission from Ref. [201].

**Table 3**
Summary of typical strategies combining gas therapy with functional NMs.

| Category | Name | Cargo | Gas Source | Gas Production Efficiency | Ref. |
|---|---|---|---|---|---|
| **NO therapy based on NMs** | NanoNOS | / | (1) NADPH oxidation generates $O_2^-$;<br>(2) $O_2^-$ dismutation by SOD-like activity yields $H_2O_2$;<br>(3) $H_2O_2$ oxidizes L-Arg to produce NO | Elevating intracellular NO levels ≥10-fold in human monocytes and ECs | [210] |
| | AASP | L-Arg | NO is enzymatically produced from L-Arg *via* NOS in gold nanocages | / | [211] |
| | B-P@PLT NP | BNN6 | NO is facilitated by the **US-triggered activation of BNN6** | BNN6 encapsulation in B-P results in a 43.4 % decrease in NO production relative to unencapsulated BNN6 | [212] |
| | ZnO NPs | $Zn^{2+}$ | NO is produced from zinc oxide NPs | / | [213] |
| | NA@MEV | MitoN | NO is produced from the amino acid L-Arg, catalyzed by NOS | / | [214] |
| **$H_2S$ therapy based on NMs** | RAPA/JK-1-PLGA@PM | JK-1 | $H_2S$ is released from JK-1 in response to the acidic, inflammatory microenvironment of the ischemic myocardium | The $H_2S$ donor JK-1 demonstrates pH-triggered release, generating $H_2S$ exclusively in acidic environments (pH 6.5) with negligible release at physiological pH 7.4 | [215] |
| | JK-1, JK-2 | $H_2S$ | $H_2S$ release from JK-1/JK-2 is regulated through ester bond hydrolysis and modulated by acidic environments | Blood analysis revealed significantly elevated $H_2S$ levels within 15 min post-treatment with JK-1/JK-2 (50–100 μg/kg) versus controls | [216] |
| | SOD/PAC@CSF | G-CSF | $H_2S$ generation occurs *via* interaction between M-Cys monomers and CSE | (1) NO/$H_2S$ co-releasing SOD/PAC@CSF showed 5.5-fold higher NO output;<br>(2) Intracellular $H_2S$ reached 660.2 nM in treated H9c2 cells | [76] |
| **CO therapy based on NMs** | M/PCOD@PLGA | PCOD585 | CO is produced from **PCOD585** in response to **$ONOO^-$** | M/PCOD@PLGA (6 mg/kg) achieved concentrations of 24.05 ± 1.96 (3 h), 20.44 ± 1.10 (6 h), and 9.40 ± 0.88 pmol/mg (24 h) | [217] |
| **$H_2$ therapy based on NMs** | $H_2$-PFOB NEs | / | $H_2$-PFOB NEs can hold up to approximately 6 mM of $H_2$ | / | [218] |

**Notes**: **NMs**, nanomaterials; **ZnO**, zinc oxide; **BNN6**, NO donor compounds; **L-Arg**, L-arginine; **B-P**, BNN6-loaded PLGA NPs; **PLT NP**, platelet membrane-coated NPs; **AASP**, PCM-modified, L-Arg-loaded, selenium-coated gold nanocages; **PCM**, peptide for cardiac muscle targeting; **NanoNOS**, NOS-like nanoplatform; **NA@MEV**, L-Arg-modified N@MEV (NO-driven nanomotor); **MitoN**, mitochondrial-targeted ROS-scavenging NADPH mimic; **RAPA/JK-1-PLGA@PM**, platelet membrane-coated RAPA/JK-1-PLGA NPs; **RAPA**, Rapamycin; **PLGA**, poly(lactic-co-glycolic acid); **JK-1**, the $H_2S$ donor; **ECs**, endothelial cell; **US**, **ultrasound.**
**JK-1**, **JK-2**, novel pH-triggered $H_2S$ donors; **SOD/PAC@CSF**, superoxide dismutase/poly(M-Arg-co-M-Cys) @ Granulocyte Colony-Stimulating Factor; **M-Cys**, N-mercaptoacryloyl-L-cysteine; **G-CSF**, Granulocyte colony-stimulating factor; **CSE**, cystathionine γ-lyase; **M/PCOD@PLGA**, MΦs membrane-coated, PCOD585-loaded Poly(lactic-co-glycolic acid) NPs; **PCOD585**, the key therapeutic agent; **$H_2$-PFOB NEs**, hydrogen-carrying perfluoroocyl bromide nanoemulsions.

of MΦs membrane-coated PLGA NPs encapsulating an $ONOO^-$-responsive CO donor (PCOD585), which enabled targeted CO delivery to ischemic myocardium for MIRI treatment [217]. The PCOD585 allows for the targeted release of CO in response to $ONOO^-$, especially, in ischemic regions, thereby enhancing the precision of treatment.

$H_2S$ has been shown to exert its protective effect in MIRI through several mechanisms, including its anti-oxidative effect *via* ROS scavenging and inhibition of oxidative stress for enhanced cell survival [226,227]. In addition, it possesses pro-vasodilatory effects and enhances myocardial perfusion to alleviate cardiac burden [228]. $H_2S$ further contributes to myocardial protection by reducing CM loss, partly through the inhibition of apoptotic signaling pathway [229–231]. Kang et al. prepared pH-responsive $H_2S$ delivery vehicles using thiophosphorylamide-based $H_2S$ donors (JK-1 and JK-2), which can effectively release $H_2S$ under mildly acidic pH conditions and significantly reduce infarct size in a MIRI mouse model *in vivo* [216]. Li et al. developed a chemotactic nanomotor (SOD/PAC@CSF), which was fabricated using N-methacryloyl-L-arginine (M-Arg) and N-methacryloyl-L-cysteine (M-Cys) monomers. The SOD/PAC@CSF facilitated targeted delivery of Granulocyte colony-stimulating factor (G-CSF) to the ischemic site (Fig. 13A) [76]. A pivotal feature of this nanosystem is its injury-responsive sequential release of $H_2S$ and NO (Fig. 13B and C). The process is initiated by the overexpressed hydrogen peroxide ($H_2O_2$) in the reperfused tissue, which reacts with the manganese dioxide ($MnO_2$) core to trigger a rapid release of $H_2S$ (Fig. 13D and E). This initial $H_2S$ burst serves to scavenge the acute oxidative stress. Subsequently, the resulting reductive microenvironment promotes the continuous release of NO, which acts to ameliorate microcirculation and suppress the inflammatory response. This orchestrated "$H_2S$-first, NO-follows" sequence ensures synergistic regulation of the injury microenvironment (Fig. 13F–H). However, the clinical translation of this chemotactic nanomotor continues to face significant challenges. For instance, physiological differences between animal models and human patients, such as the presence of comorbidities, variability in the expression of disease-related enzymes (e.g., inducible nitric oxide synthase (iNOS)), and uneven blood flow in ischemic tissues, may compromise the translational applicability of this nanomotor-based strategy. The multifunctional nature of the system further complicates regulatory approval, as it necessitates comprehensive evaluation of its pharmacokinetics, bio-distribution, immune response, and long-term toxicity. Overall, addressing these barriers is essential for its successful clinical advancement.

$H_2$ has been widely reported to exert beneficial effects in animal models of MIRI, including anti-oxidative, anti-inflammatory, and cytoprotective effects [232,233]. Nie et al. reported that the $H_2$ inhalation can significantly improve recanalization rate and cardiac function in an MIRI model *in vivo* [234]. In this work, the authors demonstrated that the therapeutic mechanism of $H_2$ primarily involves the suppression of inflammasome activation and reduction of pro-inflammatory factor release, thereby inhibiting pyroptosis. The same group further developed a $H_2$-carrying nanoemulsion system, which exhibited higher $H_2$ loading capacity and biocompatibility [218]. Additionally, by applying LIFU to trigger the release of $H_2$ in targeted tissues, the precision and therapeutic effectiveness of the treatment can be enhanced.

It should be noted that while gas signaling molecules, including $H_2$,

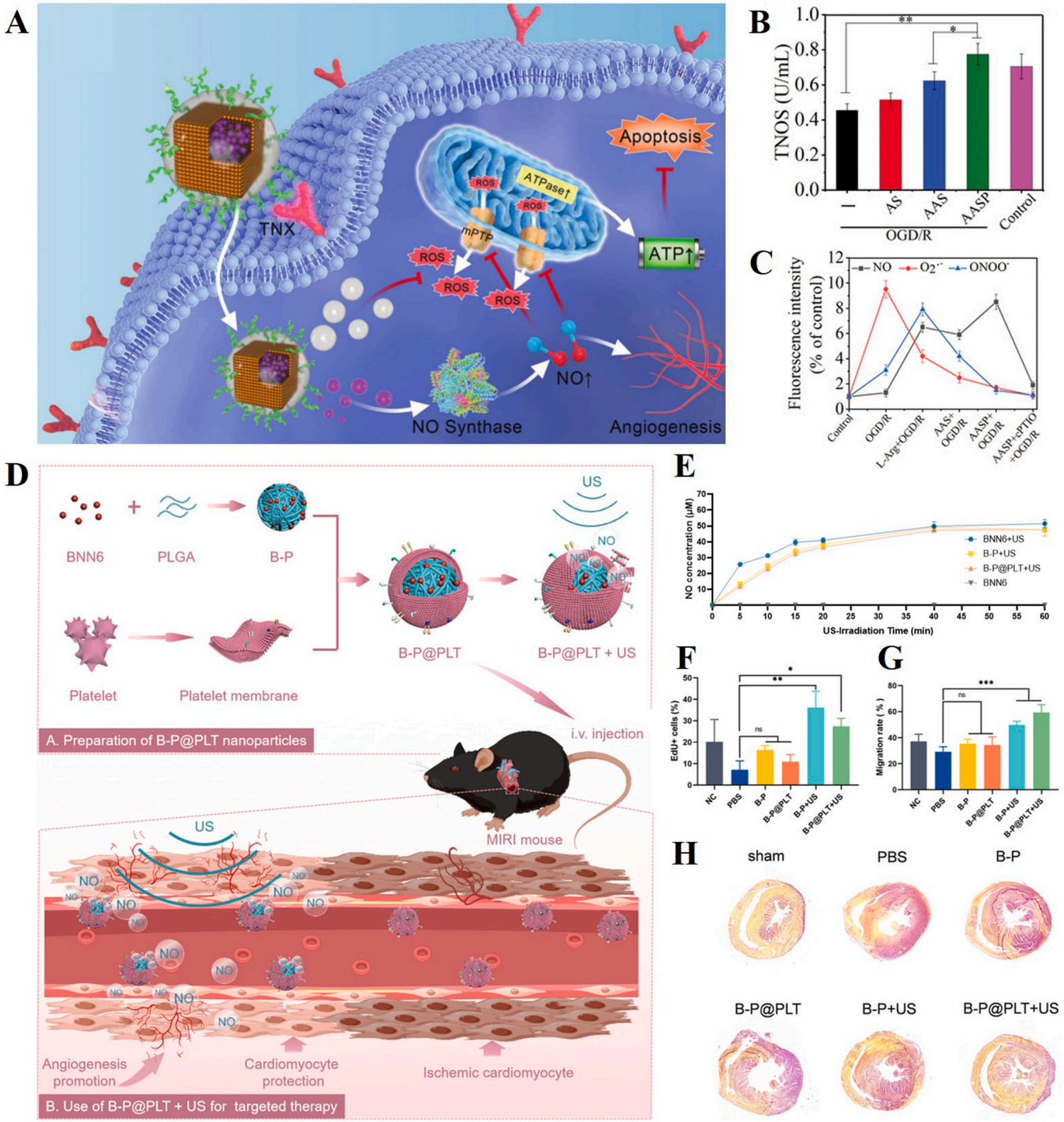


**Fig. 12.** Functional NMs promote NO generation and enhance myocardial repair. (A) AASP improved apoptosis in oxygen-glucose deprivation models *in vitro* by promoting NO production and maintaining mitochondrial function. (B) The effect of AS, AAS, and AASP (30 μg/mL) on TNOS activity in cells treated with OGD/R. (C) FI and fluorescence intensity statistics of NO, $O_2^-$, and $ONOO^-$ in cells after different treatments. Reprinted with permission from Ref. [211]. (D) Fabrication process of B-P@PLT NPs and therapeutic mechanism of B-P@PLT during MIRI. (E) Comparison of NO release behavior under continuous US irradiation versus intermittent US irradiation. (F) Quantitative data of positive cells measured using the EdU kit ($P < 0.05$). No statistical significance was found between the B-P group, B-P@PLT group, and PBS group ($P < 0.05$). (G) Quantitative data of HUVECs scratch wound healing migration. (H) Nagar-Olsen staining detects myocardial injury (red) and effect of NMs Treatment. Reprinted with permission from Ref. [212].

$H_2S$, NO, and CO exhibit distinct advantages for the treatment of MIRI, relying solely on any single gas therapy to modulate the pathological MIRI microenvironment may be insufficient. Accordingly, intelligent nanosystems capable of synergistically releasing multiple gases is emerging as a new research frontier for gas therapy, which may also help mimic the crosstalk between multiple gas signaling molecules in the physiological settings. The combined delivery of more than one gaseous molecules can target various MIRI-related pathologies, including oxidative stress, inflammation, apoptosis, and vascular dysfunction. Indeed, the combined release of NO and $H_2S$ donors has been shown to improve microvascular formation and regulate inflammatory responses [76]. Nevertheless, the concurrent delivery of multiple gaseous

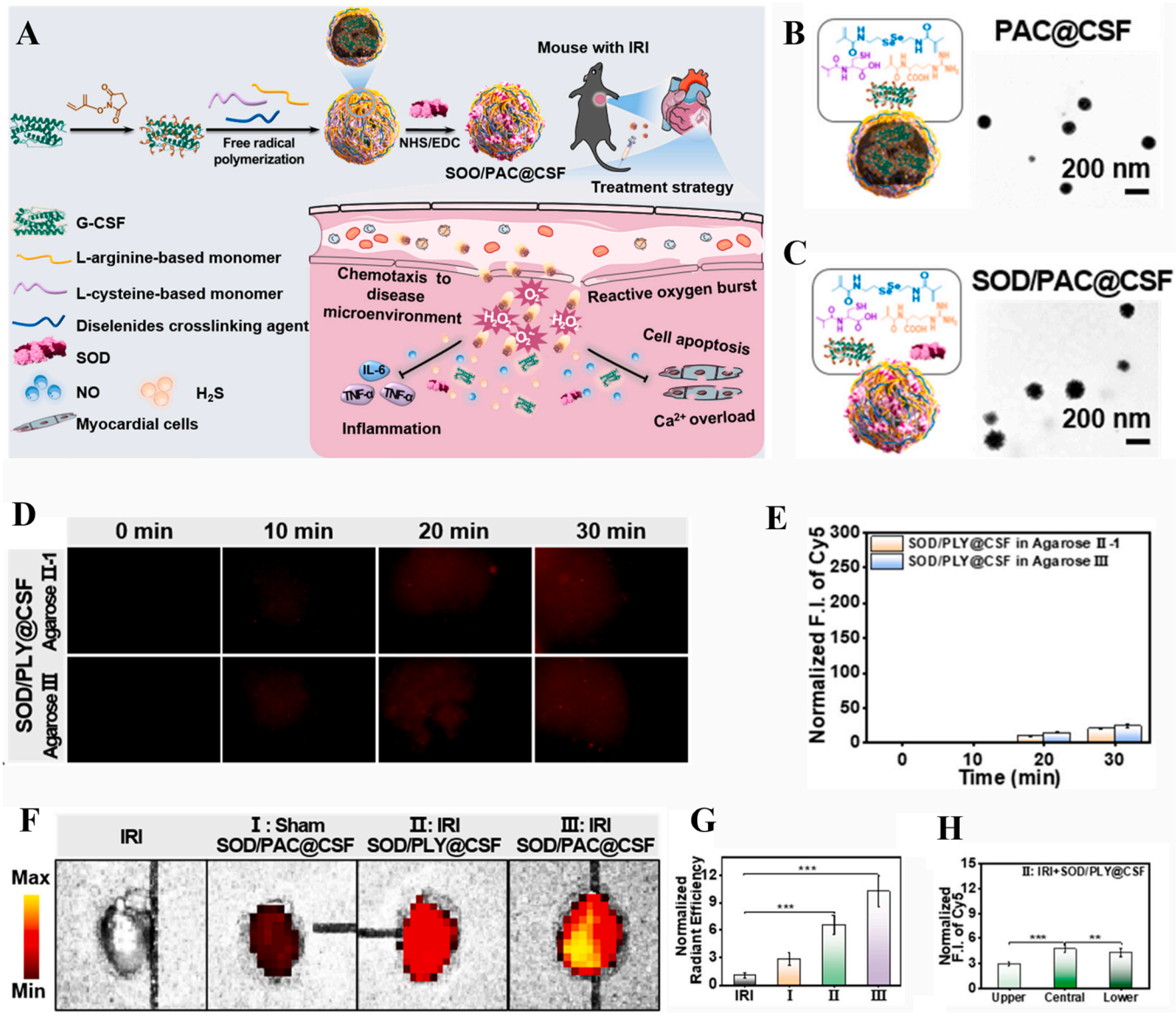


**Fig. 13. Schematic and characterization of SOD/PAC@CSF nanomotors: targeted delivery and therapeutic efficacy in MIRI.** (A) Schematic illustrating the fabrication of NO/$H_2S$ SOD/PAC@CSF nanomotors and their chemotaxis to the disease microenvironment, responsive drug release, and treatment of MIRI. (B, C) TEM images of PAC@CSF and SOD/PAC@CSF, showing the structural characteristics and size distribution. (D, E) Fluorescence images showing the chemotaxis behavior of SOD/PAC@CSF nanomotors in a static environment, quantifying their targeted motion. (F, G) *In vivo* distribution of Cy5-labeled SOD/PAC@CSF nanomotors in ischemic tissues, demonstrating their effective targeting to the ischemic heart. (H) Tissue-specific localization of G-CSF delivered by SOD/PAC@CSF nanomotors to the infarcted myocardium, confirming the therapeutic effect. Reprinted with permission from Ref. [76].

signaling molecules may require further optimizations to achieve spatiotemporal release kinetics of gases and maximize synergistic effects. Therefore, further research is required not only to unveil the biology of the pathological microenvironment but also to develop novel NMs for the on-demand delivery of various therapeutic gases.

### 3.3.3. *Nanoplatforms combining circadian rhythm for MIRI treatment*

Circadian rhythm, an evolutionarily conserved physiological mechanism, governs a wide array of physiological, psychological, and behavioral changes in organisms over a 24-h cycle. Circadian rhythm regulates critical processes including sleep-wake cycles, hormone secretion, metabolism, and cardiovascular function [235]. Notably, key cardiac activities, such as heart rate and blood pressure, exhibit robust distinct fluctuations. Growing evidence further suggests that the susceptibility of the heart to I/R injury also varies significantly throughout the day [236]. These temporal patterns highlight the potential of chronotherapy, which involves timing treatments in accordance with circadian biology, to optimize therapeutic outcomes in MIRI. Tailoring reperfusion therapy or drug administration to a patient's circadian phase may enhance efficacy and mitigate injury [35,237], opening a new dimension for personalized cardioprotective strategies.

The molecular basis for the heart's changing vulnerability lies in the rhythmic activity of its intrinsic circadian machinery. Key clock components act as master regulators, fine-tuning the myocardium's defense mechanisms across the 24-h cycle [238]. For instance, the transcription factor KLF15 oscillates to enhance the heart's antioxidant capacity during specific phases, thereby reducing injury severity [239]. Disruption of KLF15 eliminates this protective time window. In disease states such as diabetes, another clock protein, Rev-erbα, becomes dysregulated and can paradoxically exacerbate injury by activating detrimental pathways [240]. These findings confirm that the circadian system is not merely a passive timer but an active regulator of myocardial injury and

repair. This fundamental understanding provides a compelling rationale for developing therapies that are synchronized with, and even actively harness, these endogenous circadian rhythms to achieve optimal therapeutic effect.

Building upon this foundation of circadian molecular regulation, the innovative integration of chronobiology with advanced drug delivery systems has been pioneered. Zhang et al. developed hybrid NPs based on polyphenol, HA, resveratrol, oligomeric proanthocyanidins, and an MMP-responsive component (named as HA-RES-OPC-MMP NMs), that can operate in harmony with circadian rhythms (Fig. 14A) [196]. The treatment efficacy was found to be highly time-dependent: administration at ZT1 (subjective daytime in mice) enhanced myocardial repair and significantly activated the circadian regulator Sirt1. Conversely, the delivery at ZT13 (subjective nighttime) reduced Sirt1 expression and impaired regenerative effects (Fig. 14B–E). To further validate circadian dependence, Per1/2 knockout mice, which display disrupted locomotor rhythms, were examined. In these arrhythmic mice, the therapeutic benefit of NPs was nearly abolished, underscoring the essential role of an intact circadian system in mediating the nanotherapeutic effect (Fig. 14F–I). This pioneering study exemplifies the emergence of chrono-nanomedicine as a promising frontier in MIRI treatment.

## 4. Conclusions and future outlook

This review summarizes recent advances in the application of intrinsically functional NMs for the diagnosis and treatment of MIRI, emphasizing their unique potential to integrate real-time pathological sensing with targeted therapeutic intervention. By unifying imaging and therapy within single nanoplatforms, functional NMs represent a promising avenue toward precise, responsive, and personalized management of ischemic injury. Various imaging modalities, including FI, MRI, PAI, and CT, have each contributed to improved diagnostic accuracy. Notably, NM-based nano-biosensors have demonstrated increasing utility for early detection of pathological cues such as oxidative stress, inflammatory markers, and cardiac-specific enzymes. This capacity for real-time insight into disease progression provides a valuable foundation for imaging-guided therapeutic decision-making. While the clinical application of multimodal imaging remains in an early developmental stage, the convergence of multiple imaging techniques within flexible nanostructures holds strong potential to enhance diagnostic precision in the future.

On the therapeutic side, intrinsically functional NMs capable of catalytic ROS scavenging, gas release, gene delivery, and circadian rhythm modulation have shown great promise in restoring redox balance, preventing CM loss, and promoting cardiac tissue repair. The selection and prioritization of these therapeutic strategies should be informed by stage-specific pathological features and the dominant mechanisms of injury. Singular therapies may be appropriate for early or late stages of MIRI, while combinatorial regimens, particularly multifunctional nanoplatforms as outlined in Table 4, are more suitable for advanced MIRI where oxidative stress, inflammation, and tissue remodeling coexist. However, each therapeutic approach faces translational barriers. For example, nanozymes may lack sufficient catalytic specificity, potentially disrupting physiological redox signaling. Gas-based therapies require engineered carriers to overcome rapid degradation and to ensure spatial precision. In addition, gene therapies continue to be limited by delivery inefficiency and concerns regarding vector safety. Although nanoplatform-enhanced stem cell therapies can improve cell retention and functional performance, they raise issues related to long-term biosafety, complex manufacturing requirements under advanced therapy medicinal product (ATMP) regulations, and insufficient validation in models of comorbid disease.

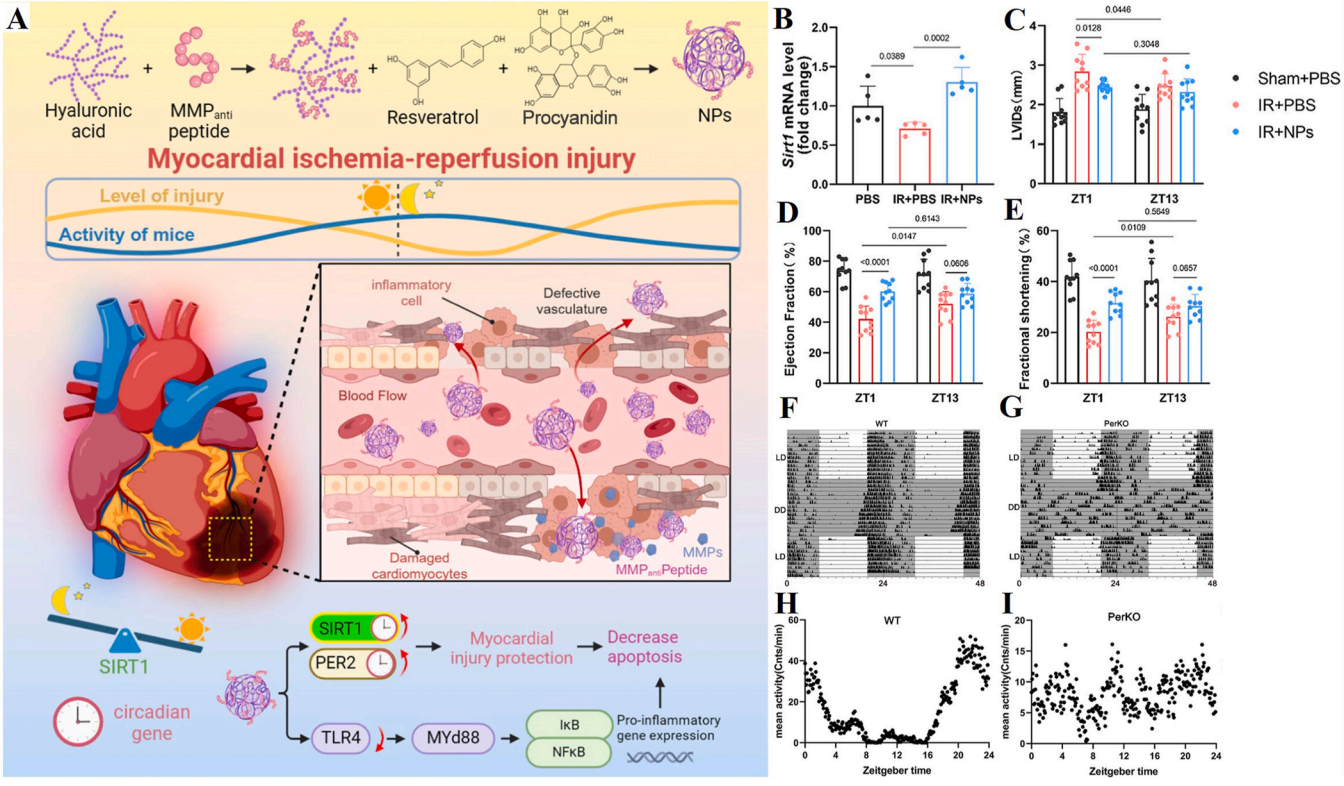


**Fig. 14. Circadian rhythm-dependent therapy by composite targeted polyphenol NPs for MIRI.** (A) Preparation of composite NPs, circadian rhythm characterization of MIRI and circadian rhythm-dependent treatment of MIRI with NPs. (B) Sirt1 was significantly activated in the left ventricle of mice treated with NPs at ZT1. (C–E) Comparison of LVID, EF, and FS in mouse hearts of different treatment groups at ZT1 and ZT13 (n = 10 mice per group). (F, G) Activity patterns of wild-type (WT) and Per1/2 knockout mice at different time periods (labeled LD and DD, representing light-dark cycles and constant darkness conditions) represented by running wheel experiments. (H, I) Movement patterns of mice in control group (WT) and experimental group (PerKO). Reprinted with permission from Ref. [196].

**Table 4**
Comparison of typical NM-mediated therapeutic strategies for MIRI.

| Strategy | Primary Mechanism | Optimal Therapeutic Phase (Post-Reperfusion) | Key Advantages | Major Limitations/Challenges |
|---|---|---|---|---|
| Nanozyme therapy | Catalytic ROS scavenging *via* enzyme mimicry | Immediate to hours post-reperfusion | High catalytic stability; broad-spectrum activity | Off-target effects; long-term biosafety |
| NM-mediated gas therapy | Controlled release of therapeutic gases (NO, $H_2S$, $H_2$, CO) | Hours to days post-reperfusion | Spatiotemporally controlled release; reduced systemic toxicity | Precise dosage control; gas toxicity risk |
| NM-mediated gene therapy | Targeted nucleic acid delivery to regulate key genes | Prior to or at reperfusion onset | High target specificity; potential for durable effects | Off-target effects; low *in vivo* transfection efficiency |
| NM-mediated stem cell therapy | Enhanced cell retention, survival, and paracrine function | 24–72 h post-reperfusion | Improved targeting and cell viability; synergistic effects | Long-term fate of engineered cells; complex manufacturing |

Beyond strategy-specific limitations, all nanoplatforms face fundamental translational challenges. One major issue is the limited cardiac enrichment efficiency of nanomedicines, which typically falls below 10 %, significantly constraining their therapeutic potential in MIRI. To address this, biomimetic strategies such as cell membrane-coated nanoparticles have been explored to prolong circulation time and evade immune recognition. However, these platforms still encounter practical limitations, including complex synthesis processes and poor batch-to-batch reproducibility. Recent advances in EC-targeted nanocarriers, which incorporate EC-specific peptides or membrane coatings, have shown potential to enhance cardiac delivery by promoting transendothelial transport into the ischemic myocardium [241,242]. Nonetheless, quantitative data on their delivery efficiency and long-term stability in clinical settings remain scarce. Furthermore, the *in vivo* behavior of nanocarriers is difficult to predict due to dynamic protein corona formation, heterogeneous target expression, and pathophysiological variability within the ischemic niche. Batch-to-batch variability in nanoparticle synthesis, affecting properties such as size, charge, encapsulation efficiency, and surface chemistry, can also alter pharmacokinetics and therapeutic outcomes. These considerations highlight the need for stringent manufacturing control, scalable and reproducible production methods, and more robust *in vivo* predictive models.

In parallel, AI and ML are poised to revolutionize the development of nanomedicine for MIRI by enabling a closed-loop workflow that integrates rational design, diagnostic imaging, and adaptive therapy. ML models can accelerate the optimization of nanoparticle formulations by precisely tuning parameters such as size, surface charge, and surface chemistry to improve cardiac targeting and biodistribution in ischemic myocardium [243]. While direct applications of deep learning models such as convolutional neural networks (CNNs) and generative adversarial networks (GANs) in analyzing NP-enhanced cardiac imaging and MIRI biodistribution patterns are still emerging, their potential is increasingly recognized. In the near term, these tools are expected to automate the quantification of myocardial injury and NM localization from multimodal imaging datasets, transforming qualitative assessments into objective, high-throughput analyses. Looking ahead, as experimental datasets expand, the integration of AI with functional NMs will enable iterative feedback loops, wherein imaging outcomes inform the computational redesign of smarter NPs that, in turn, generate richer diagnostic data. This synergy is expected to support highly personalized intervention strategies and reduce reliance on costly or high-radiation imaging modalities, thereby improving the accessibility and precision of patient-specific MIRI management.

Finally, while this review has focused on functional NMs in the context of MIRI, the underlying design principles and therapeutic frameworks discussed here may also be extended to other ischemia-reperfusion-related disorders such as cerebral or renal I/R injury. Continued interdisciplinary collaboration across materials science, nanotechnology, medicine, and computational modeling will be essential for the development of smarter, safer, and more adaptive nanotheranostic systems. These efforts are expected to drive the transformation toward precision cardiovascular and systemic ischemic care.

## CRediT authorship contribution statement

**Jie Li:** Writing – original draft, Writing – review & editing, Visualization, Investigation. **Muhammad Shafiq:** Writing – original draft, Writing – review & editing, Visualization, Investigation. **Minghua Yao:** Writing – review & editing, Funding acquisition. **Zehua Liu:** Writing – review & editing, Funding acquisition. **Ruizhi Tian:** Writing – review & editing. **Fangqiao Zheng:** Writing – review & editing. **Chan Lu:** Writing – review & editing. **Ming Ma:** Conceptualization, Writing – review & editing, Funding acquisition.

## Declaration of competing interest

The authors declare that they have no known competing financial interests or personal relationships that could have appeared to influence the work reported in this paper.

## Acknowledgement

This work was supported by the National Natural Science Foundation of China (Grant Nos. 52472290, 82171951), the Shanghai Outstanding Young Medical Talents Training Plan (Grant No. 2022YQ044), the Student Training Program for Innovation and Entrepreneurship of the Hangzhou Institute for Advanced Study, University of Chinese Academy of Sciences (UCAS), the Finnish Foundation for Cardiovascular Research, and the European Union's Horizon Europe research and innovation program under the Marie Skłodowska-Curie grant agreement (Grant No. 10112661).

## References

[1] Y. Liu, L. Li, Z. Wang, J. Zhang, Z. Zhou, Myocardial ischemia-reperfusion injury; molecular mechanisms and prevention, Microvasc. Res. 149 (2023) 104565.
[2] E. Bertero, T.A. Popoiu, C. Maack, Mitochondrial calcium in cardiac ischemia/reperfusion injury and cardioprotection, Basic Res. Cardiol. 119 (4) (2024) 569–585.
[3] P.J. Zhu, S.Y. Hu, Q.H. Jin, D.D. Li, F. Tian, S. Toan, Y. Li, H. Zhou, Y.D. Chen, Ripk3 promotes ER stress-induced necroptosis in cardiac IR injury: a mechanism involving calcium overload/XO/ROS/mPTP pathway, Redox Biol. 16 (2018) 157–168.
[4] T.J. Zhao, Y.Y. Huang, W.S. Chen, W.M. Qi, J. Wang, Y.C. Xia, J. Zhou, X.Y. Long, Y.Y. Nan, Q. Huang, K.L. Ai, Polydopamine as a biocompatible and precise mitochondrial targeted therapeutic platform for reversing myocardial ischemia-reperfusion injury, Bioact. Mater. 53 (2025) 908–931.
[5] A. Rauf, M. Shah, D.M. Yellon, S.M. Davidson, Role of caspase 1 in ischemia/reperfusion injury of the myocardium, J. Cardiovasc. Pharmacol. 74 (3) (2019) 194–200.
[6] Y.X. Li, Z.K. Lou, F. Liu, Y. Liu, C.F. Wang, Y.W. Wang, W. Qian, D.Y. Li, T.D. Xu, The impact of lipid metabolism on ferroptosis in myocardial ischemia-reperfusion injury, Apoptosis 30 (2025) 2761–2775.
[7] Q. Xiang, X. Yi, X.H. Zhu, X. Wei, D.S. Jiang, Regulated cell death in myocardial ischemia - reperfusion injury, Trends Endocrinol. Metabol. 35 (3) (2024) 219–234.
[8] M.H. Liu, R.M. Chen, Z.W. Zheng, S.L. Xu, C.Y. Hou, Y.N. Ding, M.L. Zhang, M. H. Bao, B.S. He, S. Li, Mechanisms of inflammatory microenvironment formation in cardiometabolic diseases: molecular and cellular perspectives, Front. Cardiovasc. Med. 11 (2025) 1529903.

[9] G. Heusch, Myocardial ischaemia-reperfusion injury and cardioprotection in perspective, Nat. Rev. Cardiol. 17 (12) (2020) 773–789.
[10] S. Ben-Haim, J. Kennedy, Z. Keidar, Novel cadmium zinc telluride devices for myocardial perfusion imaging-technological aspects and clinical applications, Semin. Nucl. Med. 46 (4) (2016) 273–285.
[11] P. Slomka, G. Germano, Optimizing radiation dose and imaging time with conventional myocardial perfusion SPECT: technical aspects, J. Nucl. Cardiol. 24 (3) (2016) 888–891.
[12] K. Zhu, K. Wang, R. Zhang, Z. Zhu, W. Wang, B. Yang, J. Zhao, Y. Shen, Iron chelators loaded on myocardiocyte mitochondria-targeted nanozyme system for treating myocardial ischemia-reperfusion injury in mouse models, J. Nanobiotechnol. 23 (1) (2025) 112.
[13] X. Chen, H. Chen, L. Zhu, Q. Li, P. Sun, M. Spanos, C. Su, X. Wang, L. Zhao, R. Gui, T. Wang, X. Wang, X. Zhou, Z. Chen, Cascade nanozyme delivering miRNA to ischemic heart to alleviate myocardial ischemia-reperfusion injury, Small (2025) 2502778.
[14] J. Riegler, A. Liew, S.O. Hynes, D. Ortega, T. O'Brien, R.M. Day, T. Richards, F. Sharif, Q.A. Pankhurst, M.F. Lythgoe, Superparamagnetic iron oxide nanoparticle targeting of MSCs in vascular injury, Biomaterials 34 (8) (2013) 1987–1994.
[15] J. Zhang, C. Cai, S. Razzaque, I. Hussain, Q.-W. Lu, B. Tan, Synthesis of water-soluble and highly fluorescent gold nanoclusters for $Fe^{3+}$ sensing in living cells using fluorescence imaging, J. Mater. Chem. B 5 (28) (2017) 5608–5615.
[16] E. Marin, C. Tapeinos, S. Lauciello, G. Ciofani, J.R. Sarasua, A. Larranaga, Encapsulation of manganese dioxide nanoparticles into layer-by-layer polymer capsules for the fabrication of antioxidant microreactors, Mater. Sci. Eng., C 117 (2020) 111349.
[17] E.M.Y. Chow, K.L. Foo, S.J. Tan, S.C.B. Gopinath, M. Kashif, C.Y. Heah, Y. M. Liew, J.-C. Lim, S.-M. Tan, Functionalized carbon nanotube-based biosensor for highly sensitive detection of cardiac troponin I, J. Mater. Sci. Mater. Electron. 35 (2024) 2302.
[18] A. Pourali, J. Barar, M.R. Rashidi, G. Pavon-Djavid, Y. Omidi, Ultra-sensitive facile CdS nanocrystals-based electrochemical biosensor to detect myocardial infarction marker troponin, Microchem. J. 165 (2021) 106107.
[19] J. Zhang, M. Xiao, R.G. Su, T. Kong, D. Zhang, C.W. Zhou, G.S. Cheng, Silicon nanowire FET biosensor and its application in acute myocardial infarction, Nanotechnology 35 (2023) 112001.
[20] M. Donato, P. Evelson, R.J. Gelpi, Protecting the heart from ischemia/reperfusion injury: an update on remote ischemic preconditioning and postconditioning, Curr. Opin. Cardiol. 32 (6) (2017) 784–790.
[21] J. Zhang, Y. Lu, P. Yu, Z. Li, Y. Liu, J. Zhang, X. Tang, S. Yu, Therapeutic hypothermia alleviates myocardial ischaemia-reperfusion injury by inhibiting inflammation and fibrosis via the mediation of the SIRT3/NLRP3 signalling pathway, J. Cell Mol. Med. 26 (19) (2022) 4995–5007.
[22] P. Chazelas, C. Steichen, F. Favreau, P. Trouillas, P. Hannaert, R. Thuillier, S. Giraud, T. Hauet, J. Guillard, Oxidative stress evaluation in ischemia reperfusion models: characteristics, limits and perspectives, Int. J. Mol. Sci. 22 (5) (2021) 2366.
[23] J. Hefler, B.A. Marfil-Garza, S. Campbell, D.H. Freed, A.M.J. Shapiro, Preclinical systematic review & meta-analysis of cyclosporine for the treatment of myocardial ischemia-reperfusion injury, Ann. Transl. Med. 10 (18) (2022) 954.
[24] J.-F. Peng, O.M. Salami, C. Lei, D. Ni, O. Habimana, G.-H. Yi, Targeted mitochondrial drugs for treatment of myocardial ischaemia-reperfusion injury, J. Drug Target. 30 (8) (2022) 833–844.
[25] M. Hortmann, S. Robinson, M. Mohr, M. Mauler, D. Stallmann, J. Reinoehl, D. Duerschmied, K. Peter, J. Carr, C.M. Gibson, C. Bode, I. Ahrens, The mitochondria-targeting peptide elamipretide diminishes circulating HtrA2 in ST-segment elevation myocardial infarction, Eur. Heart J. Acute Cardiovasc. Care 8 (8) (2019) 695–702.
[26] N. Li, Y. Chen, X. Xia, C. Mao, M. Wan, Progress of nanomaterials in the treatment of ischemic heart disease, J. Mater. Chem. B 13 (21) (2025) 6021–6043.
[27] Y. Jiang, R. Jiang, Z. Xia, M. Guo, Y. Fu, X. Wang, J. Xie, Engineered neutrophil membrane-camouflaged nanocomplexes for targeted siRNA delivery against myocardial ischemia reperfusion injury, J. Nanobiotechnol. 23 (1) (2025) 134.
[28] Y. Liu, S. Yan, M. Wu, Y. Xie, J. Sheng, X. Sun, L. Kang, B. Xu, N. Gu, Subaxillary implantation of mesenchymal stem cell spheroids is a novel therapy for myocardial ischemia reperfusion injury, Chem. Eng. J. 508 (2025) 160906.
[29] T. Yin, N. Wang, F. Jia, Y. Wu, L. Gao, J. Zhang, R. Hou, Exosome-based WTAP siRNA delivery ameliorates myocardial ischemia-reperfusion injury, Eur. J. Pharm. Biopharm. 197 (2024) 114218.
[30] G.J. Schena, E.K. Murray, A.N. Hildebrand, A.L. Headrick, Y. Yang, K.A. Koch, H. Kubo, D. Eaton, J. Johnson, R. Berretta, S. Mohsin, R. Kishore, T.A. McKinsey, J.W. Elrod, S.R. Houser, Cortical bone stem cell-derived exosomes' therapeutic effect on myocardial ischemia-reperfusion and cardiac remodeling, Am. J. Physiol. Heart Circ. Physiol. 321 (6) (2021) H1014–H1029.
[31] X. Zhang, Q. Liu, R. Zhao, Z. Pang, W. Zhang, T. Qi, M. Zhu, H. Kang, M. Qian, Y. Wan, R. Wang, S. Wang, X. Huang, J. Zhuang, Rational design of genetically engineered mitochondrial-targeting nanozymes for alleviating myocardial ischemic-reperfusion Injury (vol 2, pg 663, 2025), Nano Lett. 25 (9) (2025) 3681–3682.
[32] X. Bi, Z. Wang, J. He, Recent advances in biomimetic nanodelivery systems for the treatment of myocardial ischemia reperfusion injury, Colloids Surf. B Biointerfaces 247 (2025) 114414.
[33] I. Skrlec, J. Milic, M. Heffer, J. Wagner, B. Peterlin, Circadian clock genes and circadian phenotypes in patients with myocardial infarction, Adv. Med. Sci. 64 (2) (2019) 224–229.
[34] Y. Oyama, L. Walker, T. Eckle, Targeting circadian PER2 as therapy in myocardial ischemia and reperfusion injury (vol 38, pg 1262, 2021), Chronobiol. Int. 38 (9) (2021) 1262–1273.
[35] I. Rabinovich-Nikitin, L.A. Kirshenbaum, Circadian regulated control of myocardial ischemia-reperfusion injury, Trends Cardiovasc. Med. 34 (1) (2024) 1–7.
[36] B. Zhang, C. Wang, M. Guo, F. Zhu, Z. Yu, W. Zhang, W. Li, Y. Zhang, W. Tian, Circadian rhythm-dependent therapy by composite targeted polyphenol nanoparticles for myocardial ischemia-reperfusion injury, ACS Nano 18 (41) (2024) 28154–28169.
[37] A.M. Villalba-Rodriguez, L.Y. Martinez-Zamudio, S.A.H. Martinez, J. A. Rodriguez-Hernandez, E.M. Melchor-Martinez, E.A. Flores-Contreras, R. B. Gonzalez-Gonzalez, R. Parra-Saldivar, Nanomaterial constructs for catalytic applications in biomedicine: nanobiocatalysts and nanozymes, Top. Catal. 66 (9–12) (2023) 707–722.
[38] S.W. Hu, T. Ding, H. Tang, H. Guo, W. Cui, Y. Shu, Nanobiomaterial vectors for improving gene editing and gene therapy, Mater. Today 66 (2023) 114–136.
[39] I. Lugoloobi, Y. Fang, F. Jiang, G. Zhang, J. Hu, Gaseous signaling molecule-releasing hybrid nanomaterials for therapeutic applications, Giant 14 (2023) 100513.
[40] H. Yuan, H. Liang, P. Hou, J. Li, Advanced nanomaterials for multimodal molecular imaging, Chem. Res. Chin. Univ. 37 (4) (2021) 840–845.
[41] T. Repenko, A. Rix, A. Nedilko, J. Rose, A. Hermann, R. Vinokur, S. Moli, R. Cao-Milan, M. Mayer, G. von Plessen, A. Fery, L. De Laporte, W. Lederle, D.N. Chigrin, A.J.C. Kuehne, Strong photoacoustic signal enhancement by coating gold nanoparticles with melanin for biomedical imaging, Adv. Funct. Mater. 28 (7) (2018) 1705607.
[42] M. Kim, S.M. Ko, J.-M. Kim, J. Son, C. Lee, W.-K. Rhim, J.-M. Nam, Dealloyed intra-nanogap particles with highly robust, quantifiable surface-enhanced raman scattering signals for biosensing and bioimaging applications, ACS Cent. Sci. 4 (2) (2018) 277–287.
[43] J. Lin, X. Chen, P. Huang, Graphene-based nanomaterials for bioimaging, Adv. Drug Deliv. Rev. 105 (2016) 242–254.
[44] B.R. Smith, S.S. Gambhir, Nanomaterials for in vivo imaging, Chem. Rev. 117 (3) (2017) 901–986.
[45] Z. Yang, T. Xu, H. Li, M. She, J. Chen, Z. Wang, S. Zhang, J. Li, Zero-Dimensional carbon nanomaterials for fluorescent sensing and imaging, Chem. Rev. 123 (18) (2023) 11047–11136.
[46] M. Negahdary, A. Sharma, T.D. Anthopoulos, L. Angnes, Recent advances in electrochemical nanobiosensors for cardiac biomarkers, Trends Anal. Chem. 164 (2023) 117104.
[47] A. Singh, D. Bains, W.M. Hassen, N. Singh, J.J. Dubowski, Formation of a Au/$Au_9Ga_4$ alloy nanoshell on a bacterial surface through galvanic displacement reaction for high-contrast imaging, ACS Appl. Bio Mater. 3 (1) (2020) 477–485.
[48] T.-L. Ma, W.-T. Du, M.G. Mohamed, S.-W. Kuo, Luminescent hollow spherical nanoparticles with enhanced imaging contrast through hydrogen bonding connected micelles, Eur. Polym. J. 210 (2024) 112954.
[49] Z. Zhang, J. Liu, Y. Dai, M. Ye, Y. Sun, K. Zhang, J.-J. Xu, Dual-mode SERS-ECL biosensor for robust detection of circulating miRNAs based on in-situ synthesized probes, Chem. Eng. J. 495 (2024) 153607.
[50] M.S. Al Huq, B. Gururajan, P. Srinivasan, Next-generation bioinspired 2D-MXene devices for cardiovascular disease diagnosis: a state-of-the-art review on materials interface and critical challenges, Coord. Chem. Rev. 535 (2025) 216631.
[51] T. Kong, R. Su, B. Zhang, Q. Zhang, G. Cheng, CMOS-compatible, label-free silicon-nanowire biosensors to detect cardiac troponin I for acute myocardial infarction diagnosis, Biosens. Bioelectron. 34 (1) (2012) 267–272.
[52] A.L. Ferreira, L.F. de Lima, A.S. Moraes, R.J.G. Rubira, C.J.L. Constantino, F. L. Leite, A.O. Delgado-Silva, M. Ferreira, Development of a novel biosensor for Creatine Kinase (CK-MB) using Surface Plasmon Resonance (SPR), Appl. Surf. Sci. 554 (2021) 149565.
[53] L.Y. Beliaev, S. Kim, B.F.S. Nielsen, M.V. Evensen, A.-I. Bunea, R. Malureanu, L. R. Lindvold, O. Takayama, P.E. Andersen, A.V. Lavrinenko, Optical biosensors based on nanostructured silicon high-contrast gratings for myoglobin detection, ACS Appl. Nano Mater. 6 (13) (2023) 12364–12371.
[54] P. Fan, Q. Li, Z. Zhang, S. Ni, P. Jiang, S. Sun, L. Li, A novel and universal dual-channel signal amplification aptasensing platform for ultrasensitive and rapid detection of cardiac biomarkers based on the mutual regulation of bimetallic organic framework and silver nanoclusters, Talanta 288 (2025) 127745.
[55] J. Zhang, K. Sun, J. Ren, H. Wang, J. Cheng, An electrochemical metallic nanowire aptasensor for rapid and ultrasensitive detection of cardiac troponin I, Sensor. Actuator. B Chem. 401 (2023) 135001.
[56] T. Banerjee, T. Tummala, R. Elliott, V. Jain, W. Brantley, L. Hadorn, S. Santra, Multimodal magneto-fluorescent nanosensor for rapid and specific detection of blood-borne pathogens, ACS Appl. Energy Mater. 2 (9) (2019) 5587–5593.
[57] A. Pourali, M.R. Rashidi, J. Barar, G. Pavon-Djavid, Y. Omidi, Voltammetric biosensors for analytical detection of cardiac troponin biomarkers in acute myocardial infarction, Trends Anal. Chem. 134 (2020) 116123.
[58] K. Kim, C. Park, D. Kwon, D. Kim, M. Meyyappan, S. Jeon, J.-S. Lee, Silicon nanowire biosensors for detection of cardiac troponin I (cTnI) with high sensitivity, Biosens. Bioelectron. 77 (2015) 695–701.
[59] H. He, M. Long, Y. Duan, N. Gu, Prussian blue nanozymes: progress, challenges, and opportunities, Nanoscale 15 (31) (2023) 12818–12839.
[60] G. Seo, G. Lee, M.J. Kim, S.H. Baek, M. Choi, K.B. Ku, C.S. Lee, S. Jun, D. Park, H. G. Kim, S.J. Kim, J.O. Lee, B.T. Kim, E.C. Park, S.I. Kim, Rapid detection of COVID-19 causative virus (SARS-CoV-2) in human nasopharyngeal swab

specimens using field-effect transistor-based biosensor, ACS Nano 14 (4) (2020) 5135–5142.
[61] W.P. Hu, J.S. Wang, Y.P. Chiu, T.C. Huang, B.K. Yadlapalli, W.Y. Chen, The optimal ionic concentration of sensing buffer in the detection of RNA by using the DNA probe with the silicon nanowire field-effect transistor (SiNW-FET), Talanta 295 (2025) 128375.
[62] P. Li, Y. Ye, Y. Li, Z. Xie, L. Ye, J. Huang, A MoS2 nanosheet-based CRISPR/Cas12a biosensor for efficient miRNA quantification for acute myocardial infarction, Biosens. Bioelectron. 251 (2024) 116129.
[63] N. Radha Shanmugam, S. Muthukumar, S. Chaudhry, J. Anguiano, S. Prasad, Ultrasensitive nanostructure sensor arrays on flexible substrates for multiplexed and simultaneous electrochemical detection of a panel of cardiac biomarkers, Biosens. Bioelectron. 89 (2016) 764–772.
[64] Q. Liu, N. Aroonyadet, Y. Song, X. Wang, X. Cao, Y. Liu, S. Cong, F. Wu, M. E. Thompson, C. Zhou, Highly sensitive and quick detection of acute myocardial infarction biomarkers using In2O3 nanoribbon biosensors fabricated using shadow masks, ACS Nano 10 (11) (2016) 10117–10125.
[65] M.L. Yola, N. Atar, Development of cardiac troponin-I biosensor based on boron nitride quantum dots including molecularly imprinted polymer, Biosens. Bioelectron. 126 (2018) 418–424.
[66] W.Y. Li, R.R. Zhang, X.Y. Zhang, S. Wu, T.C. Ma, Y. Hou, J.F. Zeng, M.Y. Gao, Precise diagnosis of cardiac-cerebral vascular diseases with magnetic resonance imaging-based nanoprobes, Iradiology 2 (3) (2024) 264–284.
[67] A. Khalid, S. Tomljenovic-Hanic, Emerging fluorescent nanoparticles for non-invasive bioimaging, Molecules 29 (23) (2024) 5594.
[68] C. Wei, Z.Y. Jiang, C.C. Li, P.F. Li, Q.R. Fu, Nanomaterials responsive to endogenous biomarkers for cardiovascular disease theranostics, Adv. Funct. Mater. 33 (26) (2023) 2214655.
[69] X.B. Ma, Z.J. Fan, J.Y. Peng, L.M. Nie, Ischemic area-targeting and self-monitoring nanoprobes ameliorate myocardial ischemia/reperfusion injury by scavenging ROS and counteracting cardiac inflammation, Adv. Sci. 12 (11) (2025) 2414518.
[70] P.H. Kee, D. Danila, CT imaging of myocardial scar burden with CNA35-conjugated gold nanoparticles, Nanomed. Nanotechnol. Biol. Med. 14 (6) (2018) 1941–1947.
[71] L. Gong, Y. Weng, W. Zhou, K. Zhang, W. Li, J. Jiang, J. Zhu, *In vivo* CT imaging of gold nanoparticle-labeled exosomes in a myocardial infarction mouse model, Ann. Transl. Med. 9 (6) (2021) 504.
[72] Q. Wang, T. Wang, C. Lio, X. Yu, X. Chen, L. Liu, Y. Wu, H. Huang, L. Qing, P. Luo, Surface hydrolysis-designed AuNPs-zwitterionic-glucose as a novel tool for targeting macrophage visualization and delivery into infarcted hearts, J. Contr. Release 356 (2023) 678–690.
[73] Y. Li, R. Wang, W. Zheng, Y. Li, Silica-coated Ga(III)-Doped ZnO: $Yb^{3+}$, $Tm^{3+}$ upconversion nanoparticles for high-resolution in vivo bioimaging using near-infrared to near-infrared upconversion emission, Inorg. Chem. 58 (12) (2019) 8230–8236.
[74] S. Sivagnanam, K. Das, M. Basak, T. Mahata, A. Stewart, B. Maity, P. Das, Self-assembled dipeptide based fluorescent nanoparticles as a platform for developing cellular imaging probes and targeted drug delivery chaperones, Nanoscale Adv. 4 (6) (2022) 1694–1706.
[75] K. Montet-Abou, J.-L. Daire, J.-N. Hyacinthe, M. Jorge-Costa, K. Grosdemange, F. Mach, A. Petri-Fink, H. Hofmann, D.R. Morel, J.-P. Vallee, X. Montet, *In vivo* labelling of resting monocytes in the reticuloendothelial system with fluorescent iron oxide nanoparticles prior to injury reveals that they are mobilized to infarcted myocardium, Eur. Heart J. 31 (11) (2010) 1410–1420.
[76] N. Li, C. Huang, J. Zhang, J. Zhang, J. Huang, S. Li, X. Xia, Z. Wu, C. Chen, S. Tang, X. Xiao, H. Gong, Y. Dai, C. Mao, M. Wan, Chemotactic NO/$H_2S$ nanomotors realizing cardiac targeting of G-CSF against myocardial ischemia-reperfusion injury, ACS Nano 17 (13) (2023) 12573–12593.
[77] Y. Zhang, X. Chen, L. Liu, J. Tian, L. Hao, H.-t. Ran, Photoacoustic imaging of myocardial infarction region using non-invasive fibrin-targeted nanoparticles in a rat myocardial ischemia-reperfusion model, Int. J. Nanomed. 16 (2021) 1331–1344.
[78] Y. Sun, P. Zhang, Y. Li, Y. Hou, C. Yin, Z. Wang, Z. Liao, X. Fu, M. Li, C. Fan, D. Sun, L. Cheng, Light-activated gold-selenium core-shell nanocomposites with NIR-II photoacoustic imaging performances for heart-targeted repair, ACS Nano 16 (11) (2022) 18667–18681.
[79] X. Zhao, Y. Qin, B. Wang, J. Liu, Y. Wang, K. Chen, J. Zhao, L. Zhang, Y. Wu, L. Liu, A non-invasive osteopontin-targeted phase changeable fluorescent nanoprobe for molecular imaging of myocardial fibrosis, Nanoscale Adv. 6 (14) (2024) 3590–3601.
[80] X. Chen, Y. Zhang, H. Zhang, L. Zhang, L. Liu, Y. Cao, H. Ran, J. Tian, A non-invasive nanoparticles for multimodal imaging of ischemic myocardium in rats, J. Nanobiotechnol. 19 (1) (2021) 82, 20 (2022) 382.
[81] F. Li, L. Chen, S. Zhong, J. Chen, Y. Cao, H. Yu, H. Ran, Y. Yin, C. Reutelingsperger, S. Shu, Z. Ling, Collagen-targeting self-assembled nanoprobes for multimodal molecular imaging and quantification of myocardial fibrosis in a rat model of myocardial infarction, ACS Nano 18 (6) (2024) 4886–4902.
[82] W. Yang, Y. Wang, C. Fu, C. Li, F. Feng, H. Li, L. Tan, H. Qu, H. Hui, J. Wang, J. Tian, L. Long, Quantitative visualization of myocardial ischemia- reperfusion-induced cardiac lesions via ferroptosis, Theranostics 14 (3) (2024) 1081–1097.
[83] A. Varga-Szemes, F.G. Meinel, C.N. De Cecco, S.R. Fuller, R.R. Bayer II, U. J. Schoepf, CT myocardial perfusion imaging, Am. J. Roentgenol. 204 (3) (2015) 487–497.
[84] C.B. Hirschfeld, M. Dondi, T.N.B. Pascual, M. Mercuri, J. Vitola, G. Karthikeyan, N. Better, J.J. Mahmarian, S.E. Bouyoucef, H.H.-S. Bom, V. Lele, V.P.C. Magboo, E. Alexanderson, A.H. Allam, M.H. Al-Mallah, A. Flotats, S. Jerome, P. A. Kaufmann, O. Luxenburg, S.R. Underwood, M.M. Rehani, J. Vassileva, D. Paez, A.J. Einstein, I.I. Grp, Worldwide diagnostic reference levels for single-photon emission computed tomography myocardial perfusion imaging findings from INCAPS, JACC, Cardiovasc. Imaging 14 (3) (2021) 657–665.
[85] B. Abadie, N. Chan, Z. Sharalaya, P. Bhat, S. Harb, M. Jacob, W.H. Tang, P. Cremer, W. Jaber, Positron emission tomography/computed tomography perfusion imaging with myocardial blood flow has diagnostic and prognostic value for cardiac allograft vasculopathy, Eur. Heart J. 43 (2022), 305-305.
[86] M.P. Joshi, A. Chaudhari, P.S. Kharkar, S.V. Joshi, Chemistry of Iodinated Contrast Media (ICM): a mini review, Mini-Reviews Org. Chem. 18 (7) (2021) 885–901.
[87] T.C. Owens, N. Anton, M.F. Attia, CT and X-ray contrast agents: current clinical challenges and the future of contrast, Acta Biomater. 171 (2023) 19–36.
[88] M. Sharifi, F. Attar, A.A. Saboury, K. Akhtari, N. Hooshmand, A. Hasan, M.A. El-Sayed, M. Falahati, Plasmonic gold nanoparticles: optical manipulation, imaging, drug delivery and therapy, J. Contr. Release 311 (2019) 170–189.
[89] Q.L. Wang, T.T. Wang, C. Lio, X.A. Yu, X.Y. Chen, L.C. Liu, Y.J. Wu, H. Huang, L. S. Qing, P. Luo, Surface hydrolysis-designed AuNPs-zwitterionic-glucose as a novel tool for targeting macrophage visualization and delivery into infarcted hearts, J. Contr. Release 356 (2023) 678–690.
[90] B.M. King, J. Fiegel, Zwitterionic polymer coatings enhance gold nanoparticle stability and uptake in various biological environments, AAPS J. 24 (1) (2022) 18.
[91] R. Chandrasekaran, T. Madheswaran, N. Tharmalingam, R.J.C. Bose, H. Park, D. H. Ha, Labeling and tracking cells with gold nanoparticles, Drug Discov. Today 26 (1) (2020) 94–105.
[92] N. Aslan, B. Ceylan, M.M. Koc, F. Findik, Metallic nanoparticles as X-Ray computed tomography (CT) contrast agents: a review, J. Mol. Struct. 1219 (2020) 128599.
[93] H. Fang, Y. Chen, Z. Jiang, W. He, Z. Guo, Fluorescent probes for biological species and microenvironments: from rational design to bioimaging applications, Acc. Chem. Res. 56 (3) (2023) 258–269.
[94] M. Ziegler, X. Xu, M.L. Yap, H. Hu, J. Zhang, K. Peter, A self-assembled fluorescent nanoprobe for imaging and therapy of cardiac ischemia/reperfusion injury, Adv. Therapeut. 2 (3) (2019) 1800133.
[95] X.Z. Luo, C.L. Zhang, C.Y. Yue, Y.L. Jiang, F. Yang, Y.Z. Xian, A near-infrared light-activated nanoprobe for simultaneous detection of hydrogen polysulfide and sulfur dioxide in myocardial ischemia-reperfusion injury, Chem. Sci. 14 (48) (2023) 14290–14301.
[96] A.P. Shi, Y.L. Zeng, D.X. Xin, Y.Y. Zhou, L.Z. Zhao, J.J. Peng, Real-time visualization of the antioxidative potency of drugs for the prevention of myocardium ischemia-reperfusion injury by a NIR fluorescent nanoprobe, ACS Sens. 7 (12) (2022) 3867–3875.
[97] S.M. Anju, K.A. Merin, S. Varghese, A.I. Shkhair, G. Rajeevan, G. Indongo, S. George, Antibody-functionalized gold nanoclusters/gold nanoparticle platform for the fluorescence turn-on detection of cardiac troponin I, Microchim. Acta 191 (3) (2024) 124.
[98] T. Sowers, D. VanderLaan, A. Karpiouk, E.M. Donnelly, E. Smith, S. Emelianov, Laser threshold and cell damage mechanism for intravascular photoacoustic imaging, Laser Surg. Med. 51 (5) (2019) 466–474.
[99] G. Ma, X. Gao, C. Jiang, S. Xing, C. Wei, P. Huang, J. Lin, pH-Responsive nanoprobe for in vivo photoacoustic imaging of gastric acid, Anal. Chem. 91 (21) (2019) 13570–13575.
[100] H.J. Knox, J. Chan, Acoustogenic probes: a new frontier in photoacoustic imaging, Acc. Chem. Res. 51 (11) (2018) 2897–2905.
[101] P. Beard, Biomedical photoacoustic imaging, Interface Focus 1 (4) (2011) 602–631.
[102] Y.N. Zhang, X.J. Chen, L.J. Liu, J. Tian, L. Hao, H.T. Ran, Photoacoustic imaging of myocardial infarction region using non-invasive fibrin-targeted nanoparticles in a rat myocardial ischemia-reperfusion model, Int. J. Nanomed. 16 (2021) 1331–1344.
[103] O. Turgut, P. Mueller, P. Hager, S. Shit, S. Starck, M.J. Menten, E. Martens, D. Rueckert, Unlocking the diagnostic potential of electrocardiograms through information transfer from cardiac magnetic resonance imaging, Med. Image Anal. 101 (2025) 103451.
[104] Y. Yang, S. Yue, L. Shen, H. Dong, H. Li, X. Zhao, Q. Guo, X. Zhou, Ultrasensitive $^{129}$Xe Magnetic Resonamce Imagirg: From Ciinical Mfnitocing to Mmlecular Sensimg, Adv. Sci. 12 (8) (2025) 2413426.
[105] G. Joy, L.R. Lopes, M. Webber, A.M. Ardissino, J. Wilson, F. Chan, I. Pierce, R. K. Hughes, K. Moschonas, H. Shiwani, R. Jamieson, P.P. Velazquez, R. Vijayakumar, E. Dall Armellina, P.W. Macfarlane, C. Manisty, P. Kellman, R. H. Davies, M. Tome, V. Koncar, X. Tao, C. Guger, Y. Rudy, A.D. Hughes, P. D. Lambiase, J.C. Moon, M. Orini, G. Captur, Electrophysiological characterization of subclinical and overt hypertrophic cardiomyopathy by magnetic resonance imaging-guided electrocardiography, J. Am. Coll. Cardiol. 83 (11) (2024) 1042–1055.
[106] A.E. Arai, J. Schulz-Menger, D. Berman, H. Mahrholdt, Y. Han, W.P. Bandettini, M. Gutberlet, A. Abraham, P.K. Woodard, J.B. Selvanayagam, G.P. McCann, C. Hamilton-Craig, U.J. Schoepf, R.S. Tan, C.M. Kramer, M.G. Friedrich, D. Haverstock, Z. Liu, G. Brueggenwerth, C. Bacher-Stier, M. Santiuste, D. J. Pennell, C.A.D.I. Gada, Gadobutrol-enhanced cardiac magnetic resonance imaging for detection of coronary artery disease, J. Am. Coll. Cardiol. 76 (13) (2020) 1536–1547.

[107] Y. Li, Y. Gao, G. Li, Preclinical multi-target strategies for myocardial ischemia-reperfusion injury, Front. Cardiovasc. Med. 9 (2022) 967115.
[108] M. Sagris, A. Apostolos, P. Theofilis, N. Ktenopoulos, O. Katsaros, S. Tsalamandris, K. Tsioufis, K. Toutouzas, D. Tousoulis, Myocardial ischemia–reperfusion injury: unraveling pathophysiology, clinical manifestations, and emerging prevention strategies, Biomedicines 12 (4) (2024) 802.
[109] E. Gerbaud, F. Arabucki, H. Nivet, C. Barbey, L. Cetran, S. Chassaing, B. Seguy, A. Lesimple, H. Cochet, M. Montaudon, F. Laurent, O. Bar, G.J. Tearney, P. Coste, OCT and CMR for the diagnosis of patients presenting with MINOCA and suspected epicardial causes, JACC, Cardiovasc. Imaging 13 (2020) 2619–2631.
[110] H.R. Reynolds, A. Maehara, R.Y. Kwong, T. Sedlak, J. Saw, N.R. Smilowitz, E. Mahmud, J. Wei, K. Marzo, M. Matsumura, A. Seno, A. Hausvater, C. Giesler, N. Jhalani, C. Toma, B. Har, D. Thomas, L.S. Mehta, J. Trost, P.K. Mehta, B. Ahmed, K.R. Bainey, Y. Xia, B. Shah, M. Attubato, S. Bangalore, L. Razzouk, Z. A. Ali, N.B. Merz, K. Park, E. Hada, H. Zhong, J.S. Hochman, Coronary optical coherence tomography and cardiac magnetic resonance imaging to determine underlying causes of myocardial infarction with nonobstructive coronary arteries in women, Circulation 143 (2020) 624–640.
[111] F.A. Veneziano, F.A. Gioia, F. Gentile, Hybrid PET/CT and PET/MR in coronary artery disease: an update for Clinicians, with insights into AI-Guided integration, J. Cardiovasc. Dev. Dis. 12 (9) (2025) 338.
[112] L. Li, W. Ding, L. Huang, X. Zhuang, V. Grau, Multi-modality cardiac image computing: a survey, Med. Image Anal. 88 (2023) 102869.
[113] J. Bischof, G. Fletcher, P. Verkade, C. Kuntner, J. Fernandez-Rodriguez, L. Chaabane, L.A. Rose, A. Walter, M. Vandenbosch, M.A.M.J. van Zandvoort, A. Zaritsky, A. Keppler, M. Parsons, Multimodal bioimaging across disciplines and scales: challenges, opportunities and breaking down barriers, Npj Imag 2 (1) (2024) 5.
[114] M. Zubair, M. Hussain, M.A. Albashrawi, M. Bendechache, M. Owais, A comprehensive review of techniques, algorithms, advancements, challenges, and clinical applications of multi-modal medical image fusion for improved diagnosis, Comput. Methods Progr. Biomed. 272 (2025) 109014.
[115] Z. Jiang, M. Zhang, P. Li, Y. Wang, Q. Fu, Nanomaterial-based CT contrast agents and their applications in image-guided therapy, Theranostics 13 (2) (2023) 483–509.
[116] J. Xing, Z. Li, J. Yao, A. Wu, Nanomaterial-based contrast agents for common disease imaging, Sci. China Mater. 67 (2024) 1288–1291.
[117] M.H. Younis, Z. Tang, W. Cai, Multimodality imaging of nanoparticle-based vaccines: shedding light on immunology, Wiley Interdiscip. Rev. Nanomed. Nanobiotechnol. 14 (5) (2022) e1807.
[118] Z. Pang, Y. Wang, Y. Wang, Z. Sun, W. Qi, L. Xi, Multi-modality photoacoustic/ultrasound imaging based on a commercial ultrasound platform, Opt Lett. 46 (17) (2021) 4382–4385.
[119] X. Liao, M. Tang, J. Li, R. Guo, C. Zhong, X. Chen, X. Zhang, H. Mo, D. Que, W. Yu, X. Song, H. Li, Y. Cai, P. Yang, Acid-triggered cascaded responsive supramolecular peptide alleviates myocardial ischemia–reperfusion injury by restoring redox homeostasis and protecting mitochondrial function, Adv. Healthcare Mater. 14 (7) (2025) 2404319.
[120] X. Mo, L. Liu, L. Zhang, M. Hu, H. Xiang, Y. Chen, B. Zhang, Snowflake-like RuMn branched nanosheets enable topocatalytic therapy of cardiac ischemia/reperfusion injury via resisting inflammatory Cascade and neutrophil invasion, Adv. Funct. Mater. 35 (14) (2024) 2415084.
[121] X. Rossello, J.A. Riquelme, S.M. Davidson, D.M. Yellon, Role of PI3K in myocardial ischaemic preconditioning: mapping pro-survival cascades at the trigger phase and at reperfusion, J. Cell Mol. Med. 22 (2) (2017) 926–935.
[122] D.V. Korolev, G.A. Shulmeyster, M.S. Istomina, N.V. Evreinova, I.V. Aleksandrov, A.S. Krasichkov, V.N. Postnov, M.M. Galagudza, Fluorescently labeled gadolinium Ferrate/trigadolinium Pentairon(III) oxide nanoparticles: synthesis, characterization, in vivo biodistribution, and application for visualization of myocardial ischemia-reperfusion injury, Materials 15 (11) (2022) 3832.
[123] H.H. Chen, H. Yuan, H. Cho, Y. Feng, S. Ngoy, A.T.N. Kumar, R. Liao, W. Chao, L. Josephson, D.E. Sosnovik, Theranostic nucleic acid binding nanoprobe exerts anti-inflammatory and cytoprotective effects in ischemic injury, Theranostics 7 (4) (2017) 814–825.
[124] M. Shafiq, Y. Chen, R. Hashim, C. He, X. Mo, X. Zhou, Reactive oxygen species-based biomaterials for regenerative medicine and tissue engineering applications, Front. Bioeng. Biotechnol. 9 (2021) 821288.
[125] A. Zhitkovich, *N*-Acetylcysteine: Antioxidant, aldehyde Scavenger, and more, Chem. Res. Toxicol. 32 (7) (2019) 1318–1319.
[126] C. Zhang, X. Chen, Photothermal-therapy-based targeting thrombolytic therapy, ACS Appl. Bio Mater. 8 (3) (2025) 1820–1834.
[127] L.N. Pedersen, C. Valenzuela Ripoll, M. Ozcan, Z. Guo, A. Lotfinaghsh, S. Zhang, S. Ng, C. Weinheimer, J. Nigro, A. Kovacs, A. Diab, A. Klaas, F. Grogan, Y. Cho, A. Ataran, H. Luehmann, A. Heck, K. Kolb, L. Strong, R. Navara, G.M. Walls, G. Hugo, P. Samson, D. Cooper, F.J. Reynoso, J.K. Schwarz, K. Moore, K. Lavine, S.L. Rentschler, Y. Liu, P.K. Woodard, C. Robinson, P.S. Cuculich, C. Bergom, A. Javaheri, Cardiac radiation improves ventricular function in mice and humans with cardiomyopathy, Med 4 (12) (2023) 928–943.
[128] O. Sezen, B. Sonmez, A.Y. Zengin, E. Yenilmez, E. Yulug, I. Abidin, Z. Bahat, I. Dogan, Myocardial perfusion alterations observed months after radiotherapy are related to the cellular damage, Nuklearmedizin 49 (6) (2010) 209–215.
[129] X. Yang, M. Tan, J. Guo, J. Xiang, F. Yin, J. Deng, J. Luo, S. Xiao, M. Mo, H. Wang, J. Zhao, L. Zheng, J. Cheng, J. Zhong, PdZn/$Co_{SA}$-NC nanozymes with highly efficient SOD/CAT activities for treatment of osteoarthritis via regulating immune microenvironment, Adv. Funct. Mater. 34 (41) (2024) 2401963.
[130] A.-F. Jebran, T. Seidler, M. Tiburcy, M. Daskalaki, I. Kutschka, B. Fujita, S. Ensminger, F. Bremmer, A. Moussavi, H. Yang, X. Qin, S. Missbach, C. Drummer, H. Baraki, S. Boretius, C. Hasenauer, T. Nette, J. Kowallick, C. O. Ritter, J. Lotz, M. Didie, M. Mietsch, T. Meyer, G. Kensah, D. Krueger, M. S. Sakib, L. Kaurani, A. Fischer, R. Dressel, I. Rodriguez-Polo, M. Stauske, S. Diecke, K. Maetz-Rensing, E. Gruber-Dujardin, M. Bleyer, B. Petersen, C. Roos, L. Zhang, L. Walter, S. Kaulfuss, G. Yigit, B. Wollnik, E. Levent, B. Roshani, C. Stahl-Henning, P. Stroebel, T. Legler, J. Riggert, K. Hellenkamp, J.-U. Voigt, G. Hasenfuss, R. Hinkel, J.C. Wu, R. Behr, W.-H. Zimmermann, Engineered heart muscle allografts for heart repair in primates and humans, Nature 639 (8054) (2025) 503–511.
[131] I.-S. Park, C. Mahapatra, J.S. Park, K. Dashnyam, J.-W. Kim, J.C. Ahn, P.-S. Chung, D.S. Yoon, N. Mandakhbayar, R.K. Singh, J.-H. Lee, K.W. Leong, H.-W. Kim, Revascularization and limb salvage following critical limb ischemia by nanoceria-induced Ref-1/APE1-dependent angiogenesis, Biomaterials 242 (2020) 119919.
[132] G.-B. Im, Y.G. Kim, T.Y. Yoo, Y.H. Kim, K. Kim, J. Hyun, M. Soh, T. Hyeon, S. H. Bhang, Ceria nanoparticles as copper chaperones that activate SOD1 for synergistic antioxidant therapy to treat ischemic vascular diseases, Adv. Mater. 35 (16) (2023) 2208989.
[133] L. Wang, S. Qiu, X. Li, Y. Zhang, M. Huo, J. Shi, Myocardial-targeting tannic cerium nanocatalyst attenuates ischemia/reperfusion injury, Angew. Chem. Int. Ed. 62 (39) (2023) 2305576.
[134] C. Hang, M.S. Moawad, Z. Lin, H. Guo, H. Xiong, M. Zhang, R. Lu, J. Liu, D. Shi, D. Xie, Y. Liu, D. Liang, Y.-H. Chen, J. Yang, Biosafe cerium oxide nanozymes protect human pluripotent stem cells and cardiomyocytes from oxidative stress, J. Nanobiotechnol. 22 (1) (2024) 132.
[135] W. Le, Z. Sun, T. Li, H. Cao, C. Yang, T. Mei, L. Zhang, Y. Wang, W. Jia, W. Sun, Y. Hu, Z. Liu, Antioxidant nanozyme-engineered mesenchymal stem cells for in vivo MRI tracking and synergistic therapy of myocardial infarction, Adv. Funct. Mater. 34 (23) (2024) 2314328.
[136] A. Sahu, J. Jeon, M.S. Lee, H.S. Yang, G. Tae, Nanozyme impregnated mesenchymal stem cells for hepatic ischemia-reperfusion injury alleviation, ACS Appl. Mater. Interfaces 13 (22) (2021) 25649–25662.
[137] P.J. Altshuler, A.R. Schiazza, L. Luo, M.R. Helmers, B. Chhay, J.J. Han, R. Hu, D. A. Herbst, A. Tsourkas, Z. Cheng, P. Atluri, Superoxide dismutase-loaded nanoparticles attenuate myocardial ischemia-reperfusion injury and protect against chronic adverse ventricular remodeling, Adv. Therapeut. 4 (6) (2021) 2100036.
[138] L. Ding, S. Zhang, Y. Li, Y. Wu, X. Liu, D. Xu, K. Zhao, C. Xu, B. Yu, X. Huang, B. Z. Tang, W. Zhang, Superoxide dismutase mimetic nanozymes attenuate cardiac microvascular ischemia-reperfusion injury associated with hyperhomocysteinemia, Chem. Eng. J. 486 (2024) 150177.
[139] T. Ye, C. Chen, D. Wang, C. Huang, Z. Yan, Y. Chen, X. Jin, X. Wang, X. Ding, C. Shen, Protective effects of Pt-N-C single-atom nanozymes against myocardial ischemia-reperfusion injury, Nat. Commun. 15 (1) (2024) 1682.
[140] M. Long, L. Wang, L. Kang, D. Liu, T. Long, H. Ding, Y. Duan, H. He, B. Xu, N. Gu, Prussian blue nanozyme featuring enhanced superoxide dismutase-like activity for myocardial ischemia reperfusion injury treatment, ACS Nano 19 (4) (2025) 4561–4581.
[141] Y. Xiong, Y. Zhang, C. Zhou, T. Yu, ROS scavenging Manganese-loaded mesoporous silica nanozymes for catalytic anti-inflammatory therapy, Adv. Powder Technol. 34 (1) (2023) 103886.
[142] R. Cai, L. Xiao, J. Qiu, L. Zhao, Z. Li, H. Ju, M. Sun, W. Zhu, Z. Wang, F. Du, Fabrication of cerium doped carbon dots with highly radical scavenging activity alleviates ferroptosis-induced oxidative damage, Nanotechnology 32 (39) (2021) 395605.
[143] A. Othman, A. Gowda, D. Andreescu, M.H. Hassan, S.V. Babu, J. Seo, S. Andreescu, Two decades of ceria nanoparticle research: structure, properties and emerging applications, Mater. Horiz. 11 (14) (2024) 3213–3266.
[144] R.X. He, B.W. Yang, J.L. Shi, Nanocatalytic antioxidation synergizes cardioprotection and antifibrosis in cardiac injury, Nano Today 65 (2025) 102820.
[145] W.J. Liao, J.D. Lin, W.L. Wang, M. Zhang, Y.F. Chen, X. Li, H. Liu, P.X. Wang, G. J. Zhao, J.J. Fu, X.Q. Wu, Assembly of ceria-Nrf2 nanoparticles as macrophage-targeting ROS scavengers protects against myocardial infarction, Front. Pharmacol. 15 (2025) 1503757.
[146] Y. Qin, X. Han, Y. Li, A. Han, W. Liu, H. Xu, J. Liu, Hollow mesoporous metal-organic frameworks with enhanced diffusion for highly efficient catalysis, ACS Catal. 10 (11) (2020) 5973–5978.
[147] B. Zhao, H. Yang, J. Mao, J. Shi, Mof-derived hollow-open hierarchically porous carbon spheres for enzyme encapsulation and biocatalysis, Chem. Eng. J. 505 (2025) 158972.
[148] D. Menon, D. Fairen-Jimenez, Guiding the rational design of biocompatible metal-organic frameworks for drug delivery, Matter 8 (3) (2025) 101958.
[149] Z. Xu, L. Chen, Y. Luo, Y.-M. Wei, N.-Y. Wu, L.-F. Luo, Y.-B. Wei, J. Huang, Advances in metal-organic framework-based nanozymes in ROS scavenging medicine, Nanotechnology 35 (36) (2024) 362006.
[150] Z. Wang, X. Shen, X. Gao, Y. Zhao, Simultaneous enzyme mimicking and chemical reduction mechanisms for nanoceria as a bio-antioxidant: a catalytic model bridging computations and experiments for nanozymes, Nanoscale 11 (28) (2019) 13289–13299.
[151] Z. Wang, W. Wang, J. Wang, D. Wang, M. Liu, Q. Wu, H. Hu, Single-atom catalysts with ultrahigh catalase-like activity through electron filling and orbital energy regulation, Adv. Funct. Mater. 33 (2) (2023) 2209560.

[152] B. Yang, H. Yao, J. Yang, C. Chen, J. Shi, Construction of a two-dimensional artificial antioxidase for nanocatalytic rheumatoid arthritis treatment, Nat. Commun. 13 (1) (2022) 1988.
[153] S. Zhang, Y. Li, S. Sun, L. Liu, X. Mu, S. Liu, M. Jiao, X. Chen, K. Chen, H. Ma, T. Li, X. Liu, H. Wang, J. Zhang, J. Yang, X.-D. Zhang, Single-atom nanozymes catalytically surpassing naturally occurring enzymes as sustained stitching for brain trauma, Nat. Commun. 13 (1) (2022) 4744.
[154] L. Li, H. Li, L. Shi, L. Shi, T. Li, Tin porphyrin-based nanozymes with unprecedented superoxide dismutase-mimicking activities, Langmuir 38 (23) (2022) 7272–7279.
[155] J. Wu, Y. Yu, Y. Cheng, C. Cheng, Y. Zhang, B. Jiang, X. Zhao, L. Miao, H. Wei, Ligand-dependent activity engineering of glutathione peroxidase-mimicking MIL-47(V) metal-organic framework nanozyme for therapy, Angew. Chem. Int. Ed. 60 (3) (2021) 1227–1234.
[156] W. Zhou, H. Li, B. Xia, W. Ji, S. Ji, W. Zhang, W. Huang, F. Huo, H. Xu, Selenium-functionalized metal-organic frameworks as enzyme mimics, Nano Res. 11 (10) (2018) 5761–5768.
[157] J. Wang, W. Li, Y.-Q. Zheng, Nitro-functionalized metal-organic frameworks with catalase mimic properties for glutathione detection, Analyst 144 (20) (2019) 6041–6047.
[158] M. He, Y. Chen, C. Tao, Q. Tian, L. An, J. Lin, Q. Tian, H. Yang, S. Yang, Mn-porphyrin-based metal-organic framework with high longitudinal relaxivity for magnetic resonance imaging guidance and oxygen self-supplementing photodynamic therapy, ACS Appl. Mater. Interfaces 11 (45) (2019) 41946–41956.
[159] Q. Xu, G. Zhan, Z. Zhang, T. Yong, X. Yang, L. Gan, Manganese porphyrin-based metal-organic framework for synergistic sonodynamic therapy and ferroptosis in hypoxic tumors, Theranostics 11 (4) (2021) 1937–1952.
[160] K. Xiang, H. Wu, Y. Liu, S. Wang, X. Li, B. Yang, Y. Zhang, L. Ma, G. Lu, L. He, Q. Ni, L. Zhang, MOF-derived bimetallic nanozyme to catalyze ROS scavenging for protection of myocardial injury, Theranostics 13 (8) (2023) 2721–2733.
[161] Y. Liu, Y. Cheng, H. Zhang, M. Zhou, Y. Yu, S. Lin, B. Jiang, X. Zhao, L. Miao, C.-W. Wei, Q. Liu, Y.-W. Lin, Y. Du, C.J. Butch, H. Wei, Integrated cascade nanozyme catalyzes in vivo ROS scavenging for anti-inflammatory therapy, Sci. Adv. 6 (29) (2020) eabb2695.
[162] J. Estelrich, M.A. Busquets, Prussian blue: a nanozyme with versatile catalytic properties, Int. J. Mol. Sci. 22 (11) (2021) 5993.
[163] S. Sahoo, T. Kariya, K. Ishikawa, Targeted delivery of therapeutic agents to the heart, Nat. Rev. Cardiol. 18 (2021) 389–399.
[164] Q.H. Li, R. Bolli, Y.M. Qiu, X.L. Tang, Y.R. Guo, B.A. French, Gene therapy with extracellular superoxide dismutase protects conscious rabbits against myocardial infarction, Circulation 98 (17) (1998), 144-144.
[165] M. Schiffer, K. Wagner, E. Carls, J. Nicke, M. Hesse, R.M. Fratila, S. Hildebrand, D. Eberbeck, T. Mohr, M.M. Mohammadi, J.M. de la Fuente, B.K. Fleischmann, W. Roell, Nanoparticle-assisted targeting of heart lesions with cardiac myofibroblasts: combined gene and cell therapy, Theranostics 15 (10) (2025) 4287–4307.
[166] B. Baral, B. Panigrahi, A. Kar, K. Tulsiyan, U. Suryakant, D. Mandal, U. Subudhi, Peptide nanostructures-based delivery of DNA nanomaterial therapeutics for regulating gene expression, Mol. Ther. Nucleic Acids 33 (2023) 493–510.
[167] B.d.S. Rodrigues, T. Kanekiyo, J. Singh, ApoE-2 brain-targeted gene therapy through transferrin and penetratin tagged liposomal nanoparticles, Pharm. Res. 36 (11) (2019) 161.
[168] H. Wang, Y. Chen, H. Wang, X. Liu, X. Zhou, F. Wang, DNAzyme-Loaded metal-organic frameworks (MOFs) for self-sufficient gene therapy, Angew. Chem. Int. Ed. 58 (22) (2019) 7380–7384.
[169] M.P. D'Arienzo, L. Rarita, Dynamics of blood flows in the cardiocirculatory system, Computation 12 (10) (2024) 194.
[170] D.L. Brutsaert, G.W. DeKeulenaer, P. Fransen, P. Mohan, G.L. Kaluza, L.J. Andries, J.L. Rouleau, S.U. Sys, The cardiac endothelium: functional morphology, development, and physiology, Prog. Cardiovasc. Dis. 39 (3) (1996) 239–262.
[171] X. Wei, L. Zhuang, H. Li, C. He, H. Wan, N. Hu, P. Wang, Advances in multidimensional cardiac biosensing technologies: from electrophysiology to mechanical motion and contractile force, Small 16 (50) (2020) 2005828.
[172] D.C.H. Ng, D.K. Richards, R.J. Mills, U.Y. Ho, H.L. Perks, C.R. Tucker, H.K. Voges, J.K. Pagan, J.E. Hudson, Centrosome reduction promotes terminal differentiation of human cardiomyocytes, Stem Cell Rep. 15 (4) (2020) 817–826.
[173] X. Chen, H. Chen, L. Zhu, M. Zeng, T. Wang, C. Su, G. Vulugundam, P. Gokulnath, G. Li, X. Wang, J. Yao, J. Li, D. Cretoiu, Z. Chen, Y. Bei, Nanoparticle-patch system for localized, effective, and sustained miRNA administration into infarcted myocardium to alleviate myocardial ischemia-reperfusion injury, ACS Nano 18 (30) (2024) 19470–19488.
[174] Y. Zeng, M.E. Senti, M.C.I. Labonia, P. Papadopoulou, M.A.D. Brans, I. Dokter, M. H. Fens, A. van Mil, J.P.G. Sluijter, R.M. Schiffelers, P. Vader, A. Kros, Fusogenic coiled-coil peptides enhance lipid nanoparticle-mediated mRNA delivery upon intramyocardial administration, ACS Nano 17 (23) (2023) 23466–23477.
[175] M.H. Guo, G.A. Wells, D. Glineur, J. Fortier, P.M. Davierwala, K. Kikuchi, M. G. Lemma, Y.K. Mishra, J. McGinn, M. Ramchandani, P. Rabindra, S. Nambala, K. M. Chiu, B. Kiaii, S. Gibson, M. Ruel, Minimally invasive coronary surgery compared to STernotomy coronary artery bypass grafting: the MIST trial, Contemp. Clin. Trials 78 (2019) 140–145.
[176] X. Mu, J. Li, S. Yan, H. Zhang, W. Zhang, F. Zhang, J. Jiang, siRNA delivery with stem cell membrane-coated magnetic nanoparticles for imaging-guided photothermal therapy and gene therapy, ACS Biomater. Sci. Eng. 4 (11) (2018) 3895–3905.
[177] E. Briffault, P. Garcia-Garcia, R. Martinez-Borrajo, C. Evora, A. Delgado, P. Diaz-Rodriguez, Harnessing extracellular vesicle membrane for gene therapy: evs-biomimetic nanoparticles, Colloids Surf. B Biointerfaces 239 (2024) 113951.
[178] L. Zhuang, X. Zong, Q. Yang, Q. Fan, R. Tao, Interleukin-34-NF-κB signaling aggravates myocardial ischemic/reperfusion injury by facilitating macrophage recruitment and polarization, EBioMedicine 95 (2023) 104744.
[179] H. Lu, J. Wang, Z. Chen, J. Wang, Y. Jiang, Z. Xia, Y. Hou, P. Shang, R. Li, Y. Liu, J. Xie, Engineered macrophage membrane-coated S100A9-siRNA for ameliorating myocardial ischemia-reperfusion injury, Adv. Sci. 11 (41) (2024) 2403542.
[180] Y. Wang, M. Hou, S. Duan, Z. Zhao, X. Wu, Y. Chen, L. Yin, Macrophage-targeting gene silencing orchestrates myocardial microenvironment remodeling toward the anti-inflammatory treatment of ischemia-reperfusion (IR) injury, Bioact. Mater. 17 (2022) 320–333.
[181] Y. Zhou, Q. Liang, X. Wu, S. Duan, C. Ge, H. Ye, J. Lu, R. Zhu, Y. Chen, F. Meng, L. Yin, siRNA delivery against myocardial ischemia reperfusion injury mediated by reversibly camouflaged biomimetic nanocomplexes, Adv. Mater. 35 (23) (2023) 2210691.
[182] D. Boldini, L. Friedrich, D. Kuhn, S.A. Sieber, Machine learning assisted hit prioritization for high throughput screening in drug discovery, ACS Cent. Sci. 10 (4) (2024) 823–832.
[183] P. Linciano, A. Quotadamo, R. Luciani, M. Santucci, K.M. Zorn, D.H. Foil, T. R. Lane, A.C. da Silva, N. Santarem, C.B. Moraes, L. Freitas-Junior, U. Wittig, W. Mueller, M. Tonelli, S. Ferrari, A. Venturelli, S. Gul, M. Kuzikov, B. Ellinger, J. Reinshagen, S. Ekins, M.P. Costi, High-throughput phenotypic screening and machine learning methods enabled the selection of broad-spectrum low-toxicity antitrypanosomatidic agents, J. Med. Chem. 66 (22) (2023) 15230–15255.
[184] P.O. Fernandes, A.L. Dias, V.S. dos Santos Junior, M.S.M. Serafim, Y.V. Sousa, G. C. Monteiro, I.D. Coutinho, M. Valli, M.M.S.A. Verzola, F.M. Ottoni, R.M. de Padua, F.B. Oda, A.G. dos Santos, A.D. Andricopulo, V.d.S. Bolzani, B.E.F. Mota, R.J. Alves, R.B. de Oliveira, T. Kronenberger, V.G. Maltarollo, Machine learning-based virtual screening of antibacterial agents against Methicillin-susceptible and resistant *Staphylococcus aureus*, J. Chem. Inf. Model. 64 (6) (2024) 1932–1944.
[185] H. Gao, S. Li, Z. Lan, D. Pan, G.S. Naidu, D. Peer, C. Ye, H. Chen, M. Ma, Z. Liu, H. A. Santos, Comparative optimization of polysaccharide-based nanoformulations for cardiac RNAi therapy, Nat. Commun. 15 (1) (2024) 5398.
[186] C. Chang, R.-P. Cai, Y.-M. Su, Q. Wu, Q. Su, Mesenchymal stem cell-derived exosomal noncoding RNAs as alternative treatments for myocardial ischemia-reperfusion injury: current status and future perspectives, J. Cardiovasc. Transl. Res. 16 (2023) 1085–1098.
[187] Y.-A. Mao, P. Sun, X. Yin, W. Wan, H. Chen, X. Wang, R. Gui, J. Tang, X. Shi, Y. Jin, Z. Pan, X. Wang, T. Yang, H. Wang, X. Chen, J. Xiao, Conductive microneedle patch with mitochondria-localized generation of nitric oxide promotes heart repair after ischemia-reperfusion therapy, Small Methods 9 (11) (2025) e00818.
[188] D. Wu, Y. Gu, D. Zhu, Cardioprotective effects of hydrogen sulfide in attenuating myocardial ischemia-reperfusion injury, Mol. Med. Rep. 24 (6) (2021) 1–11.
[189] E. Donnarumma, M.J. Ali, A.M. Rushing, A.L. Scarborough, J.M. Bradley, C. L. Organ, K.N. Islam, D.J. Polhemus, S. Evangelista, G. Cirino, J.S. Jenkins, R.A. G. Patel, D.J. Lefer, T.T. Goodchild, Zofenopril protects against myocardial ischemia-reperfusion injury by increasing nitric oxide and hydrogen sulfide bioavailability, J. Am. Heart Assoc. 5 (7) (2016) e003531.
[190] T. Bochaton, M. Ovize, Circadian rhythm and ischaemia–reperfusion injury, Lancet 391 (10115) (2017) 8–9.
[191] G. Jin, W. Li, F. Song, J. Zhao, M. Wang, Q. Liu, A. Li, G. Huang, F. Xu, Fluorescent conjugated polymer nanovector for in vivo tracking and regulating the fate of stem cells for restoring infarcted myocardium, Acta Biomater. 109 (2020) 195–207.
[192] T.A. Tabish, M.J. Crabtree, H.E. Townley, P.G. Winyard, C.A. Lygate, Nitric oxide releasing nanomaterials for cardiovascular applications, JACC: Basic to Trans. Sci. 9 (5) (2023) 691–709.
[193] Z. Yuan, Y. Li, M. Sun, M. Yuan, Z. Han, X. Li, S. Liu, Y. Sun, J. Cao, F. Li, Recent progress in ROS-responsive biomaterials for the diagnosis and treatment of cardiovascular diseases, Theranostics 15 (11) (2025) 5172–5219.
[194] Y. Liu, C. Li, X. Yang, B. Yang, Q. Fu, Stimuli-responsive polymer-based nanosystems for cardiovascular disease theranostics, Biomater. Sci. 12 (2024) 3805–3825.
[195] D. Li, S. Zhang, Nanodrug targeting for myocardial ischemia-reperfusion injury: mechanisms, therapeutic strategies, and challenges in clinical translation, Int. J. Pharm. 684 (2025) 126153.
[196] B.S. Zhang, C. Wang, M.Y. Guo, F.X. Zhu, Z.Q. Yu, W.X. Zhang, W.Y. Li, Y. J. Zhang, W.M. Tian, Circadian rhythm-dependent therapy by composite targeted polyphenol nanoparticles for myocardial ischemia-reperfusion injury, ACS Nano 18 (41) (2024) 28154–28169.
[197] T. Eschenhagen, F. Weinberger, Challenges and perspectives of heart repair with pluripotent stem cell-derived cardiomyocytes, Nat. Cardiovasc. Res. 3 (5) (2024) 515–524.
[198] M. Shafiq, Y. Jung, S.H. Kim, Insight on stem cell preconditioning and instructive biomaterials to enhance cell adhesion, retention, and engraftment for tissue repair, Biomaterials 90 (2016) 85–115.
[199] L. Shen, Z. Tian, J. Zhang, H. Zhu, K. Yang, T. Li, J. Rich, N. Upreti, N. Hao, Z. Pei, G. Jin, S. Yang, Y. Liang, W. Chaohui, T.J. Huang, Acousto-dielectric tweezers for size-insensitive manipulation and biophysical characterization of single cells, Biosens. Bioelectron. 224 (2023) 115061.
[200] M. Rafique, O. Ali, M. Shafiq, M. Yao, K. Wang, H. Ijima, D. Kong, M. Ikeda, Insight on oxygen-supplying biomaterials used to enhance cell survival, retention, and engraftment for tissue repair, Biomedicines 11 (6) (2023) 1592.

[201] L. Pan, X. Hu, H. Yang, L. Chen, H. Tang, S. Luo, H. Hu, J. Zhang, Nanotherapy-engineered stem cells alleviate myocardial reperfusion injury by normalizing the pathological microenvironment and promoting cardiac repair, Adv. Funct. Mater. 35 (11) (2025) 2417338.
[202] N. Zhang, T. Li, P. Zhong, T. Fu, L. Li, M. Peng, Y. Wang, Y. Lu, M. Yao, Design and synthesis of a NTR-sensitive fluorescent $H_2S$ donor as a potential therapeutic agent for myocardial ischemia–reperfusion injury, J. Med. Chem. 68 (14) (2025) 14981–14994.
[203] H. Kazemirad, H.R. Kazerani, Nitric oxide plays a pivotal role in cardioprotection induced by pomegranate juice against myocardial ischemia and reperfusion, Phytother Res. 32 (10) (2018) 2069–2077.
[204] K. Hayashida, M. Sano, I. Ohsawa, K. Shinmura, K. Tamaki, K. Kimura, J. Endo, T. Katayama, A. Kawamura, S. Kohsaka, S. Makino, S. Ohta, S. Ogawa, K. Fukuda, Inhalation of hydrogen gas reduces infarct size in the rat model of myocardial ischemia-reperfusion injury, Biochem. Biophys. Res. Commun. 373 (1) (2008) 30–35.
[205] A. Kumar, S.R. Boovarahan, P.N. Prem, M. Ramanathan, D.R. Chellappan, G. A. Kurian, Evaluating the effects of carbon monoxide releasing molecule-2 against myocardial ischemia–reperfusion injury in ovariectomized female rats, N. Schmied. Arch. Pharmacol. 394 (2021) 2103–2115.
[206] Y. Cheng, J. Rong, Therapeutic potential of Heme Oxygenase-1/carbon monoxide system against ischemia-reperfusion injury, Curr. Pharm. Des. 23 (26) (2017) 3884–3898.
[207] Z. Liang, H. Chen, X. Gong, B. Shi, L. Lin, F. Tao, Q. Wu, M. Fang, H. Li, C. Lu, H. Xu, Y. Zhao, B. Chen, Ultrasound-induced destruction of nitric oxide-loaded microbubbles in the treatment of thrombus and ischemia-reperfusion injury, Front. Pharmacol. 12 (2022) 745693.
[208] W.-l. Wang, T.-y. Ge, X. Chen, Y. Mao, Y.-z. Zhu, Advances in the protective mechanism of NO, $H_2S$, and $H_2$ in myocardial ischemic injury, Front. Cardiovasc. Med. 7 (2020) 588206.
[209] D. Zhu, J. Hou, M. Qian, D. Jin, T. Hao, Y. Pan, H. Wang, S. Wu, S. Liu, F. Wang, L. Wu, Y. Zhong, Z. Yang, Y. Che, J. Shen, D. Kong, M. Yin, Q. Zhao, Nitrate-functionalized patch confers cardioprotection and improves heart repair after myocardial infarction via local nitric oxide delivery, Nat. Commun. 12 (1) (2021) 4501.
[210] H. Li, J. Yan, D. Meng, R. Cai, X. Gao, Y. Ji, L. Wang, C. Chen, X. Wu, Gold nanorod-based nanoplatform catalyzes constant NO generation and protects from cardiovascular injury, ACS Nano 14 (10) (2020) 12854–12865.
[211] Z. Wang, N. Yang, Y. Hou, Y. Li, C. Yin, E. Yang, H. Cao, G. Hu, J. Xue, J. Yang, Z. Liao, W. Wang, D. Sun, C. Fan, L. Zheng, L-Arginine-Loaded gold nanocages ameliorate myocardial Ischemia/reperfusion injury by promoting nitric oxide production and maintaining mitochondrial function, Adv. Sci. 10 (26) (2023) 2302123.
[212] L. Xu, Y. Chen, Q. Jin, T. Gao, C. Deng, R. Wang, Y. Wang, Y. Bai, J. Xu, W. Wu, H. Li, L. Fang, J. Wang, Y. Yang, L. Zhang, Q. Lv, M. Xie, A novel ultrasound-responsive biomimetic nanoparticle for targeted delivery and controlled release of nitric oxide to attenuate myocardial ischemia reperfusion injury, Small Struct. 4 (8) (2023) 2300004.
[213] A.T.A.E. Mohamed, M.A. Ragheb, M.R. Shehata, A.S. Mohamed, *In vivo* cardioprotective effect of zinc oxide nanoparticles against doxorubicin-induced myocardial infarction by enhancing the antioxidant system and nitric oxide production, J. Trace Elem. Med. Biol. 86 (2024) 127516.
[214] N. Zhang, M. Fan, Y. Zhao, X. Hu, Q. Zhu, X. Jiao, Q.D. Li, Z. Huang, G. Fu, J. Ge, H. Li, W. Zhang, Biomimetic and NOS-Responsive nanomotor deeply delivery a combination of MSC-EV and mitochondrial ROS scavenger and promote heart repair and regeneration, Adv. Sci. 10 (21) (2023) 2301440.
[215] L. Liu, Y. Yao, Y. Liu, B. Hong, Z. Li, X. Chen, Y. Zhang, H. Fu, D. Yang, C. Yang, Targeted $H_2S$-Mediated gas therapy with pH-Sensitive release property for myocardial ischemia-reperfusion injury by platelet membrane, Biomater. Res. 28 (2024) 61.
[216] J. Kang, Z. Li, C.L. Organ, C.-M. Park, C.-t. Yang, A. Pacheco, D. Wang, D.J. Lefer, M. Xian, pH-Controlled hydrogen sulfide release for myocardial ischemia-reperfusion injury, J. Am. Chem. Soc. 138 (20) (2016) 6336–6339.
[217] J. Zhang, L. Liu, Z. Dong, X. Lu, W. Hong, J. Liu, X. Zou, J. Gao, H. Jiang, X. Sun, K. Hu, Y. Yang, J. Ge, X. Luo, A. Sun, An ischemic area-targeting, peroxynitrite-responsive, biomimetic carbon monoxide nanogenerator for preventing myocardial ischemia-reperfusion injury, Bioact. Mater. 28 (2023) 480–494.
[218] C. Nie, A. Rong, J. Wang, S. Pan, R. Zou, B. Wang, S. Xi, X. Hong, M. Zhou, H. Wang, M. Yu, L. Wu, X. Sun, W. Yang, Controlled release of hydrogen-carrying perfluorocarbons for ischemia myocardium-targeting $^{19}F$ MRI-Guided Reperfusior Injury Theiapy, Adv. Sci. 10 (29) (2023) 2304178.
[219] T. Hao, G. Ji, M. Qian, Q.X. Li, H. Huang, S. Deng, P. Liu, W. Deng, Y. Wei, J. He, S. Wang, W. Gao, T. Li, J. Cheng, J. Tian, L. Pan, F. Gao, Z. Li, Q. Zhao, Intracellular delivery of nitric oxide enhances the therapeutic efficacy of mesenchymal stem cells for myocardial infarction, Sci. Adv. 9 (48) (2023) eadi9967.
[220] M. El Kazzi, H. Shi, S. Vuong, X. Wang, B. Chami, Y. Liu, B.S. Rayner, P.K. Witting, Nitroxides mitigate neutrophil-mediated damage to the myocardium after experimental myocardial infarction in rats, Int. J. Mol. Sci. 21 (20) (2020) 7650.
[221] S.M. Andrabi, N.S. Sharma, A. Karan, S.M.S. Shahriar, B. Cordon, B. Ma, J. Xie, Nitric oxide: physiological functions, delivery, and biomedical applications, Adv. Sci. 10 (30) (2023) 2303259.
[222] N. Naghavi, A. de Mel, O.S. Alavijeh, B.G. Cousins, A.M. Seifalian, Nitric oxide donors for cardiovascular implant applications, Small 9 (1) (2013) 22–35.
[223] P.N. Coneski, M.H. Schoenfisch, Nitric oxide release: part III. Measurement and reporting, Chem. Soc. Rev. 41 (10) (2012) 3753–3758.
[224] C. Farah, L.Y.M. Michel, J.-L. Balligand, Nitric oxide signalling in cardiovascular health and disease, Nat. Rev. Cardiol. 15 (5) (2018) 292–316.
[225] A. Kumar, S.R. Boovarahan, P.N. Prem, M. Ramanathan, D.R. Chellappan, G. A. Kurian, Evaluating the effects of carbon monoxide releasing molecule-2 against myocardial ischemia-reperfusion injury in ovariectomized female rats, N. Schmied. Arch. Pharmacol. 394 (10) (2021) 2103–2115.
[226] S. Jeddi, S. Gheibi, K. Kashfi, M. Carlstrom, A. Ghasemi, Protective effect of intermediate doses of hydrogen sulfide against myocardial ischemia-reperfusion injury in obese type 2 diabetic rats, Life Sci. 256 (2020) 117855.
[227] S. Du, Y. Huang, H. Jin, T. Wang, Protective mechanism of hydrogen sulfide against chemotherapy-induced cardiotoxicity, Front. Pharmacol. 9 (2018) 32.
[228] Y.J. Song, S. Cao, X.T. Sun, G.Z. Chen, The interplay of hydrogen sulfide and microRNAs in cardiovascular diseases: insights and future perspectives, Mamm. Genome 35 (3) (2024) 309–323.
[229] Z. Liang, Y. Miao, X. Teng, L. Xiao, Q. Guo, H. Xue, D. Tian, S. Jin, Y. Wu, Hydrogen sulfide inhibits ferroptosis in cardiomyocytes to protect cardiac function in aging rats, Front. Mol. Biosci. 9 (2022) 947778.
[230] J. Hao, Y. Xi, L. Jiao, X. Wen, R. Wu, G. Chang, F. Sun, C. Wei, H. Li, Exogenous hydrogen sulfide inhibits the senescence of cardiomyocytes through modulating mitophagy in rats, Cell. Signal. 100 (2022) 110465.
[231] L. Gan, P. Cheng, J. Wu, Q. Li, J. Pan, Y. Ding, X. Gao, L. Chen, Hydrogen sulfide promotes postnatal cardiomyocyte proliferation by upregulating SIRT1 signaling pathway, Int. Heart J. 65 (3) (2024) 506–516.
[232] T. Ma, L. Yang, B. Zhang, X. Lv, F. Gong, W. Yang, Hydrogen inhalation enhances autophagy via the AMPK/mTOR pathway, thereby attenuating doxorubicin-induced cardiac injury, Int. Immunopharmacol. 119 (2023) 110071.
[233] Y. Cui, Y. Li, S. Meng, Y. Song, K. Xie, Molecular hydrogen attenuates sepsis-induced cardiomyopathy in mice by promoting autophagy, BMC Anesthesiol. 24 (1) (2024) 72.
[234] C. Nie, X. Ding, A. Rong, M. Zheng, Z. Li, S. Pan, W. Yang, Hydrogen gas inhalation alleviates myocardial ischemia-reperfusion injury by the inhibition of oxidative stress and NLRP3-mediated pyroptosis in rats, Life Sci. 272 (2021) 119248.
[235] L. Pferdehirt, A.R. Damato, K.L. Lenz, M.F. Gonzalez-Aponte, D. Palmer, Q. J. Meng, E.D. Herzog, F. Guilak, A synthetic chronogenetic gene circuit for programmed circadian drug delivery, Nat. Commun. 16 (1) (2025) 1457.
[236] M.J. Sole, T.A. Martino, Circadian medicine: a critical strategy for cardiac care, Nat. Rev. Cardiol. 20 (11) (2023) 715–716.
[237] T. Eckle, J. Bertazzo, T.N. Khatua, S.R.F. Tabatabaei, N.M. Bakhtiari, L.A. Walker, T.A. Martino, Circadian influences on myocardial ischemia-reperfusion injury and heart failure, Circ. Res. 134 (6) (2024) 675–694.
[238] W. Ruan, T. Li, I.H. Bang, J. Lee, W.K. Deng, X.X. Ma, C. Luo, F. Du, S.H. Yoo, B. Kim, J.W. Li, X.Y. Yuan, K. Figarella, Y.A. An, Y.Y. Wang, Y.F. Liang, M. DeBerge, D.Z. Zhang, Z. Zhou, Y.Y. Wang, J.M. Gorham, J.G. Seidman, C. E. Seidman, S.F. Aranki, R. Nair, L. Li, J. Narula, Z.M. Zhao, A.A. Gorfe, J. D. Muehlschlegel, K.L. Tsai, H.K. Eltzschig, BMAL1-HIF2A heterodimer modulates circadian variations of myocardial injury, Nature 641 (2025) 1017–1028.
[239] L. Li, H. Li, C.L. Tien, R.L. Zhang, X.D. Liao, M.K. Jain, L.L. Zhang, KLF15 regulates the circadian susceptibility to ischemia reperfusion injury in the heart, Circ. Res. 138 (2018). A16961-A16961.
[240] H. Tian, Q. Huang, J. Cheng, Y. Xiong, Z. Xia, Rev-erbα attenuates diabetic myocardial injury through regulation of ferroptosis, Cell. Signal. 114 (2023) 111006.
[241] X. Cong, Z. Zhang, H. Li, Y.-G. Yang, Y. Zhang, T. Sun, Nanocarriers for targeted drug delivery in the vascular system: focus on endothelium, J. Nanobiotechnol. 22 (2024) 620.
[242] Y. Shao, C. Xu, S. Zhu, J. Wu, C. Sun, S. Huang, G. Li, W. Yang, T. Zhang, X.-L. Ma, J. Du, P. Li, F.-J. Xu, Y. Li, One endothelium-targeted combined nucleic acid delivery system for myocardial infarction therapy, ACS Nano 18 (11) (2024) 8107–8124.
[243] A. Ortiz-Perez, D. van Tilborg, R. van der Meel, F. Grisoni, L. Albertazzi, Machine learning-guided high throughput nanoparticle design, Digital Discov. 3 (7) (2024) 1280–1291.